Research Paper

THEMED ISSUE: Geologic Evolution of the Alaska Range and Environs

GEOSPHERE

GEOSPHERE, v. 15

https://doi.org/10.1130/GES02008.1

21 figures; 4 tables; 1 set of supplemental files

CORRESPONDENCE: jbenowitz@alaska.edu

CITATION: Terhune, P.J., Benowitz, J.A., Trop, J.M., O'Sullivan, P.B., Gillis, R.J., and Freymueller, J.T., 2019, Cenozoic tectono-thermal history of the southern Talkeetna Mountains, Alaska: Insights into a potentially alternating convergent and transform plate margin: Geosphere, v. 15, https://doi.org/10.1130/GES02008.1.

Science Editors: Raymond M. Russo, Andrea Hampel
Guest Associate Editor: James V. Jones, III

Received 8 May 2018
Revision received 20 March 2019
Accepted 15 May 2019

Cenozoic tectono-thermal history of the southern Talkeetna Mountains, Alaska: Insights into a potentially alternating convergent and transform plate margin

Patrick J. Terhune[1], Jeffrey A. Benowitz[2], Jeffrey M. Trop[3], Paul B. O'Sullivan[4], Robert J. Gillis[5], and Jeffrey T. Freymueller[2]

[1]Department of Geosciences, University of Alaska Fairbanks, 900 Yukon Drive, Fairbanks, Alaska 99775, USA
[2]Geophysical Institute, University of Alaska Fairbanks, 2156 N. Koyukuk Drive, Fairbanks, Alaska 99775, USA
[3]Department of Geology and Environmental Geosciences, Bucknell University, Moore Avenue, Lewisburg, Pennsylvania 17837, USA
[4]GeoSep Services, 1521 Pine Cone Road, Moscow, Idaho 83843, USA
[5]Alaska Division of Geological and Geophysical Surveys, 3354 College Road, Fairbanks, Alaska 99709, USA

ABSTRACT

The Mesozoic–Cenozoic convergent margin history of southern Alaska has been dominated by arc magmatism, terrane accretion, strike-slip fault systems, and possible spreading-ridge subduction. We apply $^{40}Ar/^{39}Ar$, apatite fission-track (AFT), and apatite (U-Th)/He (AHe) geochronology and thermochronology to plutonic and volcanic rocks in the southern Talkeetna Mountains of Alaska to document regional magmatism, rock cooling, and inferred exhumation patterns as proxies for the region's deformation history and to better delineate the overall tectonic history of southern Alaska. High-temperature $^{40}Ar/^{39}Ar$ thermochronology on muscovite, biotite, and K-feldspar from Jurassic granitoids indicates postemplacement (ca. 158–125 Ma) cooling and Paleocene (ca. 61 Ma) thermal resetting. $^{40}Ar/^{39}Ar$ whole-rock volcanic ages and 45 AFT cooling ages in the southern Talkeetna Mountains are predominantly Paleocene–Eocene, suggesting that the mountain range has a component of paleotopography that formed during an earlier tectonic setting. Miocene AHe cooling ages within ~10 km of the Castle Mountain fault suggest ~2–3 km of vertical displacement and that the Castle Mountain fault also contributed to topographic development in the Talkeetna Mountains, likely in response to the flat-slab subduction of the Yakutat microplate. Paleocene–Eocene volcanic and exhumation-related cooling ages across southern Alaska north of the Border Ranges fault system are similar and show no S-N or W-E progressions, suggesting a broadly synchronous and widespread volcanic and exhumation event that conflicts with the proposed diachronous subduction of an active west-east–sweeping spreading ridge beneath south-central Alaska. To reconcile this, we propose a new model for the Cenozoic tectonic evolution of southern Alaska. We infer that subparallel to the trench slab breakoff initiated at ca. 60 Ma and led to exhumation, and rock cooling synchronously across south-central Alaska, played a primary role in the development of the southern Talkeetna Mountains, and was potentially followed by a period of southern Alaska transform margin tectonics.

INTRODUCTION

The Talkeetna Mountains of south-central Alaska are positioned north of the Border Ranges fault system (BRFS) and more than 350 km inboard from the Pacific–North American plate boundary (Fig. 1). Today the Talkeetna Mountains completely overlay the subducted portion of the Yakutat microplate, a buoyant oceanic plateau that has been undergoing flat-slab subduction with southern Alaska since the late Oligocene (Figs. 1 and 2) (Benowitz et al., 2011, 2014; Lease et al., 2016). The Talkeetna Mountains region also experienced Eocene slab-window magmatism (Cole et al., 2006). The active transpressive Castle Mountain fault (CMF), which is thought to have formed as early as the Late Cretaceous (Bunds, 2001), defines the southern border of the Talkeetna Mountains (Fig. 1) (Parry et al., 2001; Haeussler et al., 2002). This spatial relationship suggests that vertical tectonics along the CMF may have contributed to the development of the Talkeetna Mountains (Fuchs, 1980; Clardy, 1974; Trop et al., 2003).

In order to better understand the overall Mesozoic–Cenozoic tectonic history of southern Alaska, we have applied $^{40}Ar/^{39}Ar$ (whole-rock, hornblende, muscovite, biotite, and K-feldspar), apatite fission-track, and apatite (U-Th)/He geochronology and thermochronology to bedrock samples collected from transects along and across the strike of the CMF and along vertical profiles throughout the glaciated high-peak region of the southern Talkeetna Mountains. The specific objectives of this study were to: (1) determine if the Talkeetna Mountains are primarily a paleotopographic expression of an earlier phase of tectonism and if the production of topography was driven by a Paleocene–Eocene plate boundary event prior to the current late Oligocene to present Yakutat flat-slab plate configuration; (2) determine if late Oligocene to present subduction of the Yakutat microplate primarily drove topographic development in the Talkeetna Mountains; (3) test the model of a west-east time transgressive sweep of Paleocene–Eocene volcanism and deformation driven by margin-parallel, spreading-ridge subduction; and (4) better understand the role of the CMF in the construction of the Talkeetna Mountains.

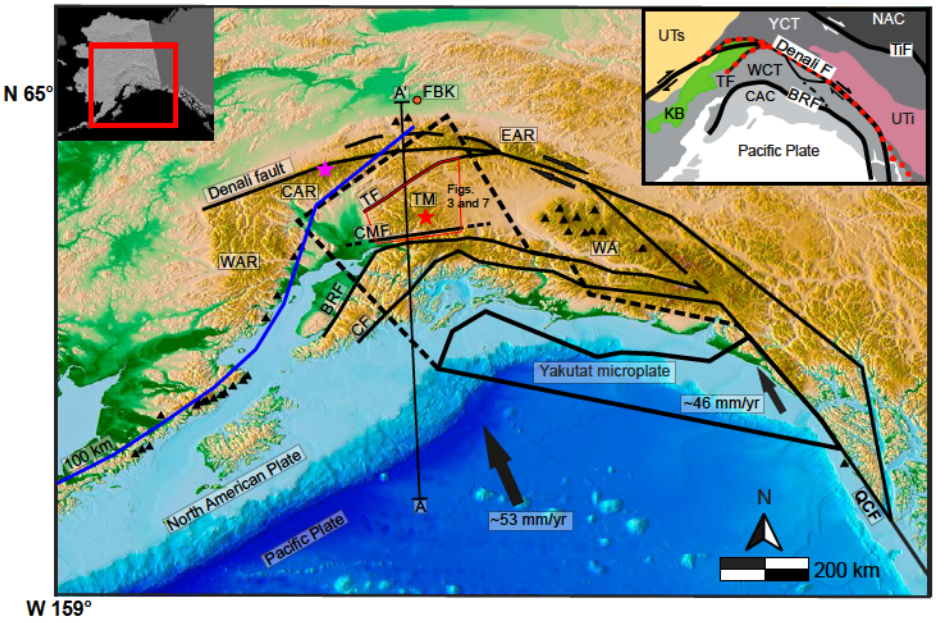

Figure 1. Simplified tectonic setting of southern Alaska. Inset map in upper left shows location in southern Alaska. Inset map in upper right shows major accreted terranes. Abbreviations: YCT—Yukon composite terrane; WCT—Wrangellia composite terrane; CAC—Chugach accretionary complex; TiF—Tintina fault; UTi—undifferentiated terranes and igneous rocks; UTs—unidentified terranes and sedimentary rocks; KB—Kahiltna Basin; NAC—North American Craton; red dotted line—Mesozoic suture zone between continental (YCT) and oceanic (WCT) terranes; TF—Talkeetna fault; BRF—Border Ranges fault; CMF—Castle Mountain fault; CF—Contact fault; QCF—Queen Charlotte–Fairweather fault; TM—Talkeetna Mountains; WAR—western Alaska Range; CAR—central Alaska Range; EAR—eastern Alaska Range; WA—Wrangell Arc; FBK—Fairbanks. Pink star—Denali; red star—Mount Sovereign; black triangles—volcanoes. Black dashed line is the subducted portion of the Yakutat microplate from Eberhart-Phillips et al. (2006). A–A' transect: on Figures 4 and 18. General location of Figures 3 and 7 denoted by red polygon.

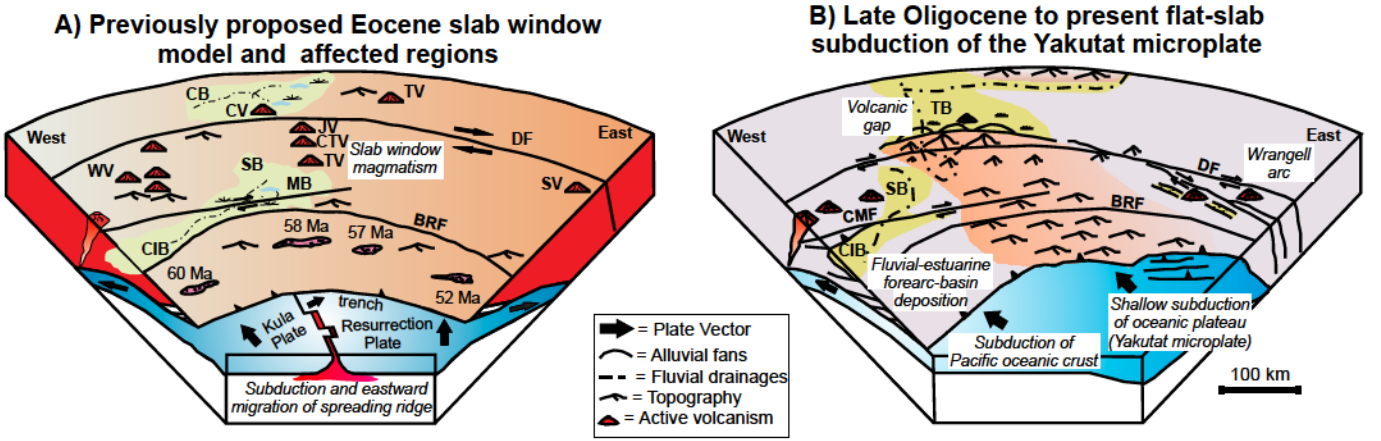

Figure 2. (A) Previously proposed Paleocene–Eocene slab window summary figure, based on the model by Haeussler et al. (2003) showing near-trench pluton emplacement ages, ages of initiation of rapid exhumation, basin formation, and regional magmatism across the region of Alaska affected by the flat-slab Paleocene–Eocene ridge subduction event. (B) Flat-slab subduction of the Yakutat microplate summary figure showing regions of basin subsidence, mountain building, the presence of an Aleutian Arc volcanic gap, and the initiation of the Wrangell Arc. Abbreviations: Cook Inlet Basin—CIB; Susitna Basin—SB; Matanuska Basin—MB; Tanana Basin—TB; Cantwell Basin—CB; Western Alaska Range volcanics—WV; Jack River volcanics—JV; Central Talkeetna volcanics—CTV; Caribou Hill volcanics—CV; Tanana Valley volcanics—TV; Sifton volcanics—SV; Denali fault—DF; Border Ranges fault system—BRF; Castle Mountain fault—CMF. Modified from Ridgway et al. (2012) and Benowitz et al. (2012a).

Our $^{40}Ar/^{39}Ar$ and fission-track results suggest that the Talkeetna Mountains are in part residual topography that formed in response to a Paleocene–Eocene thermal event, as proposed for the western Alaska Range (Fig. 1) (Benowitz et al., 2012a). A compilation of new and regional thermochronology and dating of volcanics shows no west-east progression in the timing of initiation of Paleocene–Eocene exhumation or magmatism, which is inconsistent with the current sweeping spreading-ridge subduction model. Finally, based on apatite (U-Th)/He thermochronology, we infer there has been ~2–3 km of vertical displacement along the CMF since the Miocene in response to flat-slab subduction of the Yakutat microplate which has also contributed to the creation of topography in the Talkeetna Mountains.

BACKGROUND

Southern Alaska and Talkeetna Mountains Tectonic Framework

Geology of the Talkeetna Mountains

The Talkeetna Mountains are bordered to the west by a Cenozoic intraplate and forearc composite basin (Susitna Basin) and to the east and south by remnant Cenozoic forearc basins (Copper River Basin and Matanuska Valley Basin, respectively) (Fig. 2B) (Trop and Ridgway, 2007; Stanley et al., 2014). The subvertical Talkeetna fault bisects the Talkeetna Mountains and acts as a lithospheric terrane boundary between the Wrangell composite terrane (WCT) and the Alaska Range suture zone (ARSZ) (Fig. 1) (Brennan et al., 2011; Fitzgerald et al., 2014). Three allochthonous crustal fragments making up the WCT—the Alexander, Wrangellia, and Peninsular terranes—amalgamated together by early Mesozoic time, collided with the former continental margin at lower paleolatitudes and were translated northward along regional strike-slip faults (e.g., Denali fault; Plafker and Berg, 1994; Cowan et al., 1997; Stamatakos et al., 2001; Roeske et al., 2003; Gabrielse et al., 2006). In the southern Talkeetna Mountains, our main study area, the Peninsular terrane consists of a >5-km-thick succession of lavas, tuffs, and volcaniclastic sedimentary strata and adjacent plutonic rocks that are interpreted to reflect an oceanic arc (Rioux et al., 2007, 2010).

Large batholiths intruding the WCT are referred to as the Late Triassic–Early Jurassic Talkeetna Arc; these batholiths were emplaced in this region from ca. 183–153 Ma (Hacker et al., 2011). A series of Late Jurassic trondhjemite plutons make up the bulk of bedrock exposures in the interior Talkeetna Mountains and constitute Mount Sovereign, the highest peak in the Range (~2700 m) (Fig. 3) (Rioux et al., 2007). North of the Talkeetna fault, the ARSZ primarily consists of a ~3- to ~5-km-thick package of Kahiltna Basin marine sedimentary strata; this package was subaerially uplifted during the Mesozoic WCT collision (Ridgway et al., 2002). The ARSZ is a complex suture zone between outboard accreted terranes (WCT) and inboard pericratonic terranes (e.g., Foster et al., 1994; Dusel-Bacon et al., 2006). The erosion-resistant nature of the southern Talkeetna Mountains plutonic bodies and the mafic crust of the WCT relative to the north Kahiltna Basin rocks may contribute in part to the difference in relief between the northern and southern regions of the Talkeetna Mountains.

Overall, the structural configuration of the southern Talkeetna Mountains is not well constrained due to a lack of systematic, detailed geologic mapping across the entire range. Generally northwest- and southeast-striking extensional fault systems bisect the region of the Caribou Creek volcanic field and the Hatcher Pass region (Fig. 3) (Cole et al., 2006). These extensional faults are thought to have been active during a period of Paleocene–Eocene volcanism in the Caribou Creek volcanic field and regional Paleocene–Eocene crustal extension (Cole et al., 2006). Faults also appear to partially bound the high-peak region of the southern Talkeetna Mountains, consisting primarily of the Jurassic trondhjemite pluton (Fig. 3), suggesting that the region may have exhumed as an independent crustal block. A series of mesoscale folds and reverse faults deform Paleocene–Eocene strata exposed within ~10 km of the CMF, recording post–ca. 50 Ma shortening along the CMF (Bartsch-Winkler and Schmoll, 1992; Kassab et al., 2009; Robertson, 2014).

Talkeetna Mountains Mesozoic–Cenozoic Paleogeography

Paleomagnetism studies of rocks from the Talkeetna Mountains located in the WCT of southern Alaska (Fig. 1) suggest that during the Late Cretaceous (ca. 80 Ma), the region was positioned at a paleolatitude 15° ± 8° to the south of its current location (Stamatakos et al., 2001). Northward displacement of the WCT is inferred to have occurred along structures such as the Denali fault and Tintina fault systems, which accommodated at least ~1000 km of combined dextral slip based on offset geologic features (Denali fault: Lowey, 1998; Benowitz et al., 2012b; Tintina fault: Gabrielse, 1985). The WCT was near its present-day latitude by ca. 54–40 Ma judging from paleomagnetic constraints from southern Talkeetna Mountain Eocene lava flows (Panuska et al., 1990).

The Castle Mountain Fault

The subvertical CMF extends ~250 km along the southern border of the Talkeetna Mountains without any obvious restraining or releasing bends and ends in a horsetail splay at the eastern end of the Talkeetna Mountains (Figs. 1 and 3). The CMF separates denser rocks to the south from less dense rocks to the north (Mankhemthong et al., 2013), and these strength heterogeneities may play a role in where deformation is focused along the fault zone. This fault zone is also rheologically weaker than the crust surrounding it and accommodates strain transferred inboard from the plate margin (Bunds, 2001). Approximately 130 km of Cenozoic right-lateral horizontal displacement has been suggested along the CMF (Trop et al., 2005; Pavlis and Roeske, 2007). Willis et al. (2007) constrained a Holocene horizontal slip-rate estimate along the western portion of the CMF at ~2–3 mm/yr based on an offset postglacial outwash channel, although this slip rate may decrease significantly to the east where slip is likely being partitioned

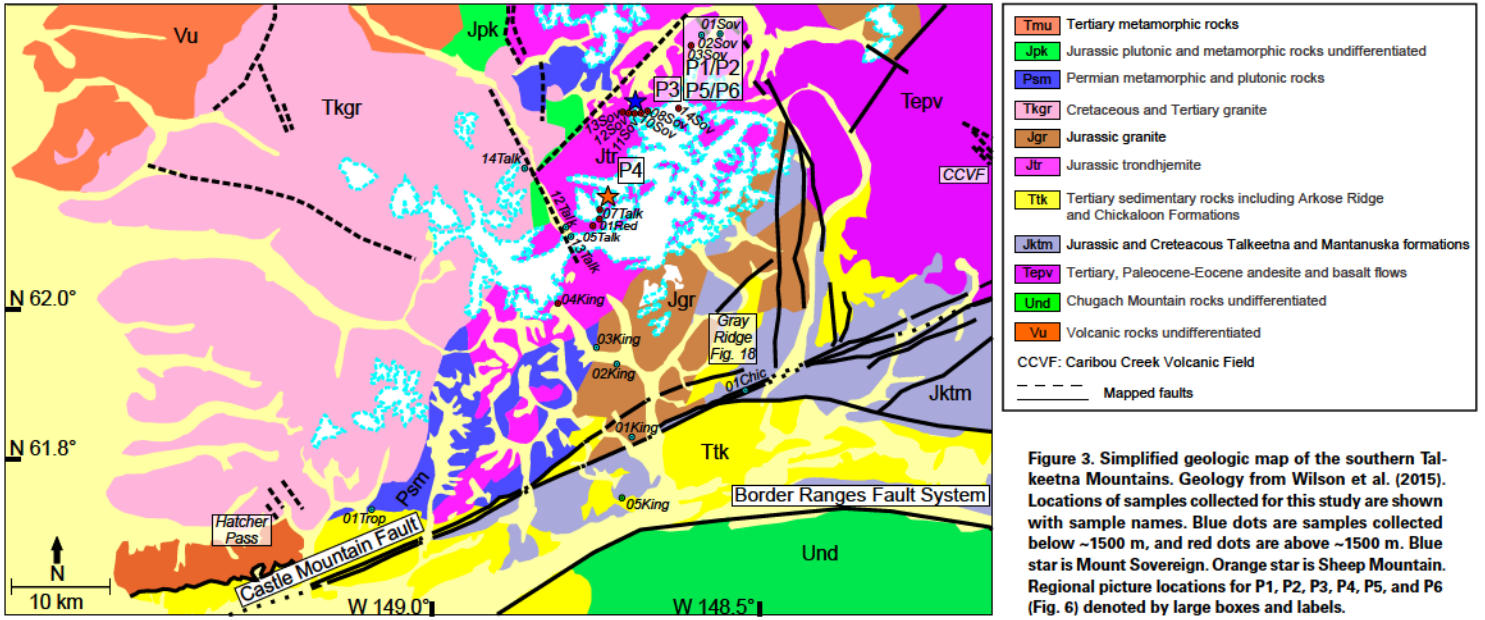

Figure 3. Simplified geologic map of the southern Talkeetna Mountains. Geology from Wilson et al. (2015). Locations of samples collected for this study are shown with sample names. Blue dots are samples collected below ~1500 m, and red dots are above ~1500 m. Blue star is Mount Sovereign. Orange star is Sheep Mountain. Regional picture locations for P1, P2, P3, P4, P5, and P6 (Fig. 6) denoted by large boxes and labels.

into an oblique component. Fuchs (1980) suggested a post-Eocene slip rate of ~0.5 mm/yr based on field mapping observations, and finite element models by Kalbas et al. (2008) suggested a Holocene slip rate of ~1 mm/yr. Conversely, light detection and ranging (lidar)–based geomorphic studies along the western segment of the CMF suggest a much-diminished Holocene dextral slip rate (<0.3 mm/yr) and vertical motion at a rate of ~0.5 mm/yr (Koehler et al., 2014). The overall vertical displacement history along the CMF is not well constrained; regional mapping studies document up to 3 km of north-side-up Neogene vertical slip based on offset Jurassic to Paleogene strata (Grantz, 1966; Detterman et al., 1976), but detailed cross sections have not been reported.

Kula-Resurrection Spreading-Ridge Subduction Hypothesis

It has been proposed that during late Paleocene–Eocene time, southern Alaska experienced diachronous subduction of the active Kula-Resurrection oceanic spreading ridge (Fig. 2A) (Bradley et al., 1993; Haeussler et al., 2003). The Kula-Resurrection ridge is interpreted to have subducted at an oblique angle and along an eastward-sweeping trajectory in a subparallel motion with respect to the paleo-trench (Haeussler et al., 2003). This model stems chiefly from a ~2000-km-long string of near-trench plutons in the accretionary prism, the Sanak-Baranof belt (Figs. 1 and 2A); the string shows an eastward progression in the timing of magmatism from ca. 63 Ma to ca. 47 Ma. Many other data sets also document a regional ca. 63–47 Ma "near-trench" thermal event within the prism, including high-temperature and low-pressure metamorphism, mafic underplating, extensive fluid circulation, and rapid exhumation and erosion (e.g., Haeussler et al., 1995; Kusky et al., 1997; Pavlis and Sisson, 2003; Gasser et al., 2011).

However, the Sanak-Baranof near-trench magmatic belt may have been positioned >~2500 km to the south along the western margin of North America ca. 63 Ma to ca. 47 Ma and subsequently translated to its current location by the late Eocene along orogeny-parallel faults such as the BRFS (Cowan, 2003; Garver and Davidson, 2015; Garver, 2017; Davidson and Garver, 2017). This competing model is based in part on a paleomagnetism study by Bol et al. (1992) and detrital-zircon studies by Garver and Davidson (2015) and Davidson and Garver (2017). If this is the case, then a relatively stationary Paleocene–Eocene slab-window or other thermal perturbation (hot spot?) led to the emplacement of the Sanak-Baranof suite ~2500 km to the south as the overlying plate was translated to the north over the thermal perturbation (Cowan, 2003).

Independent of the Sanak-Baranof near-trench plutonic suite, there is compelling supporting evidence for a widespread Paleocene–Eocene slab-window–related thermal event across southern and interior Alaska; this event drove rapid rock cooling (e.g., Yukon-Tanana: Dusel-Bacon and Murphy, 2001; western Alaska Range: Benowitz et al., 2012a; Saint Elias Range: Enkelmann et al., 2017), thermal resetting (Finzel et al., 2016), basin subsidence and inversion (Ridgway et al., 2012; Kortyna et al., 2013), and widespread volcanism

(Cole et al., 1999, 2006, 2007). If these geologic events are related to a west- to east-sweeping ridge subduction event to the south with minimal strike-slip displacement (<500 km) between the accretionary prism and region north of the BRFS since ca. 63–47 Ma, there should be a north-of-the-BRFS rock record of west to east and south to north progressions of initiation of these deformation events. Alternatively, during the Paleocene–Eocene, the accretionary prism Sanak-Baranof belt and southern Alaska north of the BRFS may have been distal from each other and experienced different slab-window mechanisms.

Flat-Slab Subduction of the Yakutat Microplate

Since ca. 30 Ma, the primary driver of orogenic processes in southern Alaska has been the ongoing flat-slab subduction of the Yakutat microplate, a buoyant ~15- to ~30-km-thick oceanic plateau (Fig. 2B) (Worthington et al., 2012; Brueseke et al., 2019). The Yakutat flat-slab extends ~350 km inboard before the dip angle increases (Eberhart-Phillips et al., 2006), and this has been suggested to cause the almost-complete gap in magmatism between the Aleutian and Wrangell Arcs (Finzel et al., 2011; Trop et al., 2012; Brueseke et al., 2019). Active transpressional fault systems across southern Alaska accommodate the oblique convergence of the Yakutat flat-slab, resulting in numerous regions of deformation far inboard from the trench interface (Haeussler, 2008; Riccio et al., 2014, Burkett et al., 2016; Waldien et al., 2018).

It has been proposed that the topographic development of the Talkeetna Mountains coincided with the flat-slab subduction of the Yakutat microplate (Figs. 1 and 2B) (Hoffman and Armstrong, 2006; Finzel et al., 2011). This is primarily based on the modern position of the Alaska Range over the subducted portion of the flat-slab, limited Miocene Talkeetna Mountain AHe bedrock cooling ages (e.g., Arkle et al., 2013), and enhanced sediment accumulation rates and sediment delivery from bedrock sources exhumed above the flat-slab region (Cook Inlet; Finzel et al., 2011, 2016; Tanana Basin; Benowitz et al., 2019).

Geodynamic computational modeling provides a potential test if the Yakutat microplate has primarily driven topographic development in the Talkeetna Mountains. Jadamec et al. (2013) used three-dimensional numerical models to test if the deformational patterns across southern Alaska can be explained by the modern plate configuration (Fig. 4A). The models produce results that match most of Alaska's modern topography. However, in the Talkeetna Mountains region, they do not predict a topographic high, but rather a basin (Figs. 4A and 4B). The models suggest that basins correlate to where the slab-dip angle increases and separates from the overriding plate, dynamically pulling down the overlying crust (Fig. 4B). The high topography of the Talkeetna Mountains contradicts the topographic predictions of Jadamec et al. (2013) unless a significant portion of the topographic relief predates the modern configuration, which would suggest that the modern plate configuration is not the dominant control of topography in the range.

The Jadamec et al. (2013) modeling also includes a rheologically weak zone where the Denali fault is located and correctly predicts topographic construction in the Alaska Range along this strike-slip structure. Conversely, this model does not account for the existence of the CMF and its potential for focusing deformation and vertical displacement, which may also contribute to its failure to correctly predict the topography of the Talkeetna Mountains. Therefore, the possibility of topographic development due to vertical tectonics

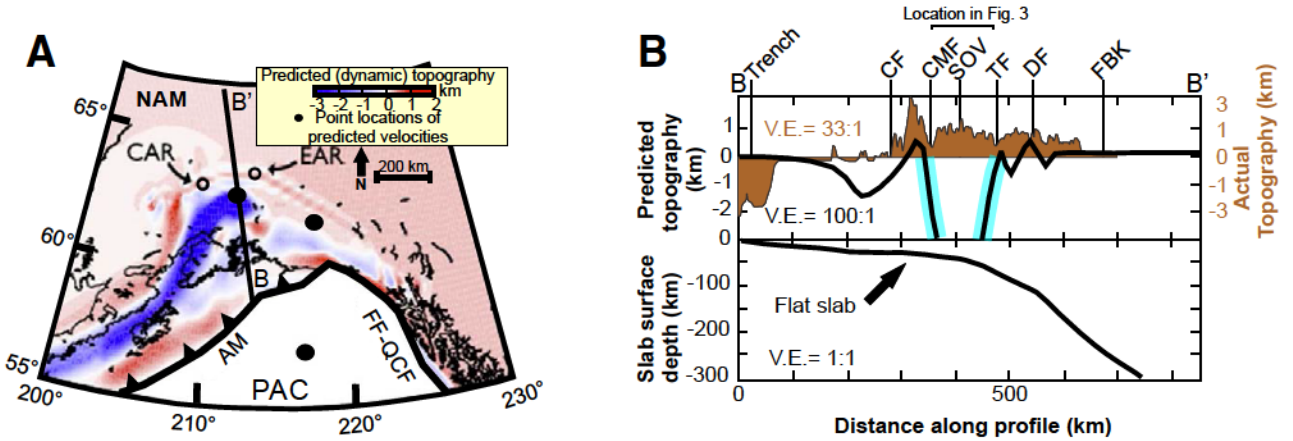

Figure 4. (A) Model results from Jadamec et al. (2013) of predicted distribution of modern dynamic topography across southern Alaska based on modern plate configuration. Red corresponds to higher dynamic topography, and blue corresponds to lower dynamic topography. Abbreviations: AM—Aleutian megathrust; CAR—Central Alaska Range; EAR—Eastern Alaska Range; NAM—North American plate; PAC—Pacific plate; FF-QCF—Fairweather Queen Charlotte fault. (B) Top: Topography predicted from model and actual topography along transect B–B′. Bottom: cross section of Yakutat flat-slab along B–B′. CF—Contact fault; CMF—Castle Mountain fault; SOV—Mount Sovereign; TF—Talkeetna thrust fault; DF—Denali fault; FBK—Fairbanks; V.E.—vertical exaggeration.

along the CMF is not eliminated by these models, if the CMF is also a rheologically weak zone, as argued by Bunds (2001).

A cross section of seismicity from the Aleutian Trench to interior Alaska displays the flat-slab subduction of the Yakutat microplate under the North American plate (Fig. 5) and highlights the significant active structural elements such as the Denali fault, which is clearly shown as a crustal-scale feature. The Yakutat slab dips subhorizontally until it reaches the Talkeetna Mountains region, where the dip angle increases to ~20°. Beneath the Talkeetna Mountains, seismicity appears to be diffuse, and the CMF does not appear to display significantly more seismicity compared to the area immediately to the north. The limited shallow seismicity and the imaged depth of the downgoing Yakutat slab suggests that the interacting plates are not highly coupled and that the buoyant slab is not acting as an upward force on the crust of the Talkeetna Mountains. Given this framework, we can use thermochronology to test if the Talkeetna Mountains reflect a paleotopography contribution that formed during a previous tectonic event and the role, if any, of the CMF in the region's topographic development history.

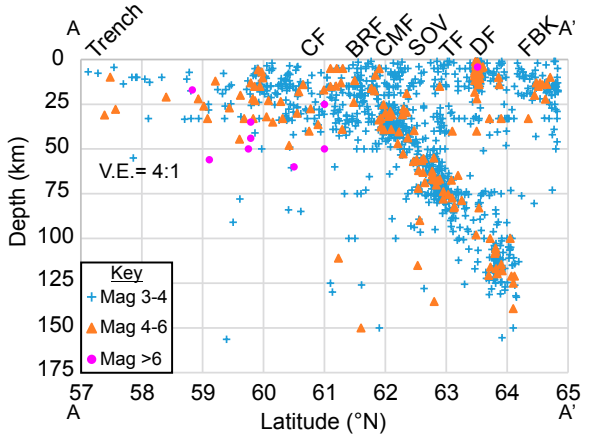

Figure 5. Seismicity along cross section A–A' from Figure 1 (100-km-wide swath). Seismic events collected, but not relocated, from the Alaska Earthquake Information Center catalog (https://earthquake.alaska.edu) from 1911 to 2015 and of magnitudes >3.0 are shown. Abbreviations: CF—Contact fault; CMF—Castle Mountain fault; SOV—Mount Sovereign; TF—Talkeetna thrust fault; DF—Denali fault; BRF—Border Ranges fault; FBK—Fairbanks; V.E.—vertical exaggeration.

Cenozoic Thermal History of Southern Alaska

The known varied convergent margin configurations that the region has undergone suggest that the thermal regime of southern Alaska has changed throughout the Cenozoic (e.g., Riccio et al., 2014; Lease et al., 2016). Thermochronology in the western Alaska Range (Fig. 1) shows evidence for a higher than normal geothermal gradient (>50 °C/km) (Benowitz et al., 2012a) during the Eocene, suggesting that high heat flow and the injection of magma into the upper crust contributed to regional mountain building. Finzel et al. (2016) also infer a possible high geothermal gradient (>100 °C) across southern Alaska during the Paleocene–Eocene based on reset detrital-zircon fission-track ages from Cretaceous–Cenozoic strata. This anomalously high geothermal gradient event likely extended across southern Alaska and persisted for ~20 m.y. (O'Sullivan and Currie, 1996; Cole and Stewart, 2009). However, it is not known when the modern thermal regime was established.

The southern Talkeetna Mountains are thought to occupy a region that was subjected to elevated heat flow above a slab window to the asthenosphere and was subsequently cooled from flat-slab subduction of the Yakutat microplate (Cole et al., 2006; Finzel et al., 2011). The basis for this inference is a package of Eocene volcanic rocks that have been linked to an inferred Paleocene–Eocene spreading-ridge subduction event (Fig. 1) (Cole et al., 2006; Cole and Stewart, 2009) and the current position of the range over the subducted portion of the Yakutat microplate (Fig. 1). Therefore, the regional rock record should register a marked shift in its thermal structure through time and space. The Talkeetna Mountains Jurassic trondhjemite plutons have been intruded by mafic dikes and K-feldspar–rich fluids (Fig. 6; P1, P2, and P3) (see Results section), providing additional evidence for a regional thermal event. Currently there are no active hot spring systems in the region; there are, however, abundant outcrops displaying hydrothermal alteration, especially within the trondhjemite plutons (Fig. 6; P3). Spatially the Talkeetna Mountains are located ~300 km from Neogene to presently active volcanoes (Fig. 1); so the region's thermal history has not been overprinted by Neogene volcanism.

Previously published low-temperature thermochronology data have generally focused on the southernmost region of the Talkeetna Mountains near the CMF (Little and Naeser, 1989; Parry et al., 2001; Hoffman and Armstrong, 2006; Hacker et al., 2011; Bleick et al., 2012) and have indicated temporal-spatial variability in the timing of Talkeetna Mountains rock cooling and inferred exhumation. AFT ages in the Hatcher Pass region (Figs. 3 and 7) record Paleocene–Eocene structural and erosional exhumation (Bleick et al., 2012). Miocene AHe ages near the CMF are indicative of a more recent rock cooling and inferred exhumation event in the southern Talkeetna Mountains (Hoffman and Armstrong, 2006). Younger (ca. 16–22 Ma) AFT ages south of the CMF suggest a period of rapid exhumation coincided with the highly coupled flat-slab subduction of the Yakutat microplate (Little and Naeser, 1989; Hoffman and Armstrong, 2006). However, only scant low-temperature thermochronology data are available in the high-peak region of the Talkeetna Mountains, and previously published ages were not collected in a systematic way that could elucidate age-elevation relationships, thermal resetting, or a CMF structural control on cooling age patterns. Hence, this study utilizes a multi-thermochronometer and geochronological approach applied to bedrock samples collected between the Talkeetna fault and the CMF and one sample south of the CMF, combined with previously published results (Hacker et al., 2011; Bleick et al., 2012; Arkle et al., 2013), to constrain rock-cooling histories.

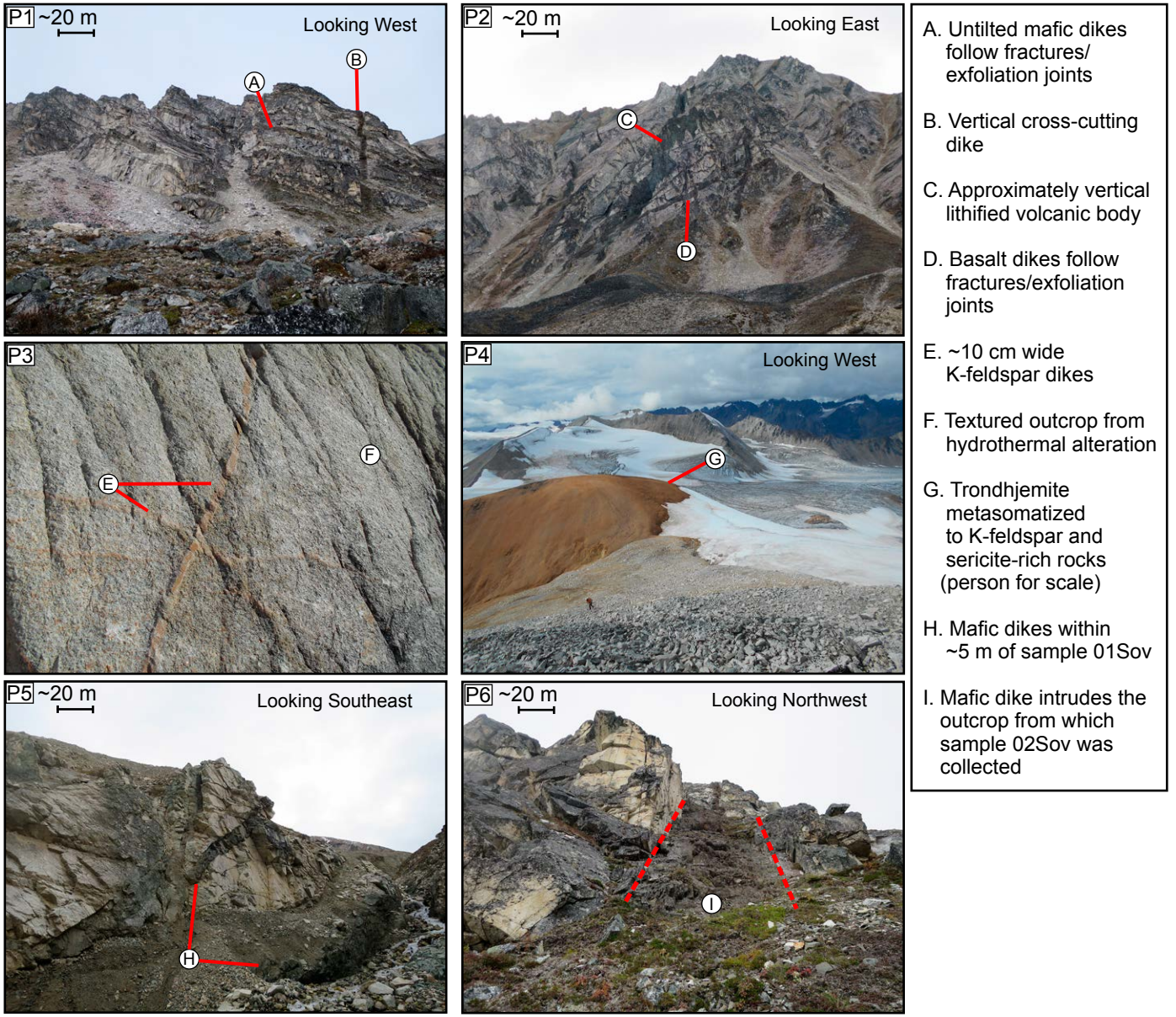

Figure 6. Photographs from our southern Talkeetna Mountains study area shown in Figure 5. (P1 and P2) The presence of Eocene dikes along exfoliation joints that are cross cut by vertical dikes and lithified volcanic bodies indicates a lack of significant tilting in the region since dike emplacement. (P3) Many outcrops in the field area have crosscutting K-feldspar dikes and have been altered by hydrothermal fluids. (P4) Along the Sheep Mountain vertical profile, trondhjemite rocks were metasomatized to K-feldspar and sericite-rich rocks (person shown for scale). (P5 and P6) Mafic dikes at a minimum distance of ~5 m from samples 01Sov and 02Sov.

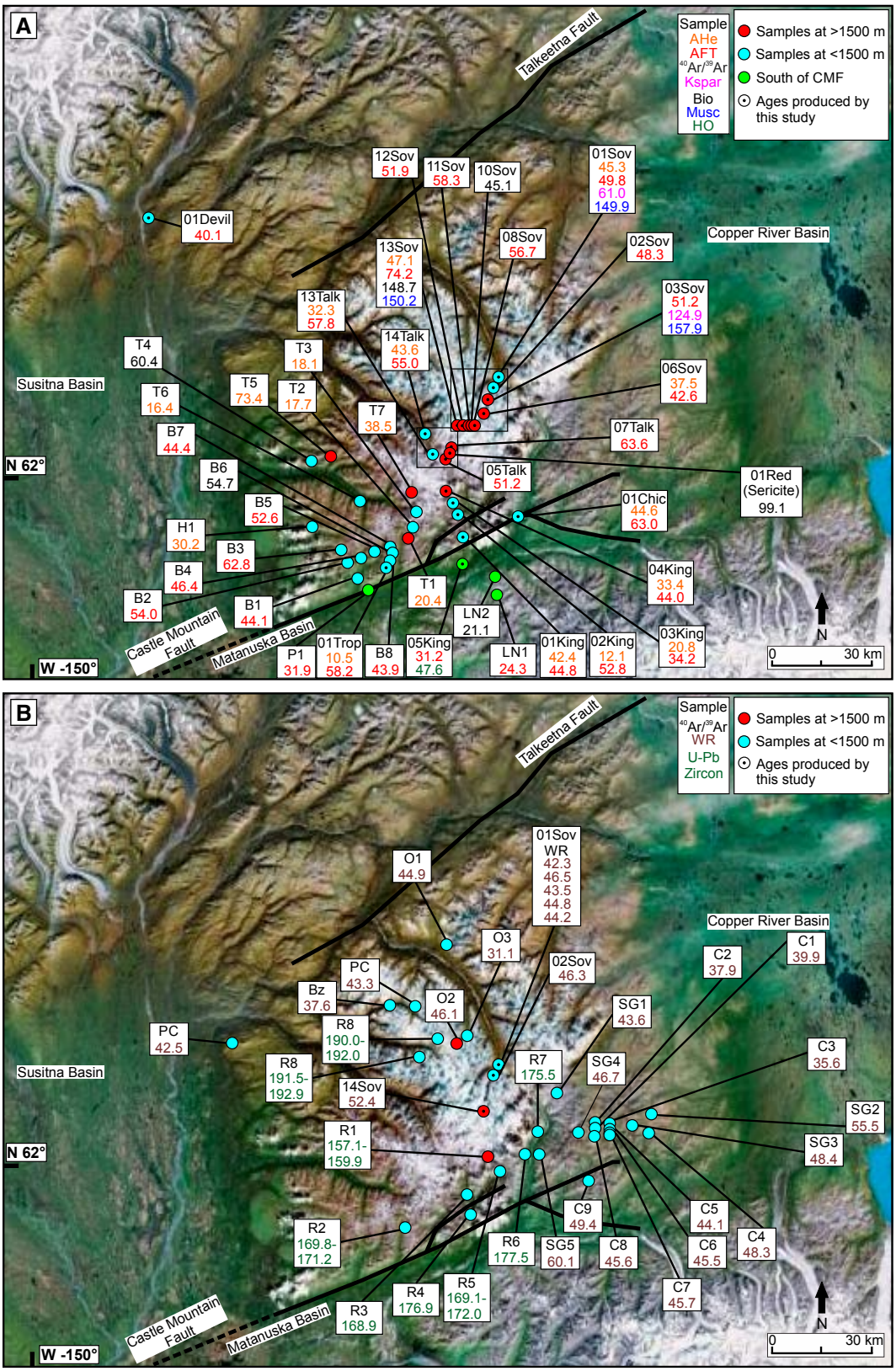

Figure 7. Satellite images of the Talkeetna Mountains and sample location maps showing cooling ages and volcanic ages from samples analyzed for this study. (A) All apatite fission-track (AFT), apatite (U-Th)/He (AHe), and $^{40}Ar/^{39}Ar$ K-feldspar, muscovite, biotite, and hornblende cooling ages published in the region south of the Talkeetna fault (upper map). (B) All whole-rock $^{40}Ar/^{39}Ar$ and zircon U-Pb ages published in the region south of the Castle Mountain fault (CMF) (lower map). Black boxes encompass Mount Sovereign (northern box) and Sheep Mountain (southern box) vertical profiles. References: B—Bleick et al., 2012; Bz—Benowitz et al., 2015; C—Cole et al., 2006; H—Hacker et al., 2011; LN—Little and Naeser, 1989; O—Oswald, 2006; P—Parry et al., 2001; PC—Ron Cole, 2017, personal commun.; R—Rioux et al., 2007; SG—Silberman and Grantz, 1984; T—Hoffman and Armstrong, 2006; WR—whole rock.

METHODS

Sampling Strategy

We use a range of geochronology ($^{40}Ar/^{39}Ar$ on whole-rock volcanics) and multi-method high-temperature ($^{40}Ar/^{39}Ar$ on hornblende, muscovite, K-feldspar, and biotite) and low-temperature (apatite fission-track [AFT] and (U-Th)/He [AHe] on apatite) thermochronology techniques to constrain regional patterns of volcanism and time and/or temperature histories for rock samples in our study area (Fig. 7). In order to discern regional cooling age patterns with respect to the CMF and elevation, our sampling strategy included bedrock sampling transects along and across strike of the CMF and over a substantial portion of the high-peak region of the Talkeetna Mountains (Fig. 7) (Spotila, 2005). We also conducted two vertical profiles collecting bedrock samples every ~100 m over a ~1300 m vertical distance. Age-elevation profiles allow the possible identification of distinct slope inflection points, which are interpreted to mark changing rock-cooling and inferred exhumation rates (e.g., Fitzgerald et al., 1993). One vertical profile was collected along Mount Sovereign (~2700 m) and one along a peak off the Sheep Glacier (~2250 m) referred to herein as Sheep Mountain (Fig. 3).

Most of our samples were collected within a large Jurassic trondhjemite pluton and a Jurassic granite pluton (Fig. 3). Sample 01Chic is a metabasalt collected in the CMF zone (Fig. 7). One tonalite sample was collected south of the CMF (05King). We collected samples at different distances from Eocene volcanic intrusions on the outskirts of the Jurassic trondhjemite pluton (Fig. 6; P5 and P6) to test for thermal resetting. Volcanic rocks representing five different phases of magmatism were sampled at a minimum distance of ~5 m from trondhjemite sample 01Sov (Figs. 6 and 7) to further test for thermal resetting. Our new ages were integrated with existing thermochronology (Silberman and Grantz, 1984; Little and Naeser, 1989; Parry et al., 2001; Cole et al., 2006; Hoffman and Armstrong, 2006; Hacker et al., 2011; Bleick et al., 2012; Arkle et al., 2013) to constrain the Cenozoic exhumation and magmatic history of the Talkeetna Mountains.

Geochronology and Thermochronology Techniques: $^{40}Ar/^{39}Ar$

$^{40}Ar/^{39}Ar$ geochronology and thermochronology were performed at the University of Alaska Fairbanks Geochronology Facility on hornblende (05King), muscovite (01Sov, 03Sov, and 13Sov), sericite (01Red), biotite (13Sov), K-feldspar (01Sov and 03Sov), and phenocryst-free groundmass separates from whole-rock volcanic samples (01Sov-1, 01Sov-2, 01Sov-3, 01Sov-4, 2Sov, and 14Sov). Samples were crushed, sieved for the 250–1000 µm grain size, washed, put through heavy liquids, and then separated using magnetic and handpicking mineral separation techniques. Samples were analyzed on a VG-3600 mass spectrometer using laser step-heating techniques described in Benowitz et al. (2014). Dating multiple minerals in the same sample provides information about a rock's thermal history from ~150–450 °C. Whole-rock volcanic ages provide information about the timing of magmatism and diking. For a more detailed description of the $^{40}Ar/^{39}Ar$ analytical methods used and how uncertainties were derived, see the Supplemental Materials[1] (Text S1).

The K-feldspar age spectra for samples 01Sov and 03Sov (Fig. 8) are interpreted using multi-domain diffusion modeling (Lovera et al., 2002) to understand their thermal histories. Instead of performing diffusion experiments, we look at the timing of closure of the high-temperature ($KFAT_{max}$: ~350 °C) and low-temperature ($KFAT_{min}$: ~150 °C) domains for K-feldspar (Benowitz et al., 2014; Löbens et al., 2017).

A summary of all the $^{40}Ar/^{39}Ar$ results is given in Table 1, with all ages quoted to ±1σ and calculated using the constants of Renne et al. (2010). For detailed isotopic tables and figures, see the Supplemental Materials (Table S1 and Fig. S1 [footnote 1]).

Thermochronology Techniques: Apatite Fission Track

Under typical continental geothermal gradients, AFT thermochronology provides information about the thermal history of a rock sample in the upper ~3–5 km of the crust (Dodson, 1973). This technique involves analysis of the damage tracks formed by the spontaneous fission of ^{238}U (Tagami and O'Sullivan, 2005). Depending on the apatite grain composition and cooling rate, fission tracks will partially anneal at temperatures >60 °C and completely anneal at temperatures >120 °C. This temperature window is referred to as the partial annealing zone (PAZ). The temperature sensitivity of fission tracks allows for analysis of a rock sample's thermal history by measuring track lengths; shorter tracks indicate a longer residence time in the PAZ (60–120 °C) and a relatively slower cooling rate (Donelick et al., 2005). Track-length distributions that include both long and partially annealed tracks indicate more complex thermal histories. For this study, AFT analyses were performed by Paul O'Sullivan at the GeoSep Services facilities in Moscow, Idaho, on 21 samples. Age and track-length information is reported in Table 2, and AFT analytical data are reported in Table 3. For a detailed description of the methods used and how uncertainties were derived, see the Supplemental Materials (Text S2 [footnote 1]).

Thermochronology Techniques: Apatite (U-Th)/He

(U-Th)/He thermochronology involves the analysis of alpha particles (^4He) accumulated in a mineral due to the radioactive decay of uranium and thorium (Reiners and Brandon, 2006). With a nominal closure temperature of 40–80 °C, apatite (U-Th)/He thermochronology (AHe) provides information about the thermal history of a rock sample in the upper ~2–4 km of the crust (Farley, 2002). ^4He particles travel ~20 microns from their parent atoms during radioactive decay, resulting in the ejection of ^4He produced near the edge of a grain, requiring corrections referred to as the F_T correction (Farley et al., 1996; Ketcham, 2005). The closure temperature of an apatite grain should vary depending on the grain size, cooling rate, and radiation damage accumulated

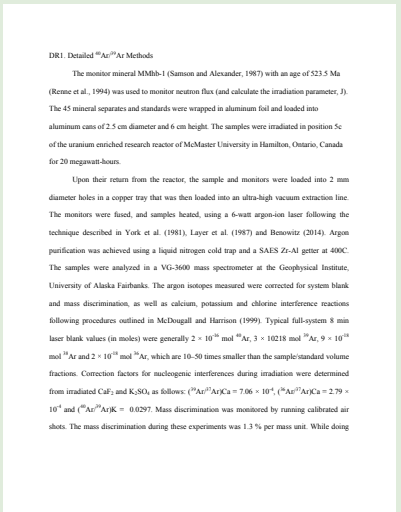

DR1. Detailed $^{40}Ar/^{39}Ar$ Methods

The monitor mineral MMhb-1 (Samson and Alexander, 1987) with an age of 523.5 Ma (Renne et al., 1994) was used to monitor neutron flux (and calculate the irradiation parameter, J). The 45 mineral separates and standards were wrapped in aluminum foil and loaded into aluminum cans of 2.5 cm diameter and 6 cm height. The samples were irradiated in position 5c of the uranium enriched research reactor of McMaster University in Hamilton, Ontario, Canada for 20 megawatt-hours.

Upon their return from the reactor, the sample and monitors were loaded into 2 mm diameter holes in a copper tray that was then loaded into an ultra-high vacuum extraction line. The monitors were fused, and samples heated, using a 6-watt argon-ion laser following the technique described in York et al. (1981), Layer et al. (1987) and Benowitz (2014). Argon purification was achieved using a liquid nitrogen cold trap and a SAES Zr-Al getter at 400C. The samples were analyzed in a VG-3600 mass spectrometer at the Geophysical Institute, University of Alaska Fairbanks. The argon isotopes measured were corrected for system blank and mass discrimination, as well as calcium, potassium and chlorine interference reactions following procedures outlined in McDougall and Harrison (1999). Typical full-system 8 min laser blank values (in moles) were generally 2×10^{-16} mol ^{40}Ar, 3×10218 mol ^{39}Ar, 9×10^{-18} mol ^{38}Ar and 2×10^{-18} mol ^{36}Ar, which are 10–50 times smaller than the sample/standard volume fractions. Correction factors for nucleogenic interferences during irradiation were determined from irradiated CaF_2 and K_2SO_4 as follows: $(^{39}Ar/^{37}Ar)Ca = 7.06 \times 10^{-4}$, $(^{38}Ar/^{37}Ar)Ca = 2.79 \times 10^{-4}$ and $(^{40}Ar/^{39}Ar)K = 0.0297$. Mass discrimination was monitored by running calibrated air shots. The mass discrimination during these experiments was 1.3 % per mass unit. While doing

[1]Supplemental Materials. Isotopic data tables and figures and detailed methods. Please visit https://doi.org/10.1130/GES02008.S1 or access the full-text article on www.gsapubs.org to view the Supplemental Material.

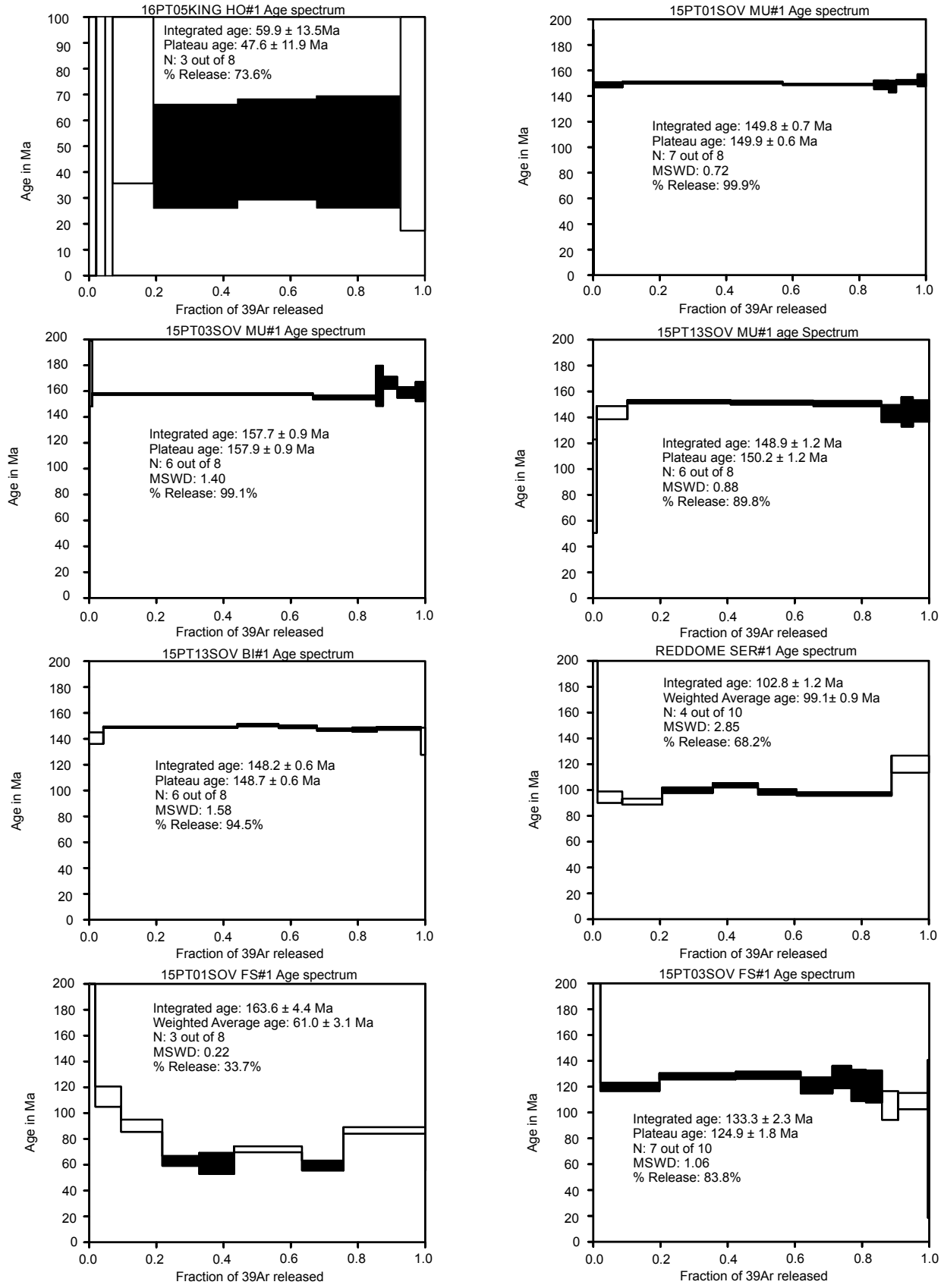

Figure 8. $^{40}Ar/^{39}Ar$ age spectra for all samples analyzed for this study. Abbreviations: BI—biotite; FS—K-feldspar; HO—hornblende; MU—muscovite; SER—sericite; WR—whole rock. (*Continued on following page.*)

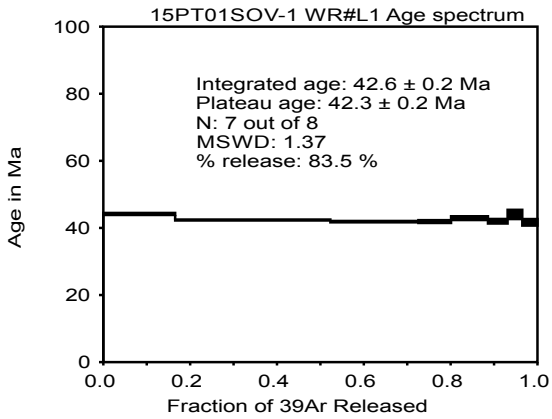

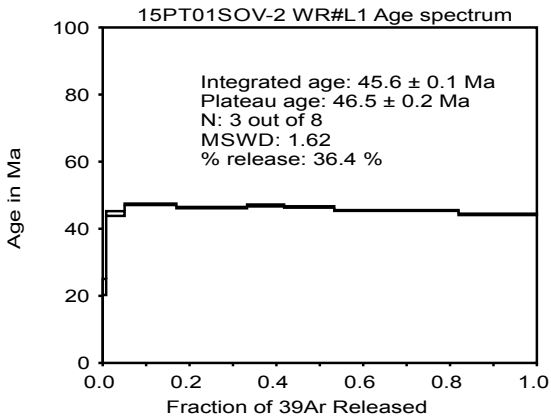

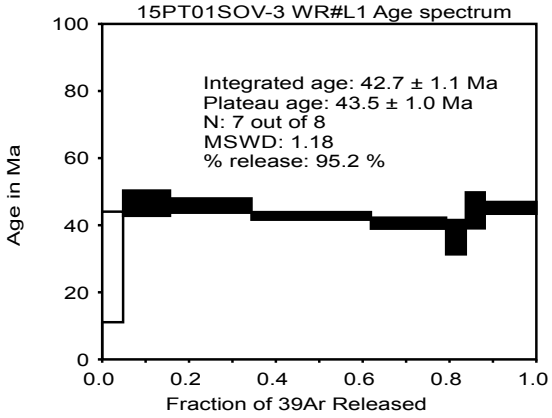

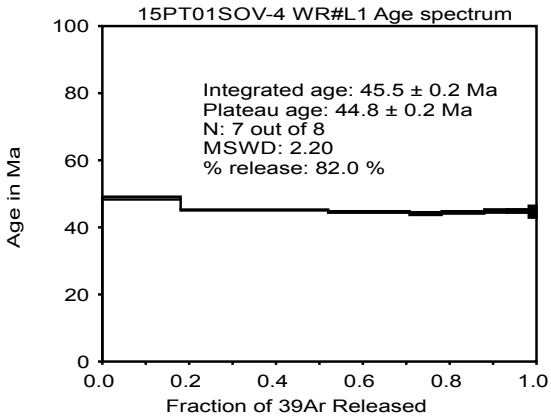

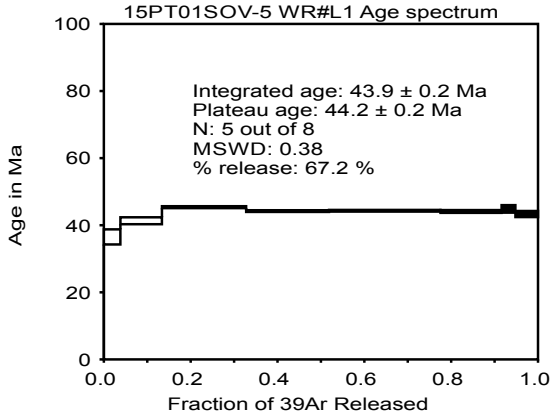

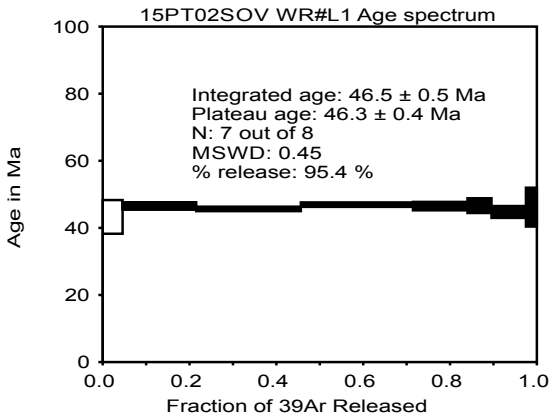

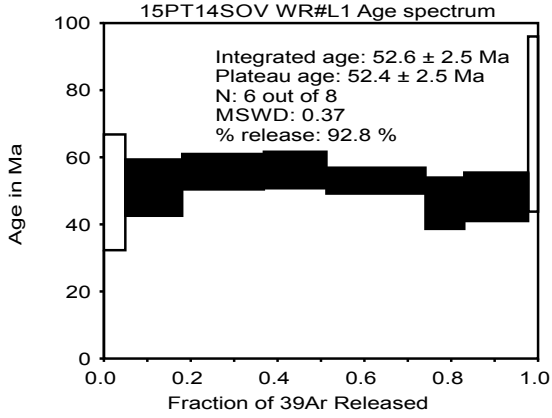

Figure 8 (*continued*).

TABLE 1. SUMMARY OF $^{40}Ar/^{39}Ar$ RESULTS

Sample	Latitude (°N)	Longitude (°W)	Elevation (m)	Mineral	Integrated age (Ma)	Plateau age (Ma)	Plateau information	Isochron age (Ma)	Isochron or other information
05King	61.77	–148.68	635	HO	59.9 ± 13.5	**47.6 ± 11.9**	3 of 8 fractions 73.6% ^{39}Ar release MSWD = 0.00	--	--
01Sov	62.19	–148.45	1333	MU	149.8 ± 0.7	**149.9 ± 0.6**	7 of 8 fractions 99.9% ^{39}Ar release MSWD = 0.72	--	--
03Sov	62.17	–148.51	1572	MU	157.7 ± 0.9	**157.9 ± 0.9**	6 of 8 fractions 99.1% ^{39}Ar release MSWD = 1.40	--	--
13Sov	62.12	–148.63	2463	MU	148.9 ± 1.2	**150.2 ± 1.2**	7 of 8 fractions 89.8% ^{39}Ar release MSWD = 0.88	--	--
13Sov	62.12	–148.63	2463	BI	148.2 ± 0.6	**148.7 ± 0.6**	6 of 8 fractions 94.5% ^{39}Ar release MSWD = 1.58	--	--
01Red	62.03	–148.69	1987	SE	102.8 ± 1.2	**99.1 ± 0.9**	4 of 10 fractions 68.2% ^{39}Ar release MSWD = 2.85	--	--
01Sov	62.19	–148.45	1333	FS	163.6 ± 4.4	**61.0 ± 3.1***	3 of 8 fractions 33.7% ^{39}Ar release MSWD = 0.22	61.1 ± 3.1	3 of 8 fractions $^{40}Ar/^{39}Ar_i$ = 295.7 ± 42.9 MSWD = 0.43
03Sov	62.17	–148.51	1572	FS	133.3 ± 2.3	**124.9 ± 1.8**	7 of 10 fractions 83.8% ^{39}Ar release MSWD = 1.06	129.1 ± 3.2	7 of 10 fractions $^{40}Ar/^{39}Ar_i$ = 269.9 ± 3.2 MSWD = 1.06
01Sov-1	62.19	–148.45	1333	WR	42.6 ± 0.2	**42.3 ± 0.2**	7 of 8 fractions 83.5% ^{39}Ar release MSWD = 1.62	42.2 ± 0.2	7 of 8 fractions $^{40}Ar/^{39}Ar_i$ = 297.7 ± 12.5 MSWD = 1.56
01Sov-2	62.19	–148.45	1333	WR	45.6 ± 0.1	**46.5 ± 0.2**	3 of 8 fractions 36.4% ^{39}Ar release MSWD = 1.62	--	--
01Sov-3	62.19	–148.45	1333	WR	42.7 ± 1.1	**43.5 ± 1.0**	7 of 8 fractions 95.2% ^{39}Ar release MSWD = 1.18	42.7 ± 1.1	7 of 8 fractions $^{40}Ar/^{39}Ar_i$ = 299.1 ± 2.5 MSWD = 1.18
01Sov-4	62.19	–148.45	1333	WR	45.5 ± 0.2	**44.8 ± 0.2**	7 of 8 fractions 82.0% ^{39}Ar release MSWD = 2.20	44.6 ± 0.6	7 of 8 fractions $^{40}Ar/^{39}Ar_i$ = 308.6 ± 25.2 MSWD = 2.34
01Sov-5	62.19	–148.45	1333	WR	43.9 ± 0.2	**44.2 ± 0.2**	5 of 8 fractions 67.2% ^{39}Ar release MSWD = 0.38	44.5 ± 0.5	5 of 8 fractions $^{40}Ar/^{39}Ar_i$ = 288.1 ± 14.0 MSWD = 0.40
02Sov	62.12	–148.49	1447	WR	46.5 ± 0.5	**46.3 ± 0.4**	7 of 8 fractions 95.4% ^{39}Ar release MSWD = 0.45	46.1 ± 0.7	7 of 8 fractions $^{40}Ar/^{39}Ar_i$ = 297.0 ± 5.8 MSWD = 0.52
14Sov	62.12	–148.55	1789	WR	52.6 ± 2.5	**52.4 ± 2.5**	6 of 8 fractions 92.8% ^{39}Ar release MSWD = 0.37	49.6 ± 5.8	6 of 8 fractions $^{40}Ar/^{39}Ar_i$ = 304.0 ± 14.1 MSWD = 0.37

Notes: Samples analyzed with standard MMHB-1 with an age of 523.5 Ma; most robust age in bold. Ages reported at ±1 sigma. Abbreviations: BI—biotite; FS—feldspar; HO—hornblende; MSWD—mean square of weighted deviates; MU—muscovite; SE—sericite; WR—whole rock.

*Does not meet all the criteria of a plateau age; therefore, weighted average age used.

TABLE 2. APATITE FISSION-TRACK AGE SUMMARY

Sample	Rock type	Latitude (°N)	Longitude (°W)	Elevation (m)	Pooled age (Ma)	– Uncertainty (Ma)	+ Uncertainty (Ma)	Mean track length (μm)	± Uncertainty (μm)
01Sov	Trondhjemite	62.19	–148.46	1332	49.82	8.09	9.65	13.74	0.15
02Sov	Trondhjemite	62.19	–148.49	1446	48.31	7.90	9.44	13.70	0.18
03Sov	Trondhjemite	62.18	–148.51	1571	51.20	6.92	7.99	14.36	0.12
06Sov	Trondhjemite	62.15	–148.53	1618	42.63	4.26	4.73	13.81	0.13
08Sov	Trondhjemite	62.12	–148.58	1928	56.73	7.09	6.31	13.83	0.16
10Sov	Trondhjemite	62.12	–148.60	2110	45.08	6.07	7.01	14.67	0.12
11Sov	Trondhjemite	62.12	–148.62	2231	58.34	13.38	17.33	13.62	0.15
12Sov	Trondhjemite	62.12	–148.63	2352	51.96	8.31	9.89	14.41	0.14
13Sov	Trondhjemite	62.12	–148.63	2463	74.23	10.39	12.06	13.80	0.23
05Talk	Trondhjemite	62.03	–148.69	1733	51.21	6.07	6.88	14.02	0.13
07Talk	Trondhjemite	62.04	–148.68	2247	63.62	7.24	8.17	14.14	0.13
13Talk	Trondhjemite	62.02	–148.74	1279	57.80	5.72	6.35	13.31	0.16
14Talk	Granodiorite	62.08	–148.82	777	55.03	7.14	8.20	12.99	0.20
01King	Granite	61.84	–148.64	1006	44.80	5.00	5.60	13.93	0.13
02King	Granite	61.90	–148.65	1046	52.79	3.06	3.25	13.73	0.14
03King	Granite	61.92	–148.70	1086	34.20	5.92	7.15	14.31	0.11
04King	Trondhjemite	61.96	–148.76	1561	44.03	5.53	6.32	13.25	0.25
05King	Tonalite	61.78	–148.68	634	31.23	4.92	5.84	14.10	0.29
01Trop	Granite	61.78	–149.11	1058	58.23	4.22	4.55	12.91	0.14
01Chic	Metabasalt	61.88	–148.43	992	63.00	20.90	31.10	12.35	0.56
01Devil	Granite	62.69	–150.24	255	41.05	12.79	18.55	14.05	0.15

Note: Apatite fission-track age uncertainties are calculated to the ±95% confidence interval. Track-length errors are 1 standard deviation.

TABLE 3. APATITE FISSION-TRACK (AFT) ANALYTICAL RESULTS

Sample	Number of grains	Mean U (ppm)	AFT age and (uncertainty) (Ma)	Mean track length (μm)	Standard deviation (μm)	Mean Dpar (μm)
01Sov	40	5.53	49.82 (–8.09, +9.65)	13.74 ± 0.15 (80)	1.30	1.74
02Sov	40	3.47	48.31 (–7.9, +9.44)	13.7 ± 0.18 (97)	1.77	1.78
03Sov	40	6.22	51.20 (–6.92, +7.99)	14.36 ± 0.12 (105)	1.19	1.73
06Sov	40	14.29	42.63 (–4.26, +4.73)	13.81 ± 0.13 (135)	1.56	1.76
08Sov	40	9.02	56.73 (–7.09, +6.31)	13.83 ± 0.16 (135)	1.86	1.78
10Sov	40	6.77	45.08 (–6.07, +7.01)	14.67 ± 0.12 (108)	1.28	1.68
11Sov	40	3.57	58.34 (–13.38, +17.33)	13.62 ± 0.15 (101)	1.50	1.72
12Sov	40	4.23	51.96 (–8.31, +9.89)	14.41 ± 0.14 (95)	1.33	1.82
13Sov	40	3.73	74.23 (–10.39, +12.06)	13.8 ± 0.23 (65)	1.87	1.78
05Talk	40	9.18	51.21 (–6.07, +6.88)	14.02 ± 0.13 (116)	1.40	1.81
07Talk	40	10.59	63.62 (–7.24, +8.17)	14.14 ± 0.13 (94)	1.21	1.84
13Talk	40	12.91	57.80 (–5.72, +6.35)	13.31 ± 0.16 (104)	1.60	1.80
14Talk	40	7.63	55.03 (–7.14, +8.2)	12.99 ± 0.2 (66)	1.63	1.82
01King	40	14.40	44.80 (–5, +5.6)	13.93 ± 0.13 (85)	1.16	1.73
02King	41	83.45	52.79 (–3.06. +3.25)	13.73 ± 0.14 (125)	1.58	2.60
03King	40	8.39	34.20 (–5.92 +7.15)	14.31 ± 0.11 (151)	1.33	2.68
04King	40	9.59	44.03 (–5.53, +6.32)	13.25 ± 0.25 (47)	1.72	1.82
05King	40	11.47	31.23 (–4.92, +5.84)	14.1 ± 0.29 (27)	1.50	2.29
01Trop	40	41.84	58.23 (–4.22, +4.55)	12.91 ± 0.14 (125)	1.55	2.12
01Chic	38	4.89	63.00 (–20.9, +31.1)	12.35 ± 0.56 (10)	1.68	2.24
01Devil	40	40.14	41.05 (–12.79, +18.55)	14.05 ± 0.15 (10)	1.12	2.09

Note: Numbers in brackets represent the number of tracks counted or measured.

in the crystal lattice and should be reflected in intra-sample and overall grain age dispersion (Reiners and Farley, 2001; Flowers et al., 2009). However, closure temperature in individual apatite grains is often not clearly controlled by these kinetic factors (Fitzgerald et al., 2006).

Twelve AHe ages were determined for this study on four to seven grains for each rock sample by Jim Metcalf at the University of Boulder, Colorado. Corrections based on grain size (F_T) were applied to raw ages to correct for alpha particle ejection effects (Farley, 2002). Single-grain outliers, which were significantly older or younger than the mean age of grains in a sample, were found in three analyses. In general, this was due to low concentrations of uranium or ^{4}He in that particular grain. We excluded these outliers from our sample average age calculations, and it did not affect our results or interpretations. Given the natural dispersion for intra-sample single grains in AHe ages, we calculated the standard deviation for each sample grain set and applied this as the best approximation of the geologic error for the analysis (Spotila and Berger, 2010). Sample AHe average ages, uncertainties, and analytical data are reported in Table 4. For a more detailed description of the AHe methods used and how uncertainties were derived, see the Supplemental Materials (Text S3 [footnote 1]).

HeFTy Thermal Modeling

Inverse thermal models were created for each of our samples using the program HeFTy (Ketcham, 2005). Using an estimate of the present-day surface temperature and higher-temperature (^{40}Ar/^{39}Ar) thermochronology data as constraints, HeFTy models the time and temperature cooling history of a sample. The program evaluates "best-fit" cooling paths and slopes based on input age and AFT track-length constraints. We present Monte Carlo method inverse models showing 50,000 acceptable and good cooling paths constrained in envelopes and weighted-mean T-t paths. Input constraints for the models include ^{40}Ar/^{39}Ar hornblende (~400–600 °C), muscovite (~400–425 °C), biotite (~250–350 °C), and K-feldspar (~180–350 °C) ages, AFT data (~60–120 °C) (single-grain ages, Dpar, track lengths, angle of tracks to the c-axis), and average AHe ages. We use a broad temperature window (~40–80 °C) for sample average AHe ages because intra-sample grain age dispersal and overall grain age dispersal were not correlated with either grain size or effective uranium (Fig. S3 [footnote 1]).

RESULTS AND INTERPRETATIONS

Field Observations

Samples collected for this study outside of the Jurassic trondhjemite pluton (Fig. 3) were spot samples collected via helicopter. Hence, this study does not document any field relationships outside of the trondhjemite pluton and the region immediately surrounding it. Samples collected outside of the trondhjemite pluton were generally granitoids (01King, 02King, 03King, and 05King) but also included a metabasalt collected in the CMF zone (01Chic).

The northeast edge of the Jurassic trondhjemite pluton is characterized by a contact with Paleocene–Eocene volcanic rocks and numerous exhumed lithified volcanic bodies and mafic dikes that intrude into the trondhjemite pluton for ~3 km from the contact (Figs. 3 and 6; P1 and P2). The mafic dikes intrude along exfoliation joints in the trondhjemite pluton and are evidence for some degree of unroofing prior to dike emplacement. Circa 60–50 Ma sedimentary strata locally overlie these Jurassic plutons and volcanic rocks along a prominent nonconformity (Sunderlin et al., 2014; Wilson et al., 2015) requiring significant unroofing prior to emplacement of these Eocene dikes. The concentration of dikes significantly decreases moving southwest from sample 03Sov. There are rare dikes diffusely dispersed across the interior trondhjemite pluton, such as samples 14Sov and 12Talk (Figs. 3 and 7).

We did not observe any faults in the region of our vertical profiles (Fig. 3), although there are mapped structures that appear to partially bound the edges of the trondhjemite pluton (Fig. 3) (Wilson et al., 2015). Between samples 13Talk and 14Talk, there is a distinct ~S-N–striking shear zone consisting of exhumed amphibolite with extensive mineralization and a mapped ~NW-SE–striking fault (Figs. 3 and 7). Throughout the trondhjemite pluton, outcrop faces show evidence for fluid infiltration, hydrothermal alteration, and subsequent mineralization (Fig. 6; P3 and P4). This is most apparent along the Sheep Mountain profile where sample 01Red was collected (Fig. 7). Here a portion of the trondhjemite pluton has been metasomatized to K-feldspar and sericite-rich rocks (Fig. 6; P4). In this area, we observed a staked mining claim that speaks to the extent of alteration.

^{40}Ar/^{39}Ar Geochronology and Thermochronology Results

Fifteen ^{40}Ar/^{39}Ar ages were produced for this study and are presented below organized by mineral type. Ages are reported at ±1σ uncertainty (Table 1). Age spectra are shown for each sample in Figures 8 and 9 (also see Fig. S1 [footnote 1]) and in general are flat, suggesting minimal argon loss. Isochron ages were calculated when possible and are shown in Figure S1 (footnote 1), and isotopic analytical data are reported in Table S1 (footnote 1).

Hornblende Age

A homogeneous hornblende separate from sample 05King, a tonalite collected from hypabyssal intrusions south of the CMF (unit Jktm on Fig. 3), was analyzed (Figs. 8 and S1 [footnote 1]; Table 1). The integrated age (59.9 ± 13.5 Ma) and the plateau age (47.6 ± 11.9 Ma) are within uncertainty. We prefer the plateau age of 47.6 ± 11.9 Ma for sample 05King because of the higher atmospheric content of the lower-temperature step-heat release. The large uncertainty is likely due to the low-K concentration of the hornblende separate.

TABLE 4. APATITE (U-Th)/He DATA AND AGE SUMMARY

Sample	Elevation (m)	Latitude (°N)	Longitude (°W)	Mass (mg)	^{4}He (nmol/g)	U (ppm)	Th (ppm)	F_T	Corrected age (Ma)	Average age (Ma)	Standard deviation (Ma)
01Sov	1332	62.19	–148.45	2.75	0.63	2.47	2.04	0.73	48.82	45.31	5.34
				1.45	0.71	3.27	1.02	0.66	48.62		(11.78%)
				1.43	0.75	4.32	1.91	0.69	37.48		
				1.30	1.77	9.75	1.24	0.66	46.31		
06Sov	1618	62.15	–148.53	3.86	2.89	19.14	1.61	0.80	32.57	37.52	4.20
				9.33	2.39	14.24	0.44	0.78	38.29		(11.18%)
				3.25	3.74	24.10	1.66	0.75	36.54		
				1.66	1.17	6.59	0.69	0.69	42.70		
13Sov	2463	62.12	–148.63	2.88	1.53	7.79	4.36	0.75	40.40	44.10	3.33
				3.08	1.01	4.52	2.26	0.75	45.07		(7.54%)
				2.49	0.99	3.90	3.22	0.73	46.83		
05Talk	1733	62.03	–148.69	4.46	2.868	16.33	0.69	0.75	40.11	Does not meet parameters for age determination	
				1.41	0.681	0.79	0.95	0.67	164.12		
				1.19	3.994	17.55	1.64	0.66	60.09		
				1.03	2.750	12.49	2.71	0.6247	59.71		
				1.32	20.825	26.43	2.93	0.64	213.55		
13Talk	1279	62.02	–148.74	0.65	2.36	20.22	0.00	0.57	36.44	32.33	3.81
				0.90	4.05	32.09	8.81	0.64	33.46		(11.78%)
				15.95	3.29	21.71	0.77	0.86	32.11		
				3.19	1.66	14.17	0.71	0.76	27.30		
14Talk	777	62.08	–148.82	1.70	3.14	14.66	0.13	0.69	56.34	43.61	11.03
				1.16	2.02	15.03	0.00	0.66	37.37		(25.29%)
				1.24	1.25	9.03	1.17	0.66	37.12		
01King	1006	61.84	–148.64	1.15	2.99	17.10	0.77	0.65	47.48	42.38	6.86
				0.49	4.98	33.31	2.09	0.57	46.48		(16.19%)
				0.50	1.84	16.26	3.10	0.55	35.15		
				0.65	4.44	27.60	3.36	0.58	48.14		
				0.48	1.87	17.62	1.42	0.54	34.63		
02King	1046	61.90	–148.65	1.29	6.26	109.13	174.32	0.63	12.31	12.13	0.76
				0.76	5.02	91.02	160.77	0.57	12.59		(6.29%)
				0.76	3.12	63.03	112.81	0.59	10.87		
				0.76	6.62	112.89	204.88	0.59	12.84		
				1.02	5.20	90.71	163.37	0.62	12.06		
03King	1086	61.92	–148.70	1.11	0.38	5.64	0.54	0.65	18.04	20.85	3.01
				0.76	9.06	90.18	141.7	0.57	23.48		(14.43%)
				0.71	3.55	42.67	8.63	0.62	23.42		

Sample	Elevation (m)	Latitude (°N)	Longitude (°W)	Mass (mg)	4He (nmol/g)	U (ppm)	Th (ppm)	F_T	Corrected age (Ma)	Pooled age (Ma)	Standard deviation (Ma)
04King	1561	61.96	–148.76	7.33	1.69	9.68	2.59	0.81	36.85	33.37	3.13
				2.69	1.57	11.02	3.44	0.74	32.62		(9.39%)
				1.33	1.30	10.99	4.05	0.66	30.01		
				1.20	0.36	3.16	0.81	0.63	30.93		
				0.67	1.74	14.23	3.32	0.58	36.44		
01Trop	1058	61.78	–149.11	1.41	1.71	33.56	47.04	0.63	11.18	10.54	0.41
				0.86	2.89	64.16	92.40	0.61	10.10		(3.90%)
				3.09	3.11	55.88	77.20	0.74	10.50		
				1.30	3.54	70.41	94.54	0.66	10.63		
				1.92	2.66	50.59	80.35	0.69	10.27		
01Chic	992	61.88	–148.43	1.39	0.99	4.94	10.73	0.66	35.80	44.62	11.18
				0.91	1.87	7.24	12.26	0.61	54.50		(25.05%)
				1.41	1.36	5.51	5.14	0.67	54.06		
				0.69	0.95	5.63	13.36	0.57	34.12		
				0.49	0.47	8.80	0.20	0.52	18.47		

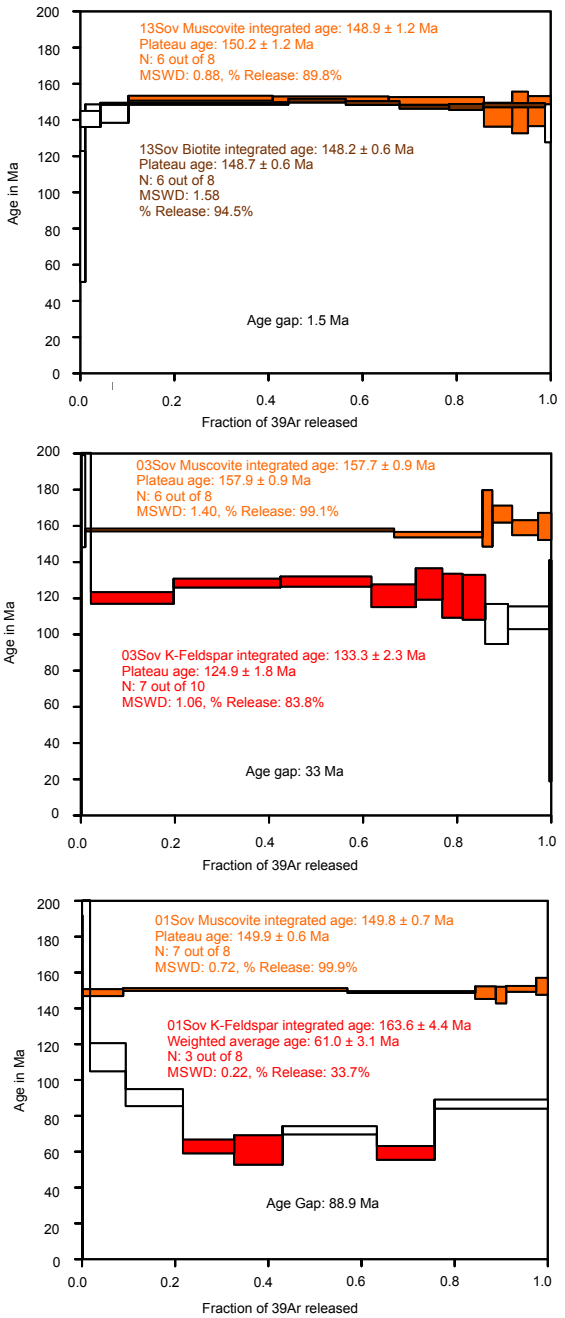

Figure 9. Muscovite/biotite and muscovite/K-feldspar $^{40}Ar/^{39}Ar$ age spectra pairs for samples 01Sov, 03Sov, and 13Sov. The "age gap" represents the closure between the two mineral phases. Filled red, brown, and orange bars represent the steps used for the muscovite, biotite, and K-feldspar steps, respectively. MSWD—mean square of weighted deviates.

Mica Ages

Homogeneous muscovite separates from samples 01Sov, 03Sov, and 13Sov, and trondhjemite samples from unit Jtr (Fig. 3) were analyzed (Figs. 8, 9, and S1 [footnote 1]; Table 1). For sample 01Sov, the integrated age (149.8 ± 0.7 Ma) and the plateau age (149.9 ± 0.6 Ma) are within uncertainty. Sample 03Sov produced both an integrated age (157.7 ± 0.9 Ma) and a plateau age (157.9 ± 0.9 Ma) within uncertainty. For sample 13Sov, the integrated age (148.9 ± 1.2 Ma) and the plateau age (150.2 ± 1.2 Ma) are within uncertainty. We prefer the plateau ages of 149.9 ± 0.6 Ma (01Sov), 157.9 ± 0.9 Ma (03Sov), and 150.2 ± 1.2 Ma (13Sov) because of the high atmospheric content of the low-temperature step heats.

A homogeneous biotite separate from sample 13Sov was analyzed (Figs. 8, 9, and Table 1). The integrated age (148.2 ± 0.6 Ma) and the plateau age (148.7 ± 0.6 Ma) are within uncertainty. We prefer the plateau age of 148.7 ± 0.6 Ma because of the high atmospheric ^{40}Ar content of the low-temperature step heat. The time between closure of the muscovite and biotite mineral systems in sample 13Sov is ca. 1.5 Ma (Fig. 9).

These overall mica ages are similar to the U-Pb zircon crystallization age of the trondhjemite pluton (Fig. 7) (157 Ma to ca. 159 Ma; Rioux et al., 2007). The duration of time between closure of the muscovite and biotite mineral phases (~100 °C) is geologically instantaneous (~1.5 m.y.) (Fig. 9). This suggests rapid rock cooling (~67 °C/m.y.) following the Late Jurassic emplacement of the trondhjemite pluton, which may have been protracted (Hacker et al., 2011).

A homogeneous sericite separate from sample 01Red, collected in unit Jtr (Fig. 3), was analyzed (Figs. 8 and S1 [footnote 1]; Table 1). The integrated age (102.8 ± 1.2 Ma) and the plateau age (99.1 ± 0.9 Ma) are not within uncertainty. We prefer the plateau age of 99.1 ± 0.9 Ma because of the anomalously older age for the lowest temperature step heat.

K-Feldspar Ages

Homogenous K-feldspar separates from samples 01Sov and 03Sov were analyzed (Figs. 8, 9, and S1 [footnote 1]; Table 1). For sample 01Sov, the age spectrum is bimodal, suggesting a more complex thermal history. The age spectrum did not meet the criteria for a plateau age (three consecutive steps); therefore, weighted average ages are reported. The integrated age (163.6 ± 4.4 Ma), maximum weighted average age (86.5 ± 2.5 Ma), and minimum weighted average age (61.0 ± 3.1 Ma) are not within uncertainty. We prefer a maximum weighted average age ($KFAT_{max}$) of 86.5 ± 2.5 Ma and a minimum weighted average age ($KFAT_{min}$) of 61.0 ± 3.1 Ma for sample 01Sov. The duration

of time between closure of the ~350 °C and ~150 °C nominal temperature domains for K-feldspar is ~26.5 m.y. The duration between closure of the muscovite and the high-temperature K-feldspar mineral phases in sample 01Sov is ~63.4 m.y. The age spectrum for sample 03Sov is flatter and suggests a less complex thermal history (Fig. 8). The integrated age (133.3 ± 2.3 Ma) and the plateau age (124.9 ± 1.8 Ma) are not within uncertainty. We prefer the plateau age of 124.9 ± 1.8 Ma for sample 03Sov because of the anomalously older age for the lowest temperature step heat. An isochron age of 129.1 ± 3.2 Ma was determined for the K-feldspar separate from sample 03SOV and is within uncertainty of the plateau age. The duration between closure of the muscovite and K-feldspar mineral phases in sample 03Sov is ~33 m.y. (Figs. 8 and 9).

Sample 03Sov records relatively slow Cretaceous rock cooling between the closure of muscovite and rapid closure K-feldspar temperature domains (~5 °C/m.y.) (Fig. 9). Sample 01Sov records relatively slow Cretaceous rock cooling between the closure of muscovite and high-temperature K-feldspar domains (~2 °C/m.y.). $^{40}Ar/^{39}Ar$ K-feldspar thermochronology on sample 01Sov, located ~200 m below sample 03Sov (Fig. 7), has a bimodal age spectrum that we infer demonstrates thermal resetting at ca. 61 Ma and subsequent rock cooling (Figs. 8 and 9; Table 1), indicating a more complex cooling history. The partial thermal resetting of K-feldspar in sample 01Sov (ca. 61 Ma) happened prior to the main episode of regional dike emplacement at ca. 50–40 Ma (Fig. 7).

We attribute the thermal resetting of K-feldspar in sample 01Sov to an elevated Paleocene geothermal gradient induced by high heat flow through a slab window beneath the Talkeetna Mountains, as proposed by Cole et al. (2006), followed by subsequent rock cooling related to exhumation. This time period (ca. 61 Ma) also overlaps with a period of thermal resetting constrained by detrital-zircon fission-track analyses on Cook Inlet (Fig. 2) Cretaceous strata (Finzel et al., 2016), and this inference is consistent with regional evidence for an elevated geothermal gradient (Benowitz et al., 2012a).

Whole-Rock Ages

Homogenous, phenocryst-free whole-rock separates from samples 01Sov-1, 01Sov-2, 01Sov-3, 01-Sov-4, and 01-Sov-5 (five different phases of magmatism sampled meters from each other), 02Sov, and 14Sov, which are mafic dikes intruding the trondhjemite pluton (unit Jtr in Fig. 3), were analyzed (Figs. 8 and S1 [footnote 1]; Table 1). The sites for the 01Sov sample series and 02Sov are located at the northeast edge of the trondhjemite pluton, and sample 14Sov is located toward its interior (Figs. 3 and 7). The five different magmatic phases of sample 01Sov (located at the contact of units Tepv and Jtr in Fig. 3) have plateau ages from ca. 46.5 Ma to ca. 42.3 Ma (Fig. 8). Four of the five different magmatic phases provided isochron ages of 42.2 ± 0.2 Ma, 42.7 ± 1.0 Ma, 44.6 ± 0.6 Ma, and 44.5 ± 0.5 Ma (see Fig. S1 [footnote 1]). We prefer plateau ages for these samples because of the higher atmospheric content of the lower-temperature step-heat releases. For sample 02Sov, the integrated age (46.5 ± 0.5 Ma), plateau age (46.3 ± 0.4 Ma), and isochron age (46.3 ± 0.4 Ma) are all within uncertainties. We prefer the plateau age of 46.3 ± 0.4 Ma because of its higher precision. For sample 14Sov, the integrated age (52.6 ± 2.5 Ma), plateau age (52.4 ± 2.5 Ma), and isochron age (49.6 ± 5.8 Ma) are all within uncertainties. We prefer the plateau age of 52.4 ± 2.5 Ma because of the anomalously high age of the highest temperature step heat.

When our new whole-rock ages are integrated with 19 previously published whole-rock $^{40}Ar/^{39}Ar$ ages in the Talkeetna Mountains (north of the CMF and south of the Talkeetna fault), ages range from ca. 61 to ca. 30 Ma (Fig. 7) (Silberman and Grantz, 1984; Cole et al., 2006; Oswald, 2006; Cole et al., 2007). Our ages support the interpretation by Cole et al. (2006) of a period of high-flux Talkeetna Mountains regional volcanism that persisted for millions of years during the Paleocene–Eocene and sparse magmatism that continued during the Oligocene.

Apatite Fission-Track Thermochronology Results

Twenty-one AFT cooling ages were produced for this study on intrusive rocks (Fig. 7 and Table 2) and are compiled with previously existing AFT cooling ages in the region (Little and Naeser, 1989; Parry et al., 2001; Bleick et al., 2012). We report pooled ages with calculated uncertainties representing the ±95% confidence interval (2σ) (ranging from ±ca. 3 Ma to ca. 31 Ma; Table 2). Dpar was measured in most dated grains, and average sample Dpar values range from ~1.7–2.7 μm (Table 3). There is no correlation between Dpar values and age (Fig. S4A [footnote 1]) or track lengths (Fig. S4B [footnote 1]), suggesting similar annealing kinetics for all samples. Confined track-length distributions are reported in Figure S2 (footnote 1).

AFT North of the CMF

Eighteen samples north of the CMF (Fig. 7) have Paleocene–Eocene cooling ages ranging from ca. 63.0 Ma to ca. 41.1 Ma (Fig. 10A). The highest elevation sample (13Sov) has a Cretaceous cooling age of ca. 74.2 Ma (Fig. 10A). Sample 03King was collected within ~5 m of the granite/metamorphic rock contact between units Jgr and PSm (Fig. 3) and has an Oligocene cooling age of ca. 34.2 Ma. These results agree with other AFT cooling ages (north of the CMF from Bleick et al., 2012), which are predominantly Paleocene–Eocene. Mean track lengths from our sample set range from 12.9 μm to 14.4 μm (Table 2).

AFT cooling ages in the southern Talkeetna Mountains have two separate cooling domains divided by elevation. Samples located outside of the trondhjemite pluton at lower elevations (less than ~1500 m) and near the CMF do not have an age-elevation relationship (Fig. 10A). AFT cooling ages from samples collected along vertical profiles of Mount Sovereign and Sheep Mountain have an age-elevation relationship with an inflection point at ca. 59 Ma that suggests more rapid rock cooling and inferred exhumation after that time at a maximum rate of ~188 m/m.y. (Fig. 10B). Samples 06Sov, 10Sov, and 12Sov

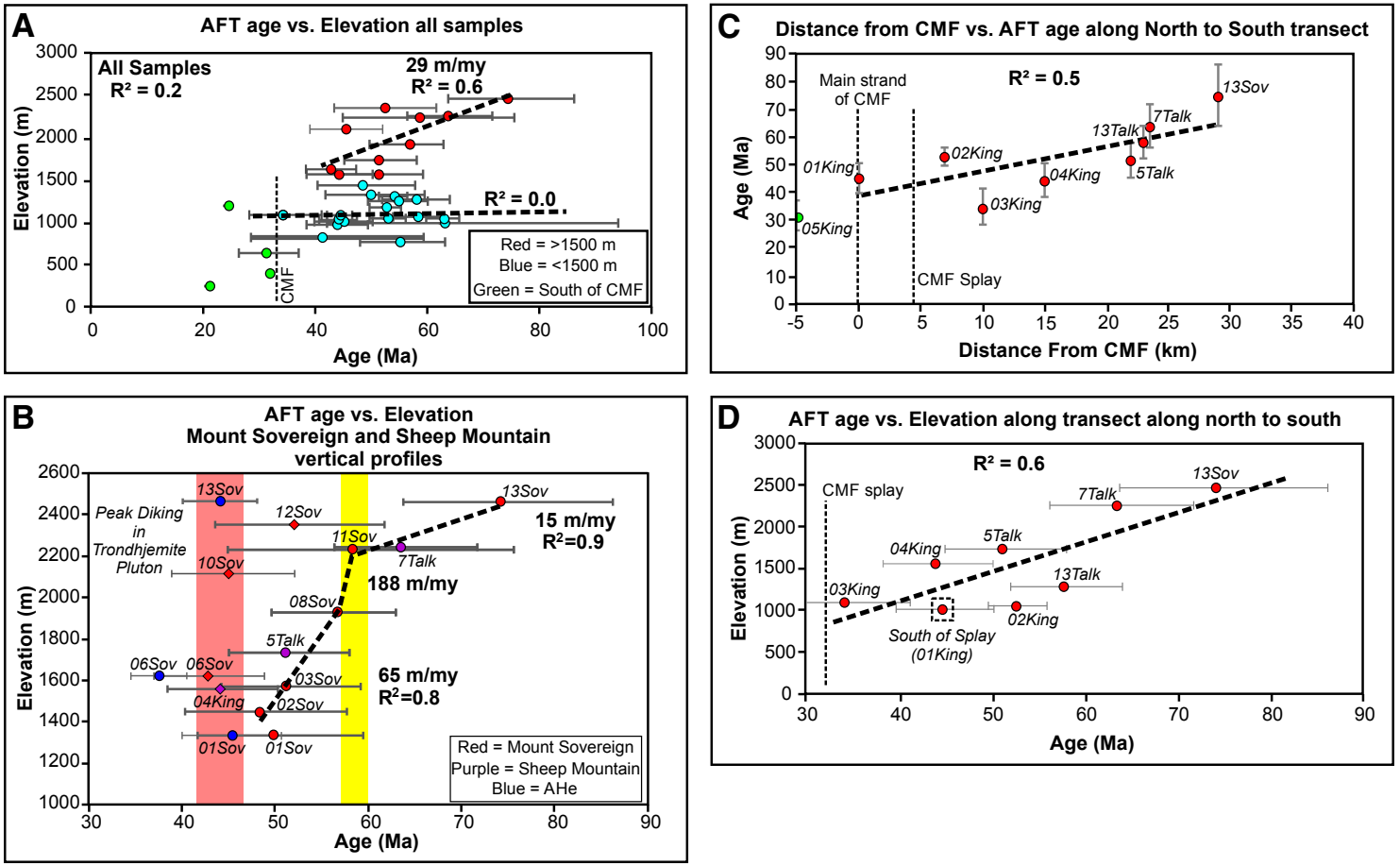

Figure 10. (A) Apatite fission-track (AFT) age versus elevation plot including all cooling ages from this study and other published sources. (B) AFT age versus elevation plot for samples (this study) from Mount Sovereign and Sheep Mountain vertical profile. Yellow bar is inflection point that we interpret reflects a change to more rapid rock cooling and inferred exhumation, and width of bar is qualitative uncertainty. Exhumation rates estimated from lines qualitatively fit through sample ages are shown in bold font. Blue circles are apatite (U-Th)/He (AHe) cooling ages that may have been thermally reset during peak regional volcanism (red bar). (C) AFT age versus distance from Castle Mountain fault (CMF) along S-N transect approaching CMF. (D) AFT age versus elevation along the same S-N transect approaching the CMF. There is an apparent relationship of AFT ages getting younger approaching the CMF in Figure 10C. However, all AFT ages in the southern Talkeetna Mountains do not show a trend of getting younger toward the CMF, and the R^2 relationship in Figure 10D is slightly stronger, suggesting these age patterns are controlled by elevation, rather than distance from CMF.

have AFT ages of ca. 42.6 Ma, ca. 45.0, and ca. 51.9 Ma, respectively, and are distinct outliers from the general age-elevation relationship (Fig. 10B). This is likely due to thermal resetting from the injection of hydrothermal fluids during middle Eocene magmatism based on field observations of hydrothermal alteration (Fig. 6; P3), new whole-rock $^{40}Ar/^{39}Ar$ constraints on Mount Sovereign Eocene magmatism (Fig. 7), and the apparent elevation-invariant AHe cooling ages along the same vertical profile (Fig. 10B).

Sample 04King has an AFT age of ca. 44.0 Ma and is another outlier to the age-elevation trend. This sample is located away from the main vertical profile sample cluster (Fig. 7) and across a mapped fault that may be affecting its age (Fig. 3). Sample 03King, the closest sample to 04King, also has a regionally young AFT age of ca. 34.2 Ma, adding credence to the possibility of an unmapped structure in the region. Alternatively, the young AFT age of sample 03King may be due to fluid flow along the unit contact with the metamorphic rocks (Fig. 3).

To test if proximity to and differential unroofing along the CMF might be controlling these AFT age-elevation patterns, we collected eight samples along a S-N transect approaching the CMF. The AFT cooling ages (Figs. 7 and 10C) have an apparent pattern of younging toward the fault. However, these samples also decrease in elevation moving toward the CMF, and the correlation between age and elevation along the same transect is slightly stronger (Fig. 10D), making it more likely that block exhumation along a vertical trajectory (reflected in age-elevation relationships) is the primary control on these cooling-age patterns rather than the proximity to the CMF.

Sample 01Devil produced an AFT age of ca. 40.1 Ma, which is relatively young compared to the full Talkeetna Mountains AFT data set. This sample is the most west and north sample in our Talkeetna Mountains AFT data set. Because sample 01Devil is a single cooling age, it is difficult to weigh its significance, but we report it for completeness.

AFT South of the CMF

Sample 05King has an AFT cooling age of ca. 31.2 Ma (Figs. 7 and 10A). This result is consistent with regional AFT cooling ages from Little and Naeser (1989) and Parry et al. (2001), who document distinctly younger cooling ages (ca. 21–32 Ma) south of the CMF. From this AFT cooling age pattern, we infer that the north side of the CMF did not have a significant vertical component during the Eocene–early Oligocene. This is consistent with mapping studies that infer chiefly Neogene vertical displacement across the fault (Grantz, 1966; Fuchs, 1980; Trop et al., 2003).

Possible Thermal Resetting of AFT Cooling Ages

To test for thermal resetting due to diking, AFT analyses were performed on samples 01Sov and 02Sov (Fig. 7 and Table 2), which are trondhjemite rocks collected at a minimum distance of ~5 m and a maximum of ~50 m from Eocene volcanic intrusions at the northeastern edge of the pluton (Fig. 6; P5 and P6). The AFT cooling ages of samples 01Sov and 02Sov (ca. 49 Ma and ca. 48 Ma, respectively) are older than the volcanic ages of the proximal dikes (ca. 46 Ma to ca. 42 Ma) (Fig. 7 and Table 1), providing evidence that the rocks of the trondhjemite pluton were not thermally reset during dike emplacement. The customary large uncertainty on the AFT ages of samples 01SOV and 02SOV (±ca. 9 Ma; Table 3) does overlap with the $^{40}Ar/^{39}Ar$ dike ages (uncertainties <±ca. 1 Ma); hence, additional approaches (HeFTy kinetic modeling and age-elevation patterns) are required to further support an interpretation of no thermal resetting as discussed below.

Throughout the trondhjemite pluton, outcrops show variable evidence for alteration from hydrothermal fluids (Fig. 6; P3) that were likely injected during the period of peak Eocene magmatism (Cole et al., 2006). Previous studies have demonstrated that the heat effects from hydrothermal fluids can result in the thermal resetting of the AFT system (Roden and Miller, 1989). Samples 06Sov, 10Sov, and 12Sov have AFT cooling ages of ca. 42 Ma, ca. 45 Ma, and ca. 51 Ma, respectively, and are distinct outliers from the Mount Sovereign to Sheep Mountain AFT age-elevation relationship (Fig. 10B), suggesting they have been thermally reset. HeFTy thermal models of these three outlier samples show more rapid Paleocene–Eocene rock-cooling rates (up to ~30 °C/m.y.) compared to the other samples in the AFT age-elevation profile (~16 °C/m.y.) (see Fig. S2 [footnote 1]), indicating the two sample sets have experienced different thermal histories. AHe cooling ages are invariant with elevation along the Mount Sovereign to Sheep Mountain vertical profile with ages generally ca. 45 Ma, adding support to this being a period of peak hydrothermal fluid injection and thermal resetting. We test this inference with HeFTy kinetic modeling and find that the thermal models provide better fits, if reheating is allowed (Fig. S2).

Apatite (U-Th)/He Thermochronology Results

Twelve AHe sample cooling ages were produced for this study on intrusive rock samples collected north of the CMF. Sample average ages and 1σ uncertainties are reported (uncertainties range from ±ca. 1 Ma to ca. 11 Ma; Table 4) and were calculated following the techniques outlined in the Methods section. Sample 05Talk yielded a large spread of individual apatite grain cooling ages (Table 4) that did not meet the parameters to calculate an average age, and it is therefore excluded from our interpretations. AHe sample cooling ages range from ca. 45.3 Ma to ca. 10.5 Ma. These new AHe results were compiled with published ages from Hoffman and Armstrong (2006) and Hacker et al. (2011) and, combined, show a distinct pattern of younging ages approaching the CMF (Fig. 11A). Sample 01King, located directly north of the continuous strand of the CMF is ca. 42.4 Ma (Fig. 7 and 11C). Sample 02King located north of a splay off of the CMF is ca. 12.1 Ma. There is no relationship between AHe cooling age and elevation (Fig. 11B). Eight samples along a S-N transect approaching the CMF show a distinct pattern of younging toward

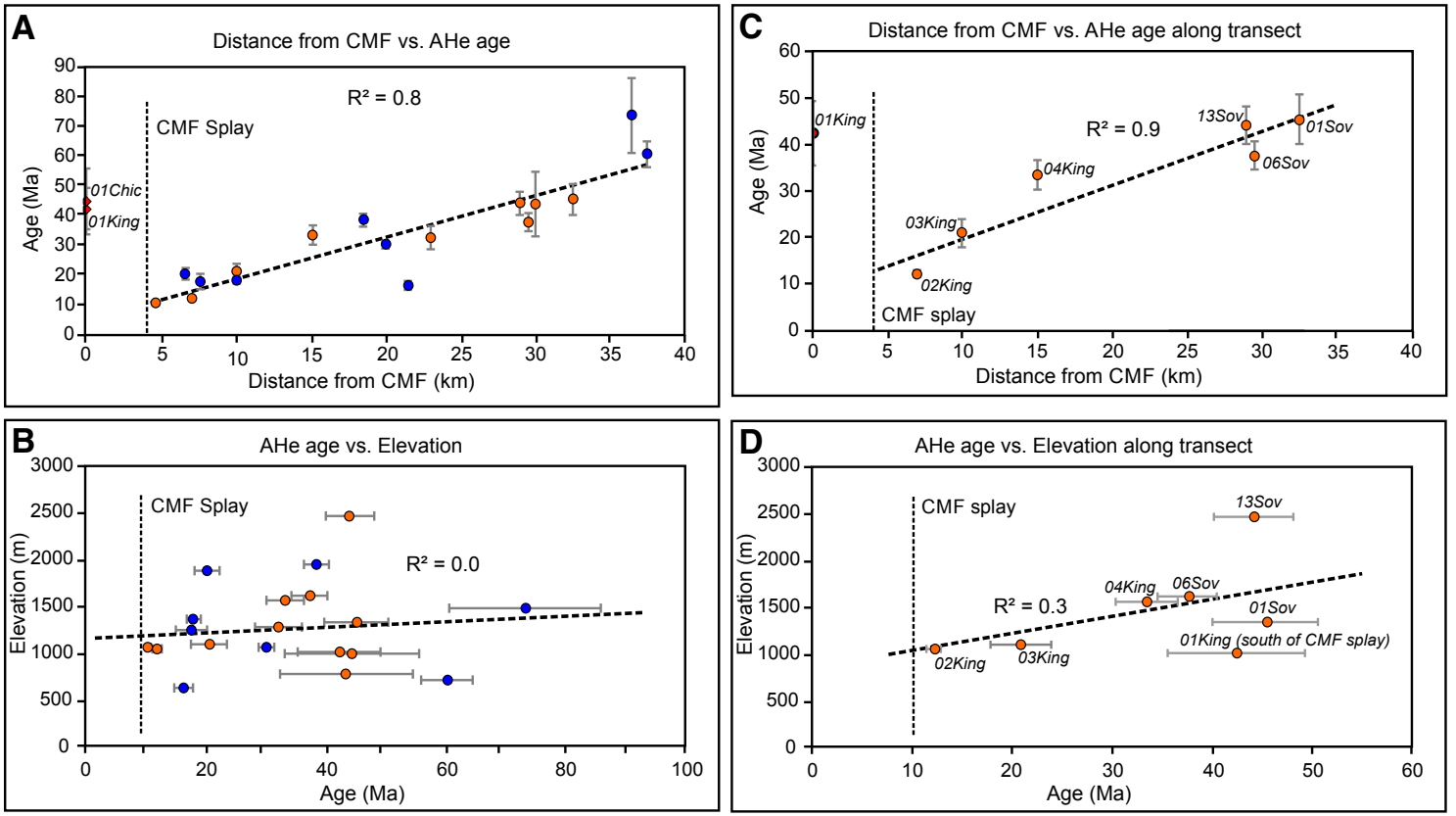

Figure 11. (A) All apatite (U-Th)/He (AHe) cooling ages existing in our study area versus distance from Castle Mountain fault (CMF). Orange circles are ages analyzed for this study, and blue dots are previously published ages (Hoffman and Armstrong, 2006; Hacker et al., 2011). Sample 01King, a distinct outlier from the data set, is north of the continuous strand of the CMF but south of the northernmost strand of the CMF, suggesting that the northernmost strand is the active strand of the CMF. (B) There is no relationship between AHe age and elevation. (C) AHe age versus distance from CMF along S-N transect approaching CMF shows a pattern of ages getting younger approaching the northernmost (and inferred active) strand of the CMF. (D) AHE age versus elevation along the same transect shows no relationship.

the fault (Fig. 11C); young cooling ages near the CMF suggest there has been exhumation along this structure since at least the Miocene. There is a weak relationship between age and elevation along the same transect (Fig. 11D), adding support to the notion that vertical displacement along the CMF is controlling AHe cooling-age patterns.

The AHe age from sample 01King located directly north of the continuous strand of the CMF is 42.4 ± 6.9 Ma (Fig. 7). The AHe age from sample 02King located north of the northern splay of the fault is 12.1 ± 0.8 Ma. This recognizably younger age is evidence that the northern splay has been the active strand of the CMF since at least the Miocene.

The compilation of AHe cooling ages (Fig. 12) indicates parts of the southern Talkeetna Mountains cooled below the ~80 °C isotherm during the Eocene. Samples 01Sov, 06Sov, and 13Sov have AHe cooling ages that may reflect thermal resetting from hydrothermal fluids during Eocene magmatism (Fig. 10B) based on their invariance with elevation-age relationship and regional evidence of hydrothermal fluid injection at the time. Overall, the AHe data support a southern Talkeetna Mountains rock-cooling event during the Oligocene–Miocene. Support for this interpretation includes deposition of Miocene fluvial strata in the footwall of the CMF in the southern Talkeetna Mountains (Bristol et al., 2017). This is consistent with our interpretation that exhumation was driven by north-side-up vertical displacement along the CMF.

In the context of regional basin analysis and the magmatic record, a compilation of the geochronology and thermochronology data from the southern Talkeetna Mountains supports Paleocene–Eocene and Oligocene–Miocene exhumation events with evidence of spatially limited thermal resetting related to hydrothermal fluid injection. The occurrence of spatially variable resetting should be taken into account by future thermochronology studies in this region (detrital studies in particular) because of the difficulty in distinguishing monotonic cooling ages from thermally reset ages without field evidence of outcrop alteration from hydrothermal fluids, age-elevation relationships, and structural control.

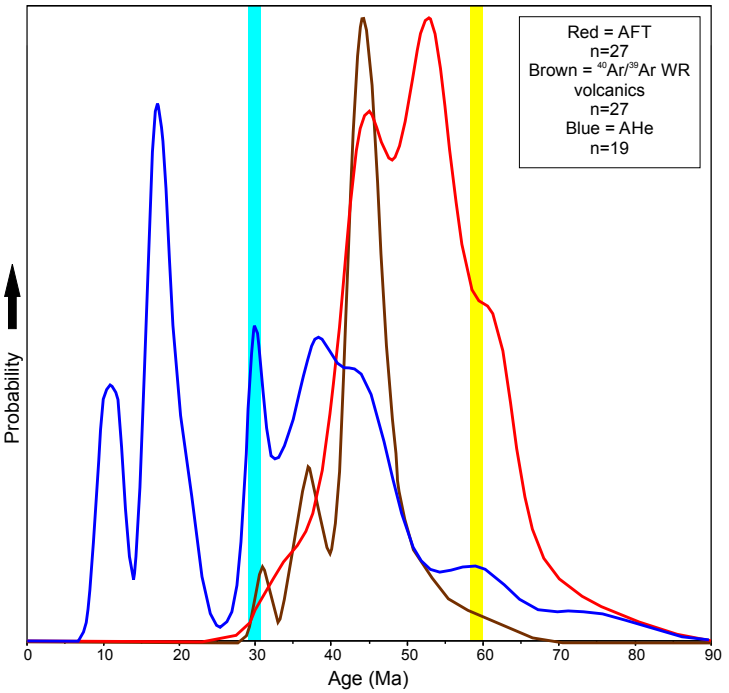

Figure 12. Normalized probability density function of all published whole-rock (WR) $^{40}Ar/^{39}Ar$, apatite fission-track (AFT), and apatite (U-Th)/He (AHe) cooling ages for samples located north of the Castle Mountain fault (CMF) and south of the Talkeetna fault (Fig. 6). Yellow bar to the right represents the inflection point from our AFT age-elevation profile (Fig. 10B). Light-blue bar to the left represents the approximate timing of initiation of Yakutat microplate flat-slab subduction.

Cooling and Magmatic Patterns in Time and Space

Previously published and our new whole-rock $^{40}Ar/^{39}Ar$, non-reset AFT, and AHe cooling ages confined to north of the CMF and south of the Talkeetna fault are compiled into a normalized probability density plot (Fig. 12) (Silberman and Grantz, 1984; Parry et al., 2001; Cole et al., 2006; Hoffman and Armstrong, 2006; Oswald, 2006; Hacker et al., 2011; Bleick et al., 2012; Arkle et al., 2013). AFT cooling ages that we interpret to be thermally reset or reflecting displacement along unmapped structures (06Sov, 10Sov, 12Sov, and 03King) are excluded. The whole-rock volcanic peak is younger than the AFT peak, suggesting that AFT cooling ages represent exhumation and not thermal resetting. Our interpretation that AFT cooling ages are exhumation-related is consistent with field observations and geochronology constraints (from the Matanuska Valley region) that document rapid accumulation of a >2-km-thick succession of ca. 60–56 Ma fluvial strata unconformably upon ca. 70 Ma and older granitoid plutons (Figs. 3 and S9 [footnote 1]) (Arkose Ridge Formation, Kortyna et al., 2013; Sunderlin et al., 2014; Trop et al., 2015).

When plotted versus latitude and longitude, whole-rock $^{40}Ar/^{39}Ar$ data in the southern Talkeetna Mountains show no S-N or W-E age progressions (Figs. 13A and 13B). When plotted versus latitude and longitude, AFT cooling ages in the southern Talkeetna Mountains show no S-N or W-E age progressions (Fig. 13A and 13B). There is also no clear evidence of regional resetting of AFT or AHe cooling age due to Eocene volcanism (Figs. 12 and 13). Similarly, region-wide, Paleocene–Eocene exhumation-related cooling ages and volcanic ages across southern Alaska have no apparent S-N or W-E age progressions: from southwest Alaska (O'Sullivan et al., 2010), the Revelation Mountains region (Reed and Lanphere, 1972), the Tordrillo Mountains (Haeussler et al., 2008; Benowitz et al., 2012a), the Kichatna Mountains (Ward et al., 2012), the Kenai Mountains (Valentino et al., 2016), the Foraker Glacier region (Reed and Lanphere, 1972; Cole and Layer, 2002), the Susitna Basin (Stanley et al., 2014), the Cantwell

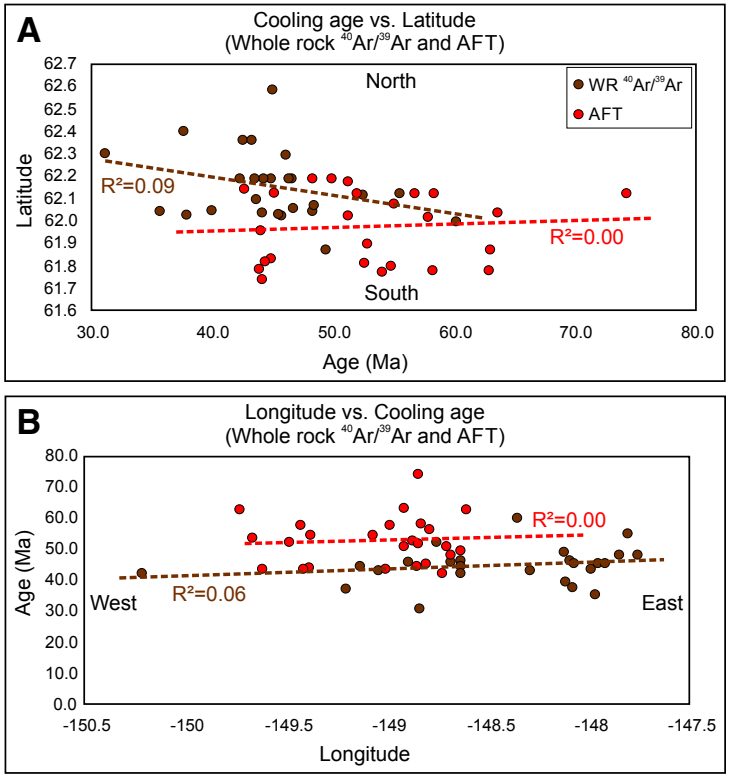

Figure 13. Spatial volcanic and cooling age patterns for all whole-rock $^{40}Ar/^{39}Ar$ (brown circles) and apatite fission-track (AFT) (red circles) cooling ages in the Talkeetna Mountains north of the Castle Mountain fault (CMF) and south of the Talkeetna fault. (A) Whole-rock $^{40}Ar/^{39}Ar$ and AFT age versus latitude. R^2 relationships show no S-N cooling-age progressions. (B) Longitude versus whole-rock $^{40}Ar/^{39}Ar$ and AFT age. R^2 relationships show no W-E cooling-age progressions.

volcanics (Cole et al., 1999), the Jack River volcanics (Cole et al., 2007), the Talkeetna Mountains (Silberman and Grantz., 1984; Parry et al., 2001; Cole et al., 2006; Hoffman and Armstrong, 2006; Oswald, 2006; Cole et al., 2007; Bleick et al., 2012; Hacker et al., 2011), the St. Elias Mountains (Enkelmann et al., 2017), and three sites in the Yukon-Tanana Terrane (Tempelman-Kluit and Wanless, 1975; Dusel-Bacon and Murphy, 2001; Enkelmann et al., 2017) (Fig. 14).

HeFTy Thermal Models

To construct a detailed thermal history of the region, inverse thermal models were produced for all our samples using all available U-Pb zircon, $^{40}Ar/^{39}Ar$, AFT, and AHe age constraints. Representative thermal models are shown in Figures 15 and 16 (for all thermal models, see Fig. S2 [footnote 1]). The thermal models display some spatially and elevation-controlled variations but in general record three main rock-cooling events: (1) The highest elevation sample from the Mount Sovereign vertical profile (13Sov) records relatively slow rock cooling from the Cretaceous to present (~1–4 °C/m.y.) (Figs. 15 and 16); (2) thermal models of lower-elevation samples (01Sov and 03Sov) show relatively slow but not well-constrained cooling until ca. 60 Ma (~1–4 °C/m.y.), when the cooling rate significantly increases for a period of ~20 m.y. (>16 °C/m.y.); and (3) slow cooling follows, and there is relative tectonic quiescence from ca. 45 Ma to present (~1 °C/m.y.). Three samples near the CMF (01Trop, 02King, and 04King) show a second relatively rapid cooling event (~4 °C/m.y.) that initiated in the Miocene (Fig. 15), although the exact timing of onset is not well constrained by our current cooling age data set.

Southern Talkeetna Mountains Paleogeothermal Gradient

Geothermal gradient constraints must be known to quantify the total amount of exhumation. We have no quantitative measurement of paleogeothermal gradients for the Talkeetna Mountains. Therefore, we use our exhumation and cooling-rate calculations along with petrological observations and other regional geothermal gradient constraints to assess qualitative variations in the geothermal gradient through time, allowing us to make inferences about the amount of southern Talkeetna Mountains exhumation. Overall, documenting variations in the regional geothermal gradient through time is integral to understanding the Cenozoic tectonic evolution of southern Alaska.

Apatite Fission-Track Cooling Age-Elevation Relationships

We use age-elevation relationships to calculate variations in the rate of exhumation through time (Fig. 10); we interpret breaks in slope as reflecting a change in the exhumation rate (Fitzgerald et al., 1993). Rock-cooling rates and estimated exhumation rates are also calculated using results from the HeFTy kinetic modeling program (Ketcham, 2005).

Seventeen samples north of the CMF have Paleocene–Eocene AFT cooling ages (ca. 63 Ma to ca. 44 Ma) (Figs. 7 and 10A; Tables 2 and 3). When these ages are compiled with previously published AFT cooling ages in the region (Parry et al., 2001; Bleick et al., 2012), there is a complex age-elevation relationship that can be divided into two different cooling domains (Fig. 10A). Samples at lower elevations (<1500 m) do not have an age-elevation relationship (Fig. 10A).

AFT cooling ages at higher elevations (>1500 m) that are within the trondhjemite pluton along the Mount Sovereign to Sheep Mountain vertical profile have a positive age-elevation relationship (Fig. 10B). As discussed above, a few of the samples along the AFT vertical profile show evidence for spatially variable thermal resetting that we infer is related to hydrothermal fluid

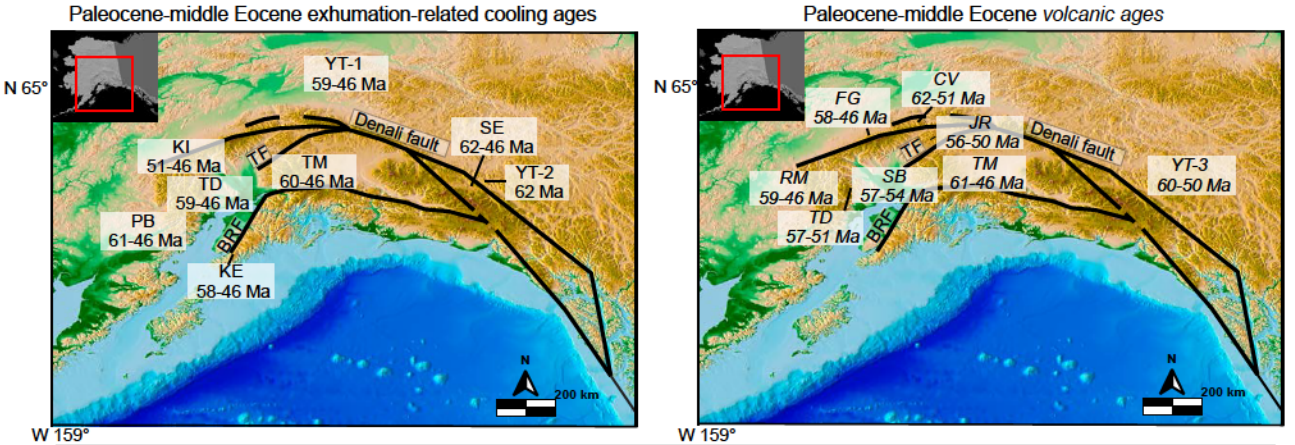

	Pebble (PB)	Revalation Mountains (RM)	Tordrillo Mountains (TD)	Kichatna Mountains (KI)	Kenai Mountains (KE)	Foraker Glacier (FG)	Susitna Basin (SB)	Cantwell Volcanics (CV)	Jack River (JR)	Talkeetna Mountains (TM)	Saint Elias (SE)	Yukon-Tanana Terrane (YT)
AHe					58-46 Ma					60-46 Ma		
AFT	61-46 Ma		59-46 Ma	51-46 Ma						58-46 Ma	50 Ma	59-46 Ma
ZFT											62-46 Ma	62 Ma
KF			57-46 Ma							*61 Ma*		
WR			*57-51 Ma*			*57-46 Ma*	*57-54 Ma*	*62-51 Ma*	*56-50 Ma*	*60-46 Ma*		*60-50 Ma*
BI		*59-46 Ma*				*58 Ma*						

Figure 14. Paleocene–middle Eocene exhumation and volcanism-related cooling ages from samples across southern Alaska show no S-N or W-E age progressions. Ages younger than ca. 46 Ma are not reported due to this being the well-constrained time of Aleutian Arc initiation (i.e., the time that normal subduction reinitiated) (Jicha et al., 2006). Abbreviations: PB—Pebble Mine (O'Sullivan et al., 2010); RM—Revelation Mountains region (Reed and Lanphere, 1972); TD—Tordrillo Mountains (Haeussler et al., 2008; Benowitz et al., 2012a); KI—Kichatna Mountains (Ward et al., 2012); KE—Kenai Mountains (Valentino et al., 2016); FG—Foraker Glacier region (Reed and Lanphere, 1972; Cole and Layer, 2002); SB—Susitna Basin (Stanley et al., 2014); CV—Cantwell volcanics (Cole et al., 1999); JR—Jack River volcanics (Cole et al., 2007); TM—Talkeetna Mountains (Silberman and Grantz., 1984; Parry et al., 2001; Cole et al., 2006; Hoffman and Armstrong, 2006; Oswald, 2006; Cole et al., 2007; Bleick et al., 2012; Hacker et al., 2011; Benowitz et al., 2012a); SE—St. Elias Mountains (Enkelmann et al., 2017); YT—Yukon-Tanana Terrane three locations (Tempelman-Kluit and Wanless, 1975; Dusel-Bacon and Murphy, 2001; Enkelmann et al., 2017). AHe—apatite (U-Th)/He; AFT—apatite fission track; ZFT—zircon fission track; KF—potassium feldspar; WR—whole rock; BI—biotite.

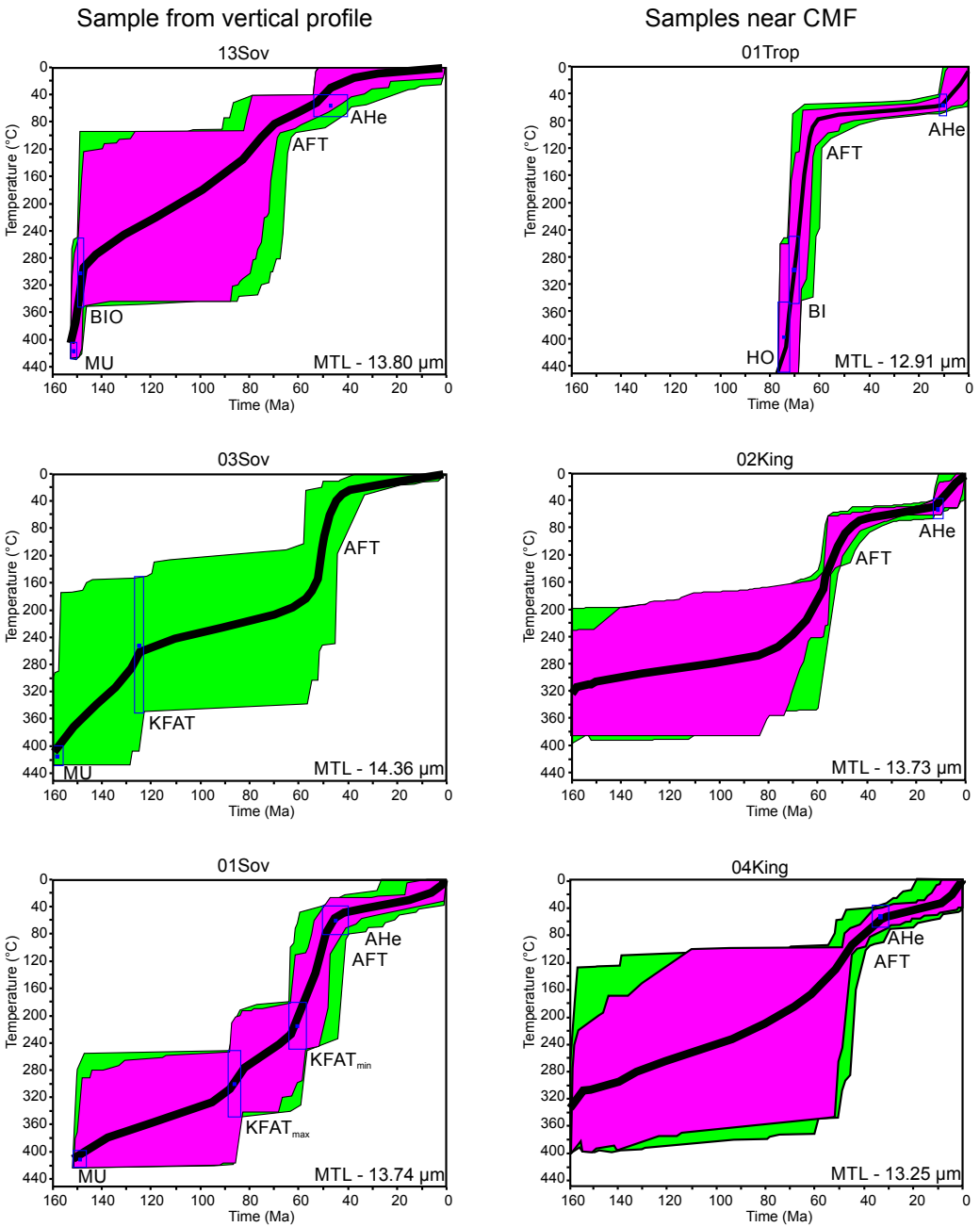

Figure 15. Inverse HeFTy thermal models for samples along the Mount Sovereign vertical profile and near the Castle Mountain fault (CMF) (Fig. 6). Models were created by generating 50,000 random cooling paths using the HeFTy kinetic modeling program (Ketcham, 2005) and all cooling-age constraints. Time/temperature envelopes and weighted-mean cooling paths are shown. Purple envelopes are defined by all good-fit cooling paths, and green envelopes are constrained by acceptable-fit cooling paths. Blue boxes are cooling-age constraints where width of box represents age uncertainty and height of box represents nominal closure temperatures for each mineral system. Red boxes represent the approximate time/temperature window for the apatite fission-track (AFT) system. AFT age and track-length information for each sample was directly input into HeFTy to generate the models. Hence, red boxes are meant to demonstrate the use of the AFT system in the making of these models but are not an input box constraint as used for other systems (blue boxes). Abbreviations: AHe—apatite (U-Th)/He; AFT—apatite fission track; BI—$^{40}Ar/^{39}Ar$ biotite; KFAT—$^{40}Ar/^{39}Ar$ K-feldspar; MU—$^{40}Ar/^{39}Ar$ muscovite; MTL—mean track-length value for each sample. For HeFTy models of all samples, see Figure S2 (text footnote 1).

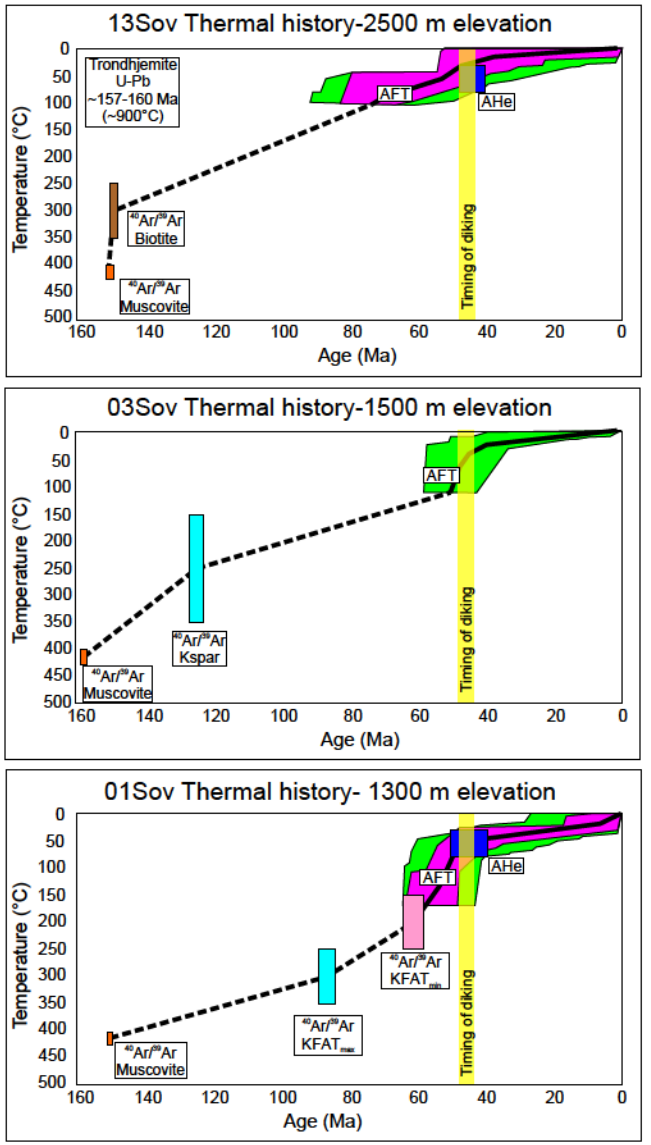

Figure 16. Thermal histories for samples 13Sov, 03Sov, and 01Sov modeled using the HeFTy kinetic modeling program (Ketcham, 2005) and $^{40}Ar/^{39}Ar$, apatite fission-track (AFT) and apatite (U-Th)/He (AHe) age constraints. U-Pb zircon crystallization ages are noted (Rioux et al., 2007). Width of boxes represents age uncertainty, and height of boxes represents nominal closure temperatures for each mineral system. Dashed line is the approximate cooling path between mineral phases. Abbreviations: KFAT—$^{40}Ar/^{39}Ar$ K-feldspar; Kspar—K-feldspar.

injection. The Mount Sovereign to Sheep Mountain AFT vertical profile shows three distinct periods of exhumation: (1) relatively slow Late Cretaceous–early Paleocene (ca. 74 to ca. 60 Ma) exhumation at a rate of ~15 m/m.y.; (2) a break in slope at ca. 60–58 Ma indicating relatively rapid exhumation at a maximum rate of ~188 m/m.y.; and (3) a second break in slope at ca. 56 Ma indicating a less rapid exhumation rate of ~65 m/m.y. Alternatively, the AFT cooling ages have large uncertainty bars that allow only one inflection point at ca. 60–58 Ma with a more moderate exhumation rate. We do not favor this interpretation because it is not supported by the HeFTy thermal models, which show a significant increase in rock-cooling rates at ca. 60 Ma and an inferred increase in exhumation rates at this time (Fig. 15). These results suggest that rapid cooling and inferred exhumation in the Talkeetna Mountains began immediately after the thermal resetting and subsequent cooling of K-feldspar from sample 01Sov (ca. 61 Ma) and continued during the main episode of dike emplacement from ca. 40–50 Ma (Figs. 7 and 12).

AFT cooling ages from samples at lower elevations (<1500 m) and closer to the CMF do not have an age-elevation relationship (Fig. 10A). The two most likely explanations for the lack of an AFT age-elevation relationship at lower elevations are potential differential erosion after the closure of the AFT system (possibly related to Cenozoic deformation or late Cenozoic glaciation) (Williams et al., 1989) and the perturbation of isotherms at lower elevations around the trondhjemite pluton by the Paleocene–Eocene volcanism, resulting in possible erratic rock-cooling profiles (Reiners, 2007).

AFT cooling ages south of the CMF are distinctly younger than those to the north (Arkle et al., 2013), which is counter to what is expected if the CMF experienced significant Eocene–Oligocene north-side-up displacement and is the primary control on Cenozoic AFT cooling age patterns. There are only four AFT cooling ages available in the Talkeetna Mountains region south of the CMF (Fig. 7), including sample 05King from this study (ca. 31 Ma), one sample located in the fault zone from Parry et al. (2001) (ca. 31 Ma), and two samples from Little and Naeser (1989) (ca. 24 Ma and ca. 21 Ma). The lack of data makes it difficult to draw interpretations from these cooling ages. However, Arkle et al. (2013) attribute these regionally younger ages to exhumation in the Chugach syntaxis driven predominantly by underplating from the Yakutat flat-slab since the Oligocene. According to their model, the exhumation effects driven by underplating die out north of the CMF, which may explain why ages south of the fault are younger than ages north of the CMF. The AFT ages south of the CMF are also located near the BRFS, and one sample is located south of a BRFS strand. Therefore, it is possible that the ages were affected by the Neogene contractional reactivation of the BRFS (Little and Naeser, 1989).

HeFTy Thermal Modeling Constraints on Rock-Cooling Events in the Talkeetna Mountains

Rock-cooling paths were constructed for all our samples using the HeFTy kinetic modeling program (Ketcham, 2005) and all available thermochronology

constraints. These time/temperature paths highlight the approximate timing and duration of multiple rock-cooling events. Representative HeFTy thermal models are shown in Figure 15. HeFTy thermal models for all samples can be found in Figure S2 (footnote 1).

Rock-cooling paths for samples 13Sov, 03Sov, and 01Sov show cooling patterns that vary with elevation (Figs. 15 and 16). The highest elevation sample (13Sov) has a much slower cooling rate relative to the lower-elevation samples. Sample 03Sov shows a cooling rate that significantly increases after ca. 60 Ma. Sample 01Sov also shows a similarly increased cooling rate after the low-temperature K-feldspar domain is thermally reset and subsequently cooled at ca. 61 Ma (Figs. 8 and 9).

All our HeFTy thermal models show distinct rock-cooling patterns that vary both spatially and with elevation. To highlight these variations, we divided the thermal models into three groups with similar cooling histories (Fig. 17): (1) The two highest elevation samples collected from the summits of Mount Sovereign and Sheep Mountain (13Sov and 07Talk) (Fig. 7); (2) seven samples from the interior Talkeetna Mountains along the two vertical profiles (01Sov, 02Sov, 03Sov, 08Sov, 11Sov, 05Talk, and 13Talk); and (3) three samples near the CMF (01Trop, 02King, and 04King).

The HeFTy thermal models suggest four distinct rock-cooling events in the southern Talkeetna Mountains topographic development history: (1) The highest elevation samples record relatively slow rock cooling from Cretaceous to present (~1–3 °C/m.y.) (Fig. 17). Mapping studies in the southern Talkeetna Mountains document Cretaceous crustal shortening (Csejtey et al., 1978; Fuchs, 1980), suggesting that rock cooling was related to exhumation. (2) The interior Talkeetna Mountains samples collected along vertical profiles and samples near the CMF both record a rapid rock-cooling event (>16 °C/m.y.) initiating at ca. 60 Ma (Fig. 17). The HeFTy models suggest that this elevated cooling rate persisted for ca. 20 Ma. This is consistent with the inferred timing of a prolonged period of Paleocene–Eocene volcanism (Cole et al., 2006) and our constrained onset of rapid exhumation at ca. 60–58 Ma (Fig. 10B) following the thermal resetting of K-feldspar in sample 01Sov at ca. 61 Ma (Figs. 8 and 9). (3) The rapid rock-cooling event is followed by a period of relative middle Eocene–Miocene tectonic quiescence with a rock-cooling rate of ~1 °C/m.y. More thermochronology data are needed to determine the exact duration of this rock-cooling event, which is unclear from our data set. (4) The samples collected near the CMF records a second, more rapid rock-cooling event (~4 °C/m.y.) during the Miocene, likely in response to vertical displacement and exhumation along the CMF. More low-temperature thermochronology data are needed near the CMF to define the timing of initiation of this rock-cooling event.

Our AFT age-elevation relationship suggests a maximum exhumation rate of 200 m/m.y. (Fig. 10B). When the maximum sustained cooling rate from our HeFTy thermal models (~16 °C/m.y.) is converted to an exhumation rate (800 m/m.y.) using a normal continental geothermal gradient of 20 °C/km, the two individual calculations disagree. Alternatively, when the ~16 °C/m.y. cooling rate is converted to an exhumation rate using a much higher geothermal gradient of ~80 °C/km, the two exhumation calculations agree well (200 m/m.y.).

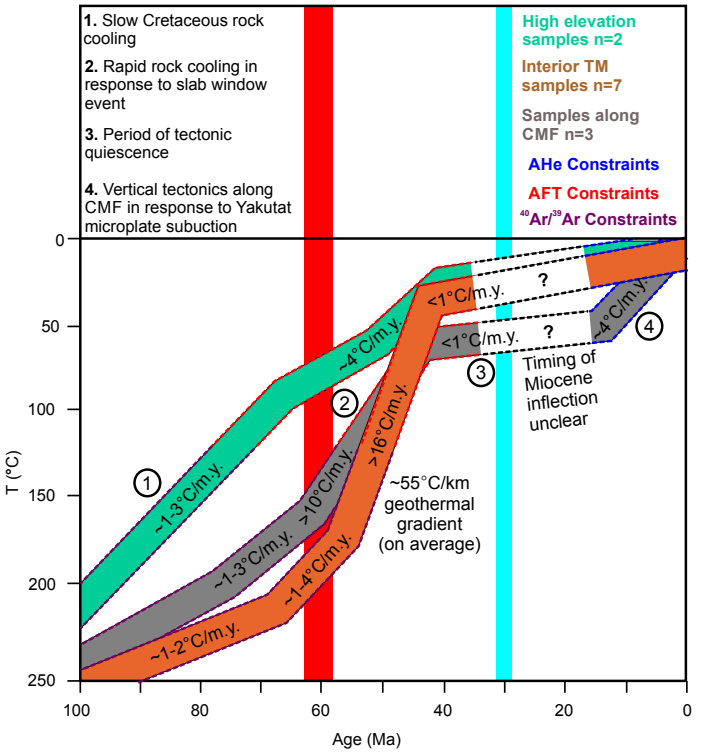

Figure 17. Time/temperature summary diagram for samples in the interior Talkeetna Mountains (TM) and along vertical profiles (brown box), at the highest elevations (teal box) and near the Castle Mountain fault (CMF) (gray box). Cooling rates are estimated from HeFTy thermal models (Fig. S2 [see text footnote 1]). Red bar at ca. 60 Ma represents the onset of the inferred thermal event discussed in the text. Light-blue bar at ca. 30 Ma represents approximate initiation of subduction of the Yakutat flat-slab. Abbreviations: AFT—apatite fission track; AHe—apatite (U-Th)/He.

When geothermal gradients are obtained from the time-averaged cooling rates between ca. 60 Ma and ca. 45 Ma from five individual HeFTy thermal models, the geothermal gradient is ~55 °C/km on average, indicating a non-steady-state geothermal gradient during this time period. This is expected given the dynamic nature of slab windows and associated upwelling of the asthenosphere (Thorkelson, 1996). Hence, thermochronology results from this study provide independent evidence for an anomalously high geothermal gradient during Paleocene–Eocene times; this evidence aligns with previous southern Alaska paleogeothermal gradient interpretations (e.g., Benowitz et al., 2012a; Finzel et al., 2016).

We acknowledge that the age-elevation profile does not provide a unique rock-cooling scenario given the large uncertainty associated with our AFT ages (±ca. 4 Ma to ca. 17 Ma; Fig. 10 and Table 3). It is also possible that large

amounts of tilting could explain the disconnect between the exhumation rate calculated from our AFT age-elevation relationship and the exhumation rate calculated from our HeFTy thermal models. However, vertical lithified volcanic bodies crosscut the mafic dikes that appear to intrude along exfoliation joints (Fig. 6; P1 and P2), suggesting there has not been significant tilting since the Eocene. Given this and the regional evidence for a high Paleocene–Eocene geothermal gradient across southern Alaska (O'Sullivan and Currie, 1996; Dusel-Bacon and Murphy, 2001; Benowitz et al., 2012a; Riccio et al., 2014; Finzel et al., 2016), we also favor the interpretation of an elevated Paleocene–Eocene southern Talkeetna Mountains geothermal gradient averaging ~55 °C/km.

DISCUSSION

Topographic Development Summary for the Southern Talkeetna Mountains

Paleocene–Eocene Paleotopography

Geophysical models of southern Alaska from Jadamec et al. (2013) predict that the modern plate configuration would result in the development of a basin in the region of the Talkeetna Mountains rather than high topography (Fig. 4). AFT cooling ages from the Talkeetna Mountains are predominantly Paleocene–Eocene (Fig. 12). These results partly reconcile the models from Jadamec et al. (2013) by suggesting that the southern Talkeetna Mountains have a significant paleotopography component that formed prior to the modern Yakutat flat-slab plate configuration (Fig. 2B).

Adding support to this interpretation, Eocene dikes intrude subhorizontally into the Mount Sovereign trondhjemite pluton along exfoliation joints and are crosscut by vertical dikes, and lithified volcanic bodies that display a visible lack of tilting (Fig. 6; P1 and P2). This suggests that southern Talkeetna Mountains unroofing initiated before dike emplacement, consistent with previous studies in the region (e.g., Trop, 2008), and the region was uplifted as a uniform crustal block. We speculate that the prolonged episode of dike emplacement, along with possible magmatic underplating during slab-window magmatism (Li et al., 2012a, 2012b), could have thickened the crust and may in part explain the sustained high topography into modern times. We interpret these overall findings to suggest that Paleocene–Eocene topographic development across the southern Talkeetna Mountains is related to the creation of a Paleocene–Eocene slab window (Cole et al., 2006; Benowitz et al., 2012a).

Structural Control on the Paleocene–Eocene Topographic Development of the Southern Talkeetna Mountains

The structures involved in accommodating southern Talkeetna Mountains exhumation related to an inferred Paleocene–Eocene slab window are not well constrained (Fig. 3). Faults appear to partially bound the edges of the trondhjemite pluton (Fig. 3) (Wilson et al., 2015). Our AFT age-elevation relationship suggests that there are two separate rock-cooling domains defined by elevation (Fig. 10A) based on the relatively well-defined age-elevation relationship within the trondhjemite pluton. Sample 04King is located across a fault on the western edge of the pluton away from the Mount Sovereign vertical profile sample cluster (Fig. 3) and is an outlier from our AFT age-elevation relationship (Fig. 10B). Similarly, samples 13Talk and 14Talk are located near a mapped fault (Fig. 3), and their AFT cooling ages fall in the cooling domain that does not display an age-elevation relationship (Fig. 10A). This is evidence that at least the structure on the western boundary of the trondhjemite pluton was active and/or a conduit for hydrothermal fluids in the Paleocene–Eocene and supports the notion that the high-peak region, established by the trondhjemite pluton, exhumed as an independent crustal block along these structures (Fig. S6 [footnote 1]).

There are also numerous mapped NW-SE–trending normal faults to the east of our study area. It is unclear whether these NW-trending normal faults were created and reactivated to allow for volcanism and exhumation driven solely by mantle processes (i.e., a slab window) (Trop et al., 2003; Cole et al., 2006), or conversely, if crustal extension and the creation and reactivation of structures were influenced by the hypothesized counterclockwise rotation and oroclinal bending of southern Alaska (Hillhouse and Coe, 1994) in the presence or absence of a slab window. The orientation of these structures is also consistent with transtension linked to dextral slip along the CMF (Cole et al., 2006).

The Castle Mountain Fault

The geophysical models by Jadamec et al. (2013) do not account for the existence of the CMF, which may in part explain the disparity between the predicted compared to actual topography (Fig. 4). To test how southern Alaska structures control patterns of deformation, we compiled the youngest AFT cooling ages along an ~S-N transect across southern Alaska (Figs. 1 and 18A) and included published data (Kveton, 1989; Parry et al., 2001; Bleick et al., 2012; Arkle et al., 2013; Frohman, 2014) and ages from this study. This compilation shows a pattern of ages abruptly changing across major faults, supporting the notion that Cenozoic deformation has been focused along these structures. However, the ages do not change as distinctly across the CMF, suggesting it has experienced less vertical displacement than other major structures along the transect. AFT ages directly to the north of the CMF are ca. 63 Ma to ca. 44 Ma (Table 2), suggesting there has been less than ~3–5 km of vertical displacement and unroofing along the CMF since the Eocene and possibly even less exhumation considering the evidence for an elevated geothermal gradient. This is consistent with previous estimates of ~3 km of Neogene vertical slip based on mapping studies (Grantz, 1966; Fuchs, 1980).

There is some regional evidence for Eocene displacement along the CMF. Wishbone Formation strata south of the CMF are deformed by footwall

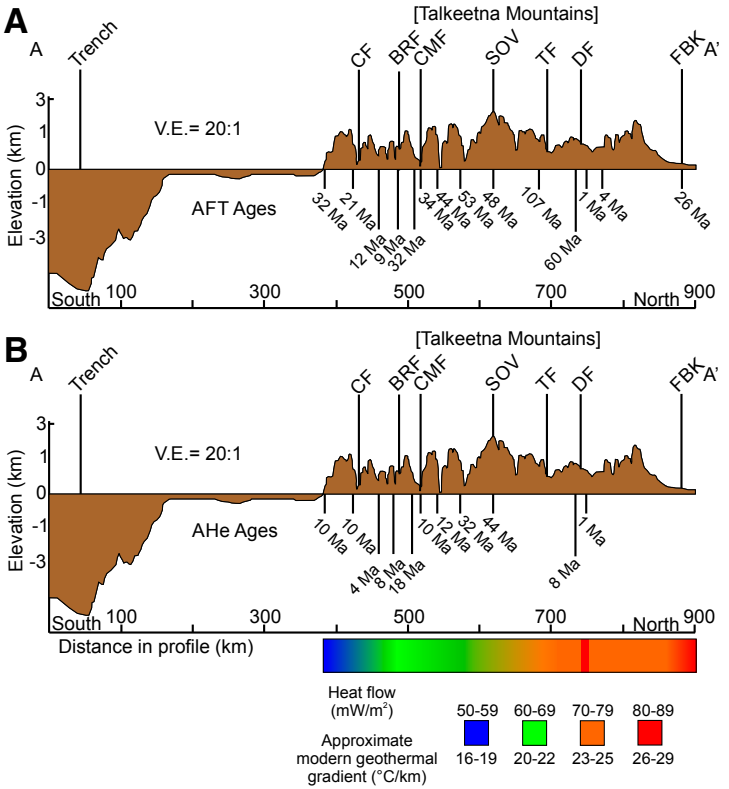

Figure 18. (A) Topographic profile and youngest apatite fission-track ages plotted along transect A–A′ (Fig. 1). Ages show a pattern of changing across major structures, with a less pronounced change across the Castle Mountain fault (CMF). (B) Topographic profile and youngest apatite (U-Th)/He ages plotted along A–A′ (Fig. 1). Ages show a pattern of changing across major structures, including a pronounced change across the CMF. Abbreviations: CF—Contact fault; BRF—Border Ranges fault; CMF—Castle Mountain fault; SOV—Mount Sovereign; TF—Talkeetna fault; DF—Denali fault; FBK—Fairbanks. Approximate geothermal gradient and heat flow shown along profile are calculated from Batir et al. (2013). V.E.—vertical exaggeration.

synclines that are consistent with syndepositional rotation and displacement (Trop et al., 2003, 2015). South of the CMF, circa 50–48 Ma lavas capping Castle Mountain and Puddingstone Hill unconformably overlie deformed conglomerates with ca. 55–52 Ma detrital zircons, indicating some footwall tilting, folding, and erosion prior to ca. 50–48 Ma (Trop et al., 2015). However, the amount of CMF vertical and horizontal displacement is not well constrained.

Miocene AHe cooling ages near the CMF are the youngest in the southern Talkeetna Mountains (Fig. 7 and Table 4). The youngest available AHe cooling ages compiled along an ~S-N transect across southern Alaska (Figs. 1 and 18B) (Arkle et al., 2013; Riccio et al., 2014) show a pattern of cooling ages abruptly changing across major faults similar to that of the AFT cooling-age transect discussed above (Fig. 18A). However, the change in AHe cooling ages across the CMF (Fig. 18B) is more pronounced than the change in AFT cooling ages (Fig. 18A).

The AHe cooling ages show a clear trend of younging toward the CMF (Fig. 11C). There is no relationship between AHe cooling age and elevation along the same transect (Fig. 11D). This provides strong evidence for vertical displacement along the CMF having a control on AHe cooling age patterns since the Miocene because rocks near the CMF have cooled more rapidly (Fig. 18).

This interpretation is consistent with HeFTy thermal models, which indicate a rapid rock-cooling event initiating by the Miocene (Fig. 17) and a study by Bristol et al. (2017) that documents the juxtaposition of Miocene fluvial strata against Cretaceous granitoids along the CMF. A Miocene 20 °C/m.y. paleo-geothermal gradient is expected due to cooling from the removal of the mantle wedge during the flat-slab subduction of the Yakutat microplate (Christeson et al., 2010), as reflected in the gross modern geothermal gradient along an ~S-N transect across southern Alaska (Figs. 1 and 19). When the Miocene rock-cooling rate from our HeFTy models (~4 °C/m.y.) is converted into an exhumation rate using a geothermal gradient of 20 °C/m.y., the approximate exhumation rate is 0.2 mm/yr.

These overall findings suggest that vertical displacement along the CMF has played a greater role in the Cenozoic exhumation of the southern Talkeetna Mountains since the Miocene. Slip on the CMF is likely in response to the flat-slab subduction of the Yakutat microplate (Haeussler, 2008).

Cenozoic Tectonic Reconstruction of Southern Alaska

Paleocene–Eocene Slab Breakoff

A ~2000-km-long string of eastward-younging Paleocene–Eocene near-trench plutons in the accretionary prism of southern Alaska (Figs. 1 and 2A) provides the basis for the proposed subduction of an active spreading ridge and an associated slab window sweeping eastward across southern Alaska (Haeussler et al., 2003). The timing and proposed slab-window mechanism for Paleocene–Eocene topographic development of the southern Talkeetna Mountains coincides with this inferred ridge-subduction event (Cole et al., 2006). The ridge-subduction model is also the presumed mechanism for the Eocene creation of topography and an elevated geothermal gradient (>~50 °C/km) in the western Alaska Range (Fig. 1) (Benowitz et al., 2012a), an elevated geothermal gradient of ~45 °C/km in the Yukon-Tanana Uplands (Dusel-Bacon and Murphy, 2001), rapid rock cooling in the St. Elias Range (Fig. 14) (Enkelmann et al., 2017), and the intrusion of dike swarms and mafic volcanic rocks throughout southern Alaska.

There are geologic predictions that can be made from the model of a Paleocene–Eocene eastward-sweeping spreading ridge across southern Alaska

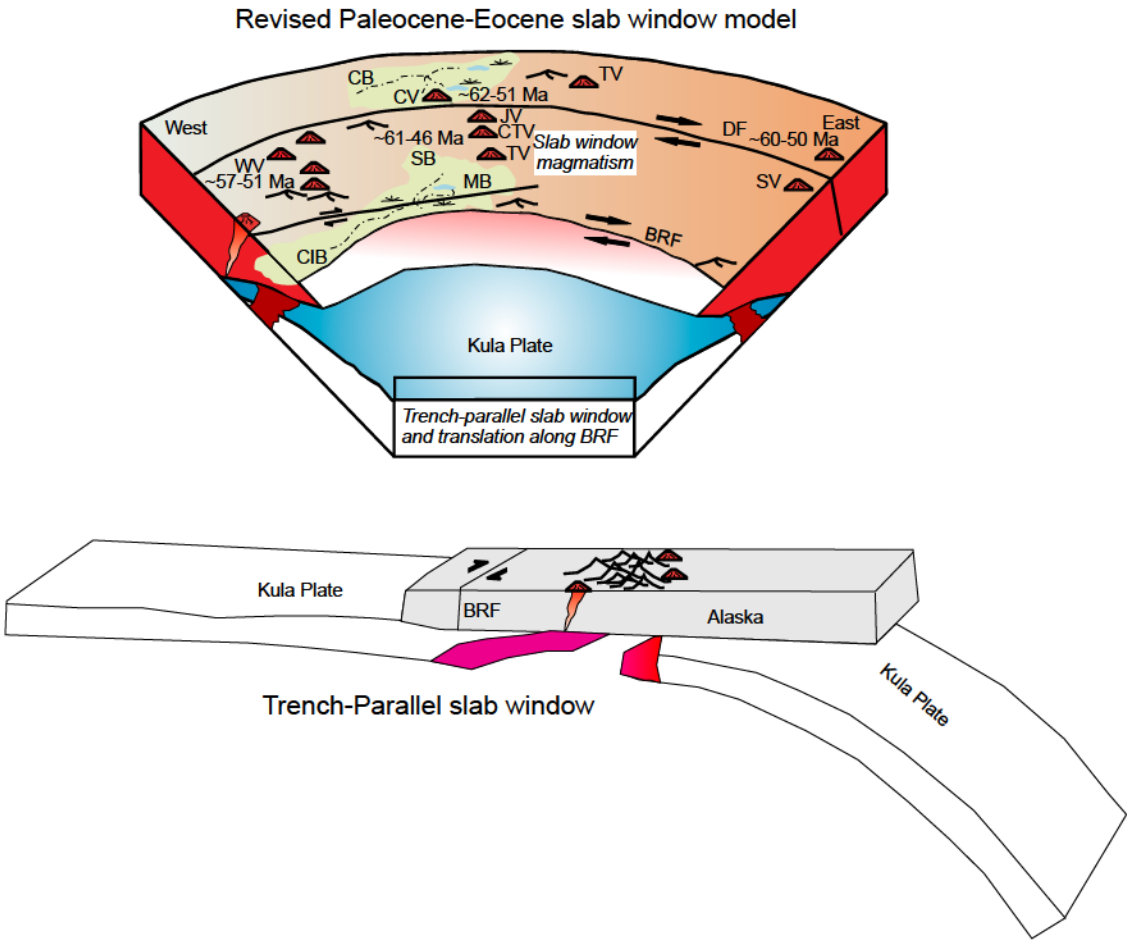

Figure 19. Paleocene–Eocene slab-window model revised from Figure 2 to show interpretations made in this study of a trench-parallel slab-window event. Abbreviations: Cook Inlet Basin—CIB; Susitna Basin—SB; Matanuska Basin—MB; Cantwell Basin—CB; Western Alaska Range volcanics—WV; Jack River volcanics—JV; Central Talkeetna volcanics—CTV; Caribou Hill volcanics—CV; Tanana Valley volcanics—TV; Sifton volcanics—SV; Denali fault—DF; Border Ranges fault system—BRF. Modified from Ridgway et al. (2012), Benowitz et al. (2012a), and Pallares et al. (2007).

(Haeussler et al., 2003). Specifically, a west-to-east and south-to-north progression in the timing of volcanism and exhumation across southern Alaska inboard from the BRFS would be expected. We applied whole-rock $^{40}Ar/^{39}Ar$ geochronology to volcanic rocks in the Talkeetna Mountains (Table 1) and compiled our results with previously published regional Paleocene–Eocene volcanic ages to test this prediction. We also applied AFT thermochronology to plutonic rocks in the Talkeetna Mountains (Table 2) and compiled our results with previously published regional Cenozoic cooling ages.

Whole-rock $^{40}Ar/^{39}Ar$ ages in the southern Talkeetna Mountains show no overall S-N or W-E relationships, suggesting no local spatial progressions in the timing of volcanism (Fig. 13). AFT cooling ages in the southern Talkeetna Mountains also show no overall S-N or W-E relationships, suggesting no local spatial progressions in the timing of exhumation (Fig. 13). More importantly, region-wide Paleocene–Eocene exhumation-related cooling ages and volcanic ages from across southern Alaska have no apparent S-N or W-E relationships: southwest Alaska (O'Sullivan et al., 2010), the Revelation Mountains region (Reed and Lanphere, 1972), the Tordrillo Mountains (Haeussler et al., 2008; Benowitz et al., 2012a), the Kichatna Mountains (Ward et al., 2012), the Kenai Mountains (Valentino et al., 2016), the Foraker Glacier region (Reed and Lanphere, 1972; Cole and Layer, 2002), the Susitna Basin (Stanley et al., 2014), the Cantwell volcanics (Cole et al., 1999), the Jack River volcanics (Cole et al., 2007), the Talkeetna Mountains (Silberman and Grantz, 1984; Parry et al., 2001; Cole

et al., 2006; Hoffman and Armstrong, 2006; Oswald, 2006; Cole et al., 2007; Bleick et al., 2012; Hacker et al., 2011), the St. Elias Mountains (Enkelmann et al., 2017), and three sites in the Yukon-Tanana Terrane (Tempelman-Kluit and Wanless, 1975; Dusel-Bacon and Murphy, 2001; Enkelmann et al., 2017) (Fig. 14).

The Paleocene–Eocene cooling and volcanic ages across southern Alaska are all broadly similar, suggesting a synchronous exhumation and volcanic event that was widespread across southern Alaska and persisted for millions of years. The apparent lack of any S-N or W-E progressions in the timing of Paleocene–Eocene volcanism and exhumation across southern Alaska north of the BRFS conflicts with the proposed model of an eastward-sweeping active spreading ridge impacting the region. The lack of any Paleocene–Eocene spatial age patterns like those observed in the prism suggests southern Alaska was likely not influenced by sweeping ridge subduction or diachronous thermal perturbation as evidenced by the varied ages in the near-trench Sanak-Baranof belt plutons in the Chugach accretionary prism to the south of the BRFS (Fig. 1). Oblique ridge-trench convergence does prompt an unzipping pattern, whereby slab-window geometry is triangular, and the opening widens progressively as the ridge descends into the mantle; thus, spatial patterns may be more diffuse farther inboard of the trench (Dickinson and Snyder, 1979; Thorkelson, 1996; Breitsprecher and Thorkelson, 2009). However, the absence of any age progression, regardless of rate, across a >800-km-wide swath of southern Alaska makes it difficult to link a Paleocene–Eocene west-to-east sweeping ridge subduction event to the overall regional geology north of the BRFS. Therefore, a different mechanism is required to explain the regional synchronous and long-lived slab-window event recorded in southern Alaska.

To reconcile this, we propose a new model for the Paleocene–Eocene tectonic configuration of southern Alaska. We suggest that a Paleocene–Eocene slab window formed subparallel to the trench (Fig. 19) and drove exhumation and volcanism synchronously across southern Alaska while also significantly increasing the regional geothermal gradient. The cause of this Paleocene–Eocene slab-window event is unclear, but Baja, California, provides an analog tectonic setting: a Miocene slab-window event has been attributed to the subduction of an active spreading ridge that was parallel to the trench and led to slab detachment and the opening of a slab window subparallel to the trench (Michaud et al., 2006). Another possible mechanism for the opening of a Paleocene–Eocene slab window across southern Alaska includes the subduction of an inactive bathymetric high (e.g., aseismic ridge or seamount chain) that was part of the Kula plate, leading to slab breakoff. Our new model of the subduction of a trench-parallel bathymetric high shutting off subduction is consistent with the lack of evidence for southern Alaska subduction-related magmatism during late Paleocene–early Eocene time (Cole et al., 2006) and stratigraphic and/or detrital geochronologic evidence for subaerial uplift and exhumation of the formerly marine forearc region followed by subsidence and nonmarine sedimentation (e.g., Trop, 2008; Ridgway et al., 2012; Kortyna et al., 2013; Finzel et al., 2015).

In our new model, southern Alaska was located ~1000 km from the Chugach accretionary prism during late Paleocene–early Eocene time, while the ca. 63 to ca. 47 Ma near-trench plutons were emplaced into the Chugach accretionary prism. The Paleocene–early Eocene margin outboard of southern Alaska was likely a transform setting characterized by dextral slip along the BRFS or unidentified faults to the south of the BRFS. Both regions were subsequently shuffled laterally by dextral displacement along orogen-parallel strike-slip faults, consistent with paleomagnetic data indicating that southern Alaska (WCT) and the Chugach accretionary prism were positioned hundreds of kilometers south of their current position during latest Cretaceous–Paleocene time, but still distal from each other (Bol et al., 1992; Stamatakos et al., 2001; Cowan, 2003; Garver and Davidson, 2015). Rocks making up our study area in southern Alaska at ca. 80 Ma were positioned at a paleolatitude ~15° to the south of their current location (Stamatakos et al., 2001) and were translated to near their current latitude by ca. 54–40 Ma judging from paleomagnetic data (Panuska et al., 1990), consistent with significant northward translation of the WCT during late Paleocene–early Eocene time (Figs. 20 and 21).

Large-scale translation of the Chugach accretionary prism and Sanak-Baranof belt was likely accommodated along the BRFS and other orogen-parallel fault systems (Fig. 20). The slip history of the BRFS is prolonged and complex with multiple episodes of displacement suggested during the Late Cretaceous–Paleogene and reactivation during the Neogene (Pavlis and Roeske, 2007). Roeske et al. (2003) proposed at least ~600–1000 km of Late Cretaceous–Eocene BRFS slip. Slip may have been partitioned onto other structures across southern Alaska (Fig. 1), such as the Castle Mountain fault, which has been suggested to accommodate ~130 km of dextral slip (Pavlis and Roeske, 2007); the Denali fault, which has an inferred ~400 km of post–Early Cretaceous dextral displacement (Lowey, 1998; Benowitz et al., 2012b); or faults within the Chugach accretionary prism with poorly understood slip histories such as the Eagle River fault (Kochelek et al., 2011) or Glacier Creek fault (Little, 1990).

Eocene Oroclinal Bending

Paleo-vectors of Pacific plate motion relative to the North American plate do not favor large translation along the North American plate boundary, driven by Pacific plate motion, given the modern geographic configuration of North America (Fig. 21) (Doubrovine and Tarduno, 2008). However, if the southern Alaska orocline was unbent during the Paleocene–middle Eocene (Fig. 21), the paleo-vectors are more compatible with the northward translation of the near-trench plutons along the western margin of North America (Garver and Davidson, 2015). Paleomagnetic declinations of Late Cretaceous–Paleocene rocks support ~30°–50° counterclockwise rotation of southern Alaska by the late Eocene (Hillhouse and Coe, 1994; e.g., Betka et al., 2017). This oft-cited but loosely constrained model explains the curvature of regional structures and mountain ranges (e.g., Denali fault and Alaska Range) and is known as the southern Alaska orocline (e.g., Cole et al., 2007).

Given the heating of the southern Alaska thermal regime during the inferred slab-window event (Figs. 19 and 20), it is possible that oroclinal bending may

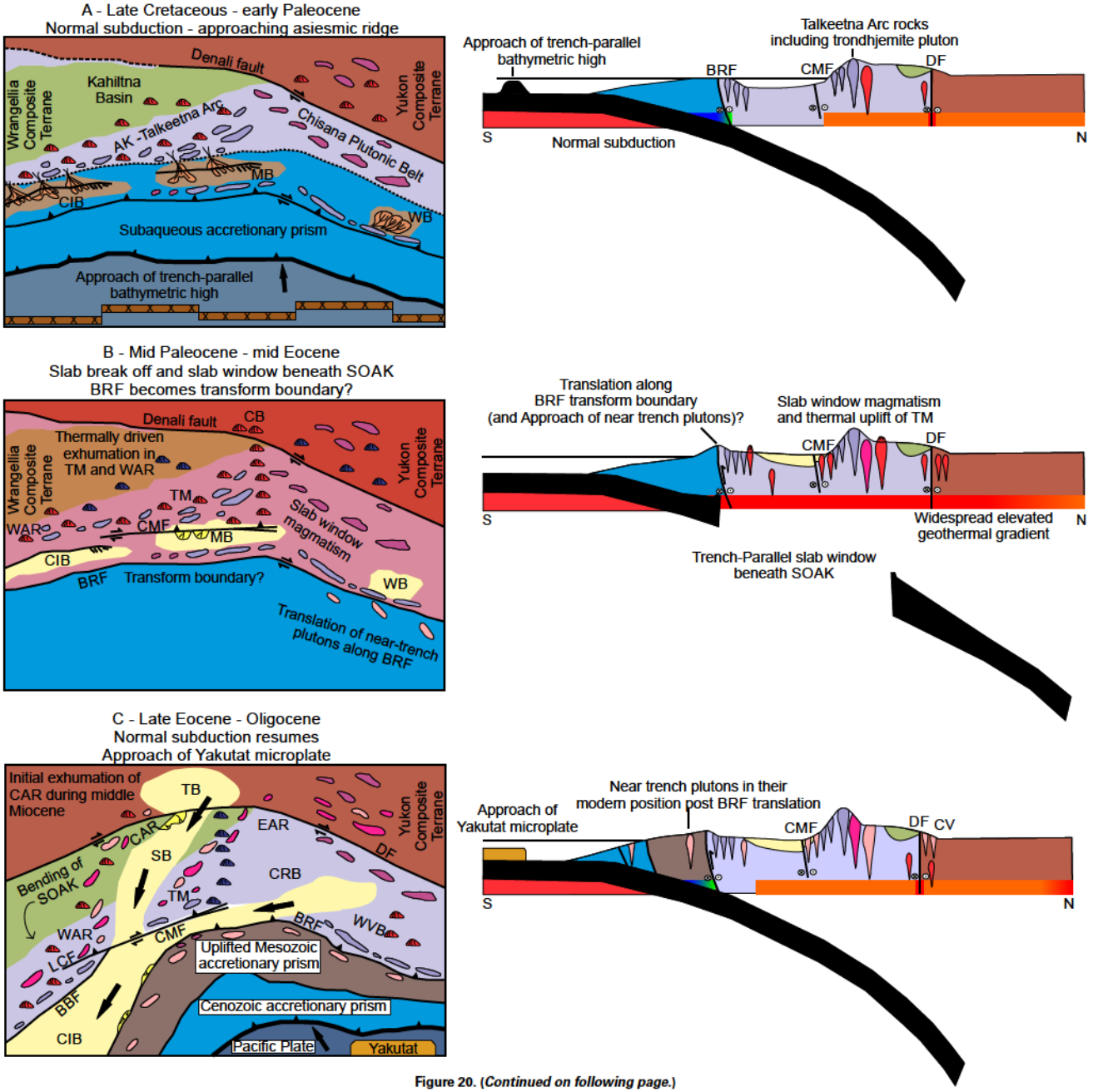

Figure 20. (***Continued on following page.***)

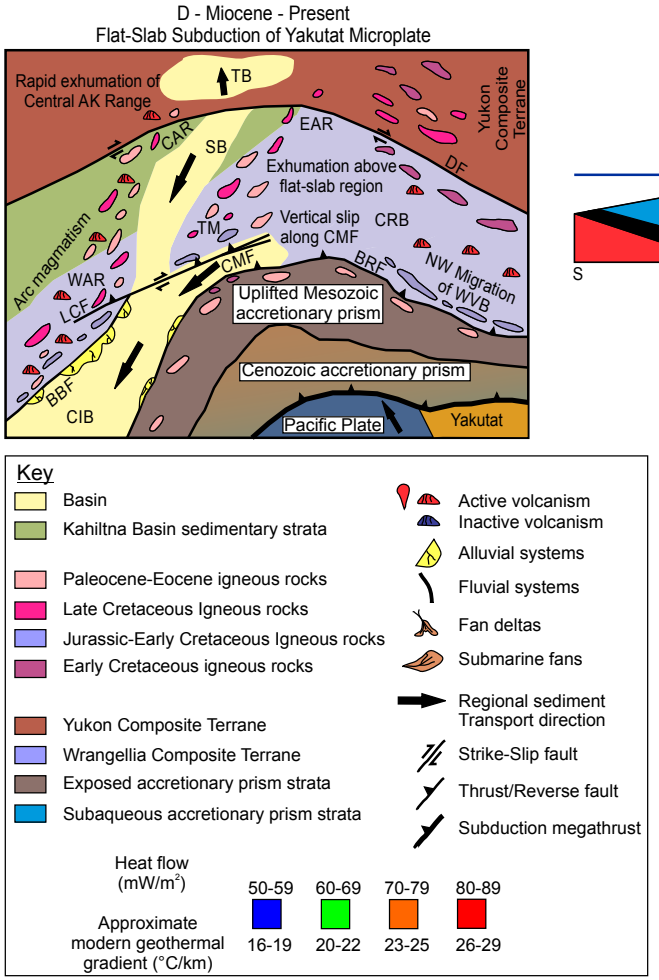

Figure 20 (*continued*). Paleogeographic maps and cross sections showing the inferred tectono-thermal evolution of southern Alaska (SOAK) from Late Cretaceous to present (modified from Trop and Ridgway, 2007, and Trop et al., 2015). (A) Late Cretaceous–early Paleocene paleogeographic map and cross section illustrating normal subduction and approach of inferred trench-parallel aseismic ridge. Abbreviations: CIB—Cook Inlet Basin; MB—Matanuska Basin; WB—Wrangell Basin. (B) Mid-Paleocene–mid-Eocene paleographic map illustrating slab-window event beneath southern Alaska, heating of the thermal regime, thermally driven exhumation and topographic development, and approach of near-trench plutons along inferred Border Ranges fault transform boundary. Abbreviations: BRF—Border Ranges fault; CB—Cantwell Basin; CMF—Castle Mountain fault; DF—Denali fault; TM—Talkeetna Mountains; WAR—western Alaska Range. (C) Late Eocene–Oligocene paleogeographic map and cross section illustrating resumption of normal subduction, oroclinal bending of southern Alaska, approach of Yakutat microplate, and cooling of the thermal regime. Abbreviations: BBF—Bruin Bay fault; CAR—central Alaska Range; CRB—Copper River Basin; CV—Cantwell volcanics; EAR—eastern Alaska Range; LCF—Lake Clark fault; SB—Susitna Basin; TB—Tanana Basin; WVB—Wrangell volcanic belt. (D) Miocene to present paleographic map and cross section illustrating modern tectonic configuration of southern Alaska including flat-slab subduction of the Yakutat microplate and subsequent inboard deformation and cooling of the thermal regime due to the subduction of the mantle wedge. Abbreviations: MC—McHugh Complex; OG—Orca Group; VG—Valdez Group; DF—Denali fault; CMF—Castle Mountain fault, BRF—Border Ranges fault; LCF—Lake Clark fault; BBF—Bruin Bay fault; TM—Talkeetna Mountains; EAR—Eastern Alaska Range; CAR—Central Alaska Range; WAR—Western Alaska Range; MB—Matanuska Basin; WB—Wrangell Mountains Basin; CB—Cantwell Basin; CIB—Cook Inlet Basin; CRB—Copper River Basin; SB—Susitna Basin; TB—Tanana Basin; WVB—Wrangell Volcanic Belt.

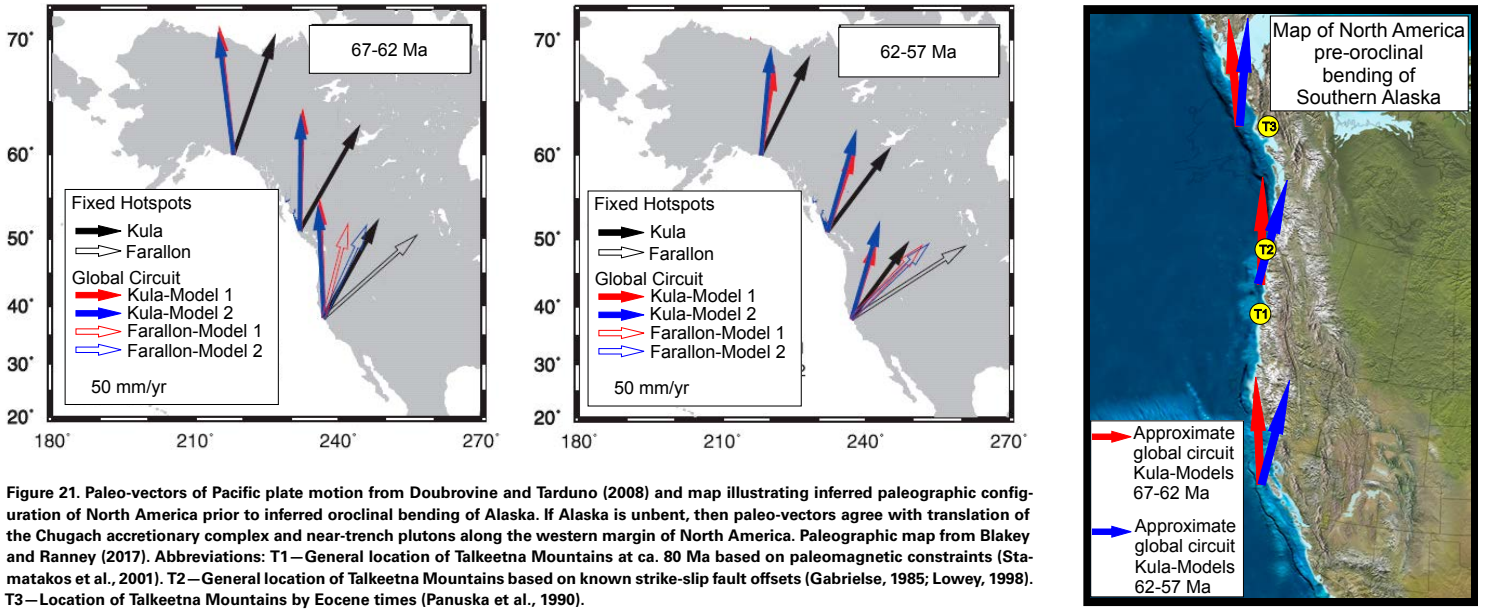

Figure 21. Paleo-vectors of Pacific plate motion from Doubrovine and Tarduno (2008) and map illustrating inferred paleographic configuration of North America prior to inferred oroclinal bending of Alaska. If Alaska is unbent, then paleo-vectors agree with translation of the Chugach accretionary complex and near-trench plutons along the western margin of North America. Paleographic map from Blakey and Ranney (2017). Abbreviations: T1—General location of Talkeetna Mountains at ca. 80 Ma based on paleomagnetic constraints (Stamatakos et al., 2001). T2—General location of Talkeetna Mountains based on known strike-slip fault offsets (Gabrielse, 1985; Lowey, 1998). T3—Location of Talkeetna Mountains by Eocene times (Panuska et al., 1990).

have been facilitated in part due to the thermally induced weakening of the crust, making it less elastic and more deformable. A similar mechanism for oroclinal bending due to thermal weakening has been suggested for the Pamir Mountains of Central Asia (Yin et al., 2001). As southern Alaska was rotated, the angle of convergence between the plate boundary and the Pacific plate would increase, allowing for normal subduction to resume by the late Eocene (Fig. 20) (Jicha et al., 2006; Stern and Gerya, 2017). The re-initiation of normal subduction by the late Eocene is also supported by a study of the Hawaii-Emperor chain bend documenting a major change in Pacific plate motion by ca. 47 Ma (Torsvik et al., 2017). The new increased convergence angle of the Pacific plate would favor subduction along the southern Alaska plate boundary. Our results and interpretations align with the proposed middle-late Eocene oroclinal bending of southern Alaska. However, the loosely constrained orocline model would benefit from higher-resolution integrated paleomagnetic and geochronologic studies across southern Alaska.

Furthermore, the unbending of the southern Alaska orocline may not be necessary for a Paleocene–Eocene plate boundary configuration that favored a transform margin. Paleomagnetism studies of Eocene volcanic rocks in the southern Talkeetna Mountains (Panuska et al., 1990; Stamatakos et al., 2001) suggest the sampled rocks (and the underlying WCT north of the BRFS) were not in their current location, but rather were positioned at lower latitudes at the time of our proposed Paleocene–Eocene slab breakoff event. The southern Talkeetna Mountains are thought to have then been translated northward along structures such as the Denali fault and Tintina fault systems, which are believed to have accommodated at least ~1000 km of combined displacement since the Cretaceous (Denali fault: Lowey, 1998; Benowitz et al., 2012b; Tintina fault: Gabrielse, 1985). This paleoposition would favor transform margin tectonics given known constraints on the incoming plate convergence angle with North America (Fig. 21). Hence, if the Talkeetna Mountains were located ~1000 km to the southeast of the present location at the time of our proposed slab breakoff event, their position along western North America would still favor transform margin tectonics with or without Cenozoic oroclinal bending of southern Alaska. The Sanak-Baranof near-trench magmatic belt located south of the BRFS (Cowan, 2003) would have been ~1000 km south of the Talkeetna Mountains in this palinspastic reconstruction.

Farris and Paterson (2009) proposed an alternative Kula-Resurrection ridge model that involves varying obliquity of the incoming sweeping ridge along a convergent margin that becomes progressively more curved due to oroclinal bending (Hillhouse and Coe, 1994). However, the Farris and Paterson (2009) model assumes the Sanak-Baranof belt was translated <100 km since emplacement and infers the incoming ridge was mostly parallel to the margin ca. 53–50 Ma. This model does not fit our interpretation of the initiation of a slab window across interior south-central Alaska (north of the BRFS) by ca. 60 Ma nor inferred large Paleocene–Eocene translation of the Sanak-Baranof belt along western North America (Cowan, 2003; Garver, 2017). Convergent margins and oceanic ridge segments can both have very complex geometries

(Thorkelson, 1996) leading to variations in obliquity regardless of the strike of the margin. We do not have enough geologic constraints to infer the plate configuration or bathymetric high responsible for the Paleocene–Eocene slab window that we infer synchronously affected interior south-central Alaska. We acknowledge an extremely modified Kula-Resurrection ridge configuration can be reconciled with large translation of the Sanak-Baranof belt and a Paleocene–Eocene slab window under southern Alaska.

Summary

Our proposed Cenozoic tectonic evolution of southern Alaska is summarized in Figure 20 and can be divided into four separate plate configurations: (1) the Late Cretaceous–early Paleocene plate configuration was characterized by normal subduction and the approach of what we infer to be a trench-parallel bathymetric high (e.g., aseismic or active ridge or seamount chain) (Fig. 20A). (2) The middle Paleocene–middle Eocene plate configuration was characterized by a slab-window event beneath southern Alaska, related region-wide volcanism and exhumation, the increase of the regional geothermal gradient (Fig. 20B), and synorogenic sedimentation. We infer that at this time southern Alaska had a transform margin, allowing for the northward translation of the near-trench intrusions within the prism along the western margin of North America. The rotation and oroclinal bending of southern Alaska, possibly due in part to the thermally induced weakening of the crust above a slab window, may have initiated by the middle Eocene. (3) The late Eocene–Oligocene plate configuration was characterized by the resumption of normal subduction (Fig. 20C) and a period of relative tectonic quiescence. (4) The Miocene–present plate configuration is characterized by the flat-slab subduction of the Yakutat microplate, displacement and mountain building along southern Alaska structures, and the lowering of the geothermal gradient due to the removal of the mantle wedge during flat-slab subduction (Fig. 20D).

CONCLUSIONS

$^{40}Ar/^{39}Ar$ (hornblende, muscovite, biotite, K-feldspar, and whole-rock), AFT, and AHe thermochronology data indicate that the southern Talkeetna Mountains have a polyphase topographic development history (Fig. S6 [footnote 1]) that can be divided into four distinct rock-cooling events (Fig. 17): (1) slow rock cooling (~1–3 °C/m.y.) and exhumation from the Late Cretaceous–early Paleocene (ca. 74 Ma to ca. 60 Ma); (2) rapid rock cooling (>16 °C/m.y.) and exhumation initiating by the middle Paleocene (ca. 60 Ma) and persisting for ~15 m.y.; (3) a period of slow rock cooling (~1 °C/m.y.) and relative tectonic quiescence during the late Eocene–Oligocene (starting by ca. 45 Ma with Oligocene constraints not well defined by our results); and (4) more rapid rock cooling (~4 °C/m.y.) and exhumation that were focused along the CMF and initiated by the Miocene (ca. 12 Ma).

$^{40}Ar/^{39}Ar$ whole-rock volcanic ages and AFT cooling ages in the southern Talkeetna Mountains are predominantly Paleocene–Eocene (Fig. 12), suggesting that the Talkeetna Mountains has a component of paleotopography that formed prior to the current Yakutat flat-slab plate configuration. Our thermochronology data set also provides evidence for an elevated Paleocene–Eocene geothermal gradient (~55 °C/km on average) and suggests that the thermal effects of a slab window beneath southern Alaska drove exhumation. Miocene AHe cooling ages near the CMF (Fig. 7) suggest ~2–3 km of near fault vertical displacement since ~11 Ma, which is consistent with vertical offset of Paleocene–Eocene strata across the CMF and that the CMF played a role in the Miocene topographic development history of the Talkeetna Mountains. Miocene–Holocene vertical slip along the CMF was likely driven by the highly coupled flat-slab subduction of the Yakutat microplate (Fig. 20D).

Paleocene–Eocene volcanic ages and cooling ages across southern Alaska north of the BRFS are generally similar and show no apparent S-N or W-E relationships (Figs. 13 and 14), suggesting a synchronous and widespread volcanic and exhumation event. To reconcile this, we propose a new model for the Paleocene–Eocene tectonic configuration of southern Alaska. We suggest that region-wide Paleocene–Eocene volcanism and exhumation were driven by a trench-parallel slab-window event beneath southern Alaska (Fig. 19) and that at this time southern Alaska had a transform margin, allowing for the northward translation of the near-trench plutons and the Chugach accretionary prism to their current position. The combination of possible oroclinal bending of Alaska and a change in the vector of Pacific plate to more northerly led to a more convergent southern Alaska margin and the resumption of normal subduction during the middle-late Eocene. Finally, the Oligocene to present-day flat-slab subduction of the Yakutat microplate developed the modern tectono-thermal regime of southern Alaska.

ACKNOWLEDGMENTS

We acknowledge reviewer Paul Umhoefer, an anonymous reviewer, and the associate editor Jamey Jones for their constructive comments and suggestions that helped improve this manuscript greatly. This research was supported by NSF award 1828023 to Benowitz, NSF award 0910545 to Trop, the Wes Wallace Memorial Scholarship, the University of Alaska Fairbanks Undergraduate Research and Scholarly Activity Research Grant, the Alaska Geological Society and American Association of Petroleum Geologists Research Scholarships, and the Geological Society of America Graduate Student Research Grant.

REFERENCES CITED

Arkle, J.C., Armstrong, P.A., Haeussler, P.J., Prior, M.G., Hartman, S., Sendziak, K.L., and Brush, J.A., 2013, Focused exhumation in the syntaxis of the western Chugach Mountains and Prince William Sound, Alaska: Geological Society of America Bulletin, v. 125, p. 776–793, https://doi.org/10.1130/B30738.1.

Bartsch-Winkler, S., and Schmoll, H.R., 1992, Utility of radiocarbon-dated stratigraphy in determining late Holocene earthquake recurrence intervals, upper Cook Inlet region, Alaska: Geological Society of America Bulletin, v. 104, p. 684–694, https://doi.org/10.1130/0016-7606(1992)104<0684:UORDSI>2.3.CO;2.

Batir, J.F., Blackwell, D.D., and Richards, M.C., 2013, Updated Heat Flow of Alaska: Alaska Energy Authority/Alaska Center for Energy and Power, 47 p.

Benowitz, J.A., Layer, P.W., Armstrong, P., Perry, S.E., Haeussler, P.J., Fitzgerald, P.G., and VanLaningham, S., 2011, Spatial variations in focused exhumation along a continental-scale strike-slip fault: The Denali fault of the eastern Alaska Range: Geosphere, v. 7, p. 455–467, https://doi.org/10.1130/GES00589.1.

Benowitz, J.A., Haeussler, P.J., Layer, P.W., O'Sullivan, P.B., Wallace, W.K., and Gillis, R.J., 2012a, Cenozoic tectono-thermal history of the Tordrillo Mountains, Alaska: Paleocene–Eocene ridge subduction, decreasing relief, and late Neogene faulting: Geochemistry, Geophysics, Geosystems, v. 13, https://doi.org/10.1029/2011GC003951.

Benowitz, J., Benowitz, J., Vansant, G., Vansant, G., Roeske, S., Roeske, S., Layer, P.W., Layer, P.W., Hults, C.P., Hults, C.P., O'Sullivan, P., O'Sullivan, P., and Anonymous, 2012b, Geochronological constraints on the Eocene to present slip rate history of the eastern Denali fault system: Geological Society of America Abstracts with Programs, v. 44, p. 634.

Benowitz, J.A., Layer, P.W., and Vanlaningham, S., 2014, Persistent long-term (c. 24 Ma) exhumation in the Eastern Alaska Range constrained by stacked thermochronology, *in* Jourdan, F., et al., eds., Advances in $^{40}Ar/^{39}Ar$ Dating: From Archaeology to Planetary Sciences: Geological Society of London Special Publication 378, p. 225–243, https://doi.org/10.1144/SP378.12.

Benowitz, J.A., Davis, K., and Roeske, S., 2019, A river runs through it both ways across time: $^{40}Ar/^{39}Ar$ detrital and bedrock muscovite geochronology constraints on the Neogene paleodrainage history of the Nenana River system, Alaska Range: Geosphere, v. 15, p. 682–701, https://doi.org/10.1130/GES01673.1.

Betka, P.M., Gillis, R.J., and Benowitz, J.A., 2017, Cenozoic sinistral transpression and polyphase slip within the Bruin Bay fault system, Iniskin-Tuxedni region, Cook Inlet, Alaska: Geosphere, v. 13, p. 1806–1833, https://doi.org/10.1130/GES01464.1.

Blakey, R.C., and Ranney, W.D., 2017, Ancient Landscapes of Western North America: A Geologic History with Paleogeographic Maps: Springer, 228 p., https://doi.org/10.1007/978-3-319-59636-5.

Bleick, H.A., Till, A.B., Bradley, D.C., O'Sullivan, P.B., Wooden, J.L., Bradley, D.B., Taylor, T.A., Friedman, S.B., and Hults, C.P., 2012, Early Tertiary exhumation of the flank of a forearc basin, southwest Talkeetna Mountains, Alaska: U.S. Geological Survey Open-File Report 2012-1232, 1 map sheet, https://doi.org/10.3133/ofr20121232.

Bol, A.J., Coe, R.S., Grommé, C.S., and Hillhouse, J.W., 1992, Paleomagnetism of the Resurrection Peninsula, Alaska: Implications for the tectonics of southern Alaska and the Kula-Farallon ridge: Journal of Geophysical Research. Solid Earth, v. 97, p. 17,213–17,232, https://doi.org/10.1029/92JB01292.

Bradley, D.C., Haeussler, P.J., and Kusky, T.M., 1993, Timing of early Tertiary ridge subduction in southern Alaska, *in* Dusel-Bacon, C., and Till, A.B., Geologic Studies in Alaska by the U.S. Geological Survey, 1992: U.S. Geological Survey Bulletin 2068, p. 163–177, https://doi.org/10.3133/70180223.

Breitsprecher, K., and Thorkelson, D.J., 2009, Neogene kinematic history of Nazca-Antarctic-Phoenix slab windows beneath Patagonia and the Antarctic Peninsula: Tectonophysics, v. 464, p. 10–20, https://doi.org/10.1016/j.tecto.2008.02.013.

Brennan, P.R.K., Gilbert, H., and Ridgway, K.D., 2011, Crustal structure across the central Alaska Range: Anatomy of a Mesozoic collisional zone: Geochemistry, Geophysics, Geosystems, v. 12, https://doi.org/10.1029/2011GC003519.

Bristol, I., Trop, J., Benowitz, J., and Davis, K., 2017, Major Miocene paleodrainage in south-central Alaska: Sedimentology, depositional age and provenance of strata exposed in the southwestern Talkeetna Mountains: Geological Society of America Abstracts with Programs, v. 49, no. 4, https://doi.org/10.1130/abs/2017CD-292545.

Brueseke, M.E., Benowitz, J.A., Trop, J.M., Davis, K.N., Berkelhammer, S.E., Layer, P.W., and Morter, B.K., 2019, The Alaska Wrangell Arc: ~30 Ma of subduction-related magmatism along a still active arc-transform junction: Terra Nova, v. 31, no. 1, p. 59–66.

Bunds, M.P., 2001, Fault strength and transpressional tectonics along the Castle Mountain strike-slip fault, southern Alaska: Geological Society of America Bulletin, v. 113, p. 908–919, https://doi.org/10.1130/0016-7606(2001)113<0908:FSATTA>2.0.CO;2.

Burkett, C.A., Bemis, S.P., and Benowitz, J.A., 2016, Along-fault migration of the Mount McKinley restraining bend of the Denali fault defined by late Quaternary fault patterns and seismicity, Denali National Park & Preserve, Alaska: Tectonophysics, v. 693, part B, p. 489–506, https://doi.org/10.1016/j.tecto.2016.05.009.

Christeson, G.L., Gulick, S.P.S., van Avendonk, H.J.A., Worthington, L.L., Reece, R.S., and Pavlis, T.L., 2010, The Yakutat terrane: Dramatic change in crustal thickness across the transition fault, Alaska: Geology, v. 38, p. 895–898, https://doi.org/10.1130/G31170.1.

Clardy, B.I., 1974, Origin of the Lower and Middle Tertiary Wishbone and Tsadaka formations, Matanuska Valley, Alaska [M.S. thesis]: Fairbanks, Alaska, University of Alaska, 50 p.

Cole, R.B., and Layer, P.W., 2002, Stratigraphy, age and geochemistry of Tertiary volcanic rocks and associated synorogenic deposits, Mount McKinley quadrangle, Alaska, *in* Wilson, F.H., and Galloway, J.P., eds., U.S. Geological Survey Professional Paper 1662, p. 19–43.

Cole, R.B., and Stewart, B.W., 2009, Continental margin volcanism at sites of spreading ridge subduction: Examples from southern Alaska and western California: Tectonophysics, v. 464, p. 118–136, https://doi.org/10.1016/j.tecto.2007.12.005.

Cole, R.B., Ridgway, K.D., Layer, P.W., and Drake, J., 1999, Kinematics of basin development during the transition from terrane accretion to strike-slip tectonics, Late Cretaceous–early Tertiary Cantwell Formation, south central Alaska: Tectonics, v. 18, no. 6, p. 1224–1244, https://doi.org/10.1029/1999TC900033.

Cole, R.B., Nelson, S.W., Layer, P.W., and Oswald, P.J., 2006, Eocene volcanism above a depleted mantle slab window in southern Alaska: Geological Society of America Bulletin, v. 118, p. 140–158, https://doi.org/10.1130/B25658.1.

Cole, R.B., Layer, P.W., Hooks, B., Cyr, A., and Turner, J., 2007, Magmatism and deformation in a terrane suture zone south of the Denali fault, northern Talkeetna Mountains, Alaska, *in* Ridgway, K.D., Trop, J.M., Glen, J.M.G., and O'Neill, J.M., eds., Tectonic Growth of a Collisional Continental Margin: Crustal Evolution of Southern Alaska: Geological Society of America Special Paper 431, p. 477–506, https://doi.org/10.1130/2007.2431(19).

Cowan, D.S., 2003, Revisiting the Baranof–Leech River hypothesis for early Tertiary coastwise transport of the Chugach–Prince William terrane: Earth and Planetary Science Letters, v. 213, p. 463–475, https://doi.org/10.1016/S0012-821X(03)00300-5.

Cowan, D.S., Brandon, M.T., and Garver, J.I., 1997, Geologic tests of hypotheses for large coastwise displacements—A critique illustrated by the Baja British Columbia controversy: American Journal of Science, v. 297, no. 2, p. 117–173, https://doi.org/10.2475/ajs.297.2.117.

Csejtey, B., Nelson, W.H., Jones, D.L., Silberling, N.J., Dean, R.M., Morris, M.S., Lanphere, M.A., Smith, J.G., and Silberman, M.L., 1978, Reconnaissance geologic map and geochronology, Talkeetna Mountains quadrangle, northern part of Anchorage Quadrangle and southwest corner of Healy quadrangle, Alaska: U.S. Geological Survey Open-File Report 78-558A, scale 1:250,000.

Davidson, C., and Garver, J.I., 2017, Age and origin of the resurrection ophiolite and associated turbidites of the Chugach–Prince William Terrane, Kenai Peninsula, Alaska: The Journal of Geology, v. 125, p. 681–700, https://doi.org/10.1086/693926.

Detterman, R.L., Flafker, G., Tysdal, R.G., and Hudson, T., 1976, Geology and surface features along part of the Talkeetna segment of the Castle Mountain-Caribou fault system, Alaska: U.S. Geological Survey Miscellaneous Field Studies Map 738.

Dickinson, W.R., and Snyder, W.S., 1979, Geometry of subducted slabs related to the San Andreas transform: The Journal of Geology, v. 87, p. 609–627, https://doi.org/10.1086/628456.

Dodson, M.H., 1973, Closure temperature in cooling geochronological and petrological systems: Contributions to Mineralogy and Petrology, v. 40, p. 259–274, https://doi.org/10.1007/BF00373790.

Donelick, R.A., O'Sullivan, P.B., and Ketcham, R.A., 2005, Apatite fission-track analysis: Reviews in Mineralogy and Geochemistry, v. 58, p. 49–94, https://doi.org/10.2138/rmg.2005.58.3.

Doubrovine, P.V., and Tarduno, J.A., 2008, A revised kinematic model for the relative motion between Pacific oceanic plates and North America since the Late Cretaceous: Journal of Geophysical Research. Solid Earth, v. 113, https://doi.org/10.1029/2008JB005585.

Dusel-Bacon, C., and Murphy, J.M., 2001, Apatite fission-track evidence of widespread Eocene heating and exhumation in the Yukon-Tanana Upland, interior Alaska: Canadian Journal of Earth Sciences, v. 38, p. 1191–1204, https://doi.org/10.1139/e01-015.

Dusel-Bacon, C., Hopkins, M.J., Mortenson, J.K., Dashevsky, S.S., Bressler, J.R., and Day, W.C., 2006, Paleozoic tectonic and metallogenic evolution of the pericratonic rocks of east central Alaska and adjacent Yukon Territory, *in* Colpron, M., and Nelson, J.L., eds., Paleozoic Evolution and Metallogeny of Pericratonic Terranes at the Ancient Pacific Margin of North America, Canadian and Alaskan Cordillera: Geological Association of Canada Special Paper 45, p. 25–74.

Eberhart-Phillips, D., Christensen, D.H., Brocher, T.M., Hansen, R., Ruppert, N.A., Haeussler, P.J., and Abers, G.A., 2006, Imaging the transition from Aleutian subduction to Yakutat collision in central Alaska, with local earthquakes and active source data: Journal of Geophysical Research. Solid Earth, v. 111, https://doi.org/10.1029/2005JB004240.

Enkelmann, E., Piestrzeniewicz, A., Falkowski, S., Stübner, K., and Ehlers, T.A., 2017, Thermochronology in southeast Alaska and southwest Yukon: Implications for North American Plate response to terrane accretion: Earth and Planetary Science Letters, v. 457, p. 348–358, https://doi.org/10.1016/j.epsl.2016.10.032.

Farley, K.A., 2002, (U-Th)/He dating: Techniques, calibrations, and applications: Reviews in Mineralogy and Geochemistry, v. 47, p. 819–844, https://doi.org/10.2138/rmg.2002.47.18.

Farley, K.A., Wolf, R.A., and Silver, L.T., 1996, The effects of long alpha-stopping distances on (U-Th)/He ages: Geochimica et Cosmochimica Acta, v. 60, p. 4223–4229, https://doi.org/10.1016/S0016-7037(96)00193-7.

Farris, D.W., and Paterson, S.R., 2009, Subduction of a segmented ridge along a curved continental margin: Variations between the western and eastern Sanak-Baranof belt, southern Alaska: Tectonophysics, v. 464, p. 100–117, https://doi.org/10.1016/j.tecto.2007.10.008.

Finzel, E.S., Trop, J.M., Ridgway, K.D., and Enkelmann, E., 2011, Upper plate proxies for flat-slab subduction processes in southern Alaska: Earth and Planetary Science Letters, v. 303, p. 348–360, https://doi.org/10.1016/j.epsl.2011.01.014.

Finzel, E.S., Flesch, L.M., Ridgway, K.D., Holt, W.E., and Ghosh, A., 2015, Surface motions and intraplate continental deformation in Alaska driven by mantle flow: Geophysical Research Letters, v. 42, p. 4350–4358, https://doi.org/10.1002/2015GL063987.

Finzel, E.S., Enkelmann, E., Falkowski, S., and Hedeen, T., 2016, Long-term fore-arc basin evolution in response to changing subduction styles in southern Alaska: Tectonics, v. 35, p. 1735–1759, https://doi.org/10.1002/2016TC004171.

Fitzgerald, P.G., Stump, E., and Redfield, T.F., 1993, Late Cenozoic uplift of Denali and its relation to relative plate motion and fault morphology: Science, v. 259, p. 497–499, https://doi.org/10.1126/science.259.5094.497.

Fitzgerald, P.G., Baldwin, S.L., Webb, L.E., and O'Sullivan, P.B., 2006, Interpretation of (U-Th)/He single grain ages from slowly cooled crustal terranes: A case study from the Transantarctic Mountains of southern Victoria Land: Chemical Geology, v. 225, no. 1–2, p. 91–120, https://doi.org/10.1016/j.chemgeo.2005.09.001.

Fitzgerald, P.G., Roeske, S.M., Benowitz, J.A., Riccio, S.J., Perry, S.E., and Armstrong, P.A., 2014, Alternating asymmetric topography of the Alaska range along the strike-slip Denali fault: Strain partitioning and lithospheric control across a terrane suture zone: Tectonics, v. 33, p. 1519–1533, https://doi.org/10.1002/2013TC003432.

Flowers, R.M., Ketcham, R.A., Shuster, D.L., and Farley, K.A., 2009, Apatite (U–Th)/He thermochronometry using a radiation damage accumulation and annealing model: Geochimica et Cosmochimica Acta, v. 73, no. 8, p. 2347–2365, https://doi.org/10.1016/j.gca.2009.01.015.

Foster, H.L., Keith, T.E.C., and Menzie, W.D., 1994, Geology of the Yukon–Tanana area of east-central Alaska, *in* Plafker, G., and Berg, H.C., eds., The Geology of Alaska: Boulder, Colorado, Geological Society of America, The Geology of North America, v. G-1, p. 205–240, https://doi.org/DNAG-GNA-G1.205.

Frohman, R.A., 2014, Identification and evolution of tectonic faults in the greater Fairbanks Area, Alaska [M.S. thesis]: Fairbanks, Alaska, University of Alaska Fairbanks, 247 p.

Fuchs, W.A., 1980, Tertiary tectonic history of the Castle Mountain fault system in the Talkeetna Mountains: [Ph.D. dissertation]: Salt Lake City, University of Utah, 152 p.

Gabrielse, H., 1985, Major dextral transcurrent displacements along the Northern Rocky Mountain Trench and related lineaments in north-central British Columbia: Geological Society of America Bulletin, v. 96, no. 1, p. 1–14, https://doi.org/10.1130/0016-7606(1985)96<1:MDTDAT>2.0.CO;2.

Gabrielse, H., Murphy, D.C., Mortensen, J.K., Haggart, J.W., Enkin, R.J., and Monger, J.W.H., 2006, Cretaceous and Cenozoic dextral orogen-parallel displacements, magmatism, and paleogeography, north-central Canadian Cordillera, *in* Haggart, J.W., Enkin, R.J., and Monger, J.W.H., eds., Paleogeography of the North American Cordillera: Evidence For and Against Large-Scale Displacements: Geological Association of Canada Special Paper, 46, p. 255–276.

Garver, J.I., 2017, Accretion and translation of the Chugach, Prince William and Yakutat Terranes in Alaska: Geological Society of America Abstracts with Programs, v. 49, no. 6, https://doi.org/10.1130/abs/2017AM-302956.

Garver, J.I., and Davidson, C.M., 2015, Southwestern Laurentian zircons in Upper Cretaceous flysch of the Chugach–Prince William terrane in Alaska: American Journal of Science, v. 315, p. 537–556, https://doi.org/10.2475/06.2015.02.

Gasser, D., Bruand, E., Stüwe, K., Foster, D.A., Schuster, R., Fügenschuh, B., and Pavlis, T., 2011, Formation of a metamorphic complex along an obliquely convergent margin: Structural and thermochronological evolution of the Chugach Metamorphic Complex, southern Alaska: Tectonics, v. 30, https://doi.org/10.1029/2010TC002776.

Grantz, A., 1966, Strike-slip faults in Alaska: U.S. Geological Survey Open-File Report 66-53, 82 p., https://doi.org/10.3133/ofr6653.

Hacker, B.R., Kelemen, P.B., Rioux, M., McWilliams, M.O., Gans, P.B., Reiners, P.W., Layer, P.W., Söderlund, U., and Vervoort, J.D., 2011, Thermochronology of the Talkeetna intraoceanic arc of Alaska: Ar/Ar, U-Th/He, Sm-Nd, and Lu-Hf dating: Tectonics, v. 30, TC1011, https://doi.org/10.1029/2010TC002798.

Haeussler, P.J., 2008, An Overview of the Neotectonics of Interior Alaska : Far-Field Deformation From the Yakutat Microplate Collision, *in* Freymueller, J.T., Haeussler, P.J., Wesson, R.L., and Ekström, G., eds., Active Tectonics and Seismic Potential of Alaska: American Geophysical Union Geophysical Monograph Series, v. 179, p. 83–108, https://doi.org/10.1029/179GM05.

Haeussler, P.J., Bradley, D., Goldfarb, R., Snee, L., and Taylor, C., 1995, Link between ridge subduction and gold mineralization in southern Alaska: Geology, v. 23, p. 995–998, https://doi.org/10.1130/0091-7613(1995)023<0995:LBRSAG>2.3.CO;2.

Haeussler, P.J., Best, T.C., and Waythomas, C.F., 2002, Paleoseismology at high latitudes: Seismic disturbance of upper Quaternary deposits along the Castle Mountain fault near Houston, Alaska: Geological Society of America Bulletin, v. 114, p. 1296–1310, https://doi.org/10.1130/0016-7606(2002)114<1296:PAHLSD>2.0.CO;2.

Haeussler, P.J., Bradley, D.C., Wells, R.E., and Miller, M.L., 2003, Life and death of the resurrection plate: Evidence for its existence and subduction in the northeastern Pacific in Paleocene-Eocene time: Bulletin of the Geological Society of America, v. 115, p. 867–880, https://doi.org/10.1130/0016-7606(2003)115<0867:LADOTR>2.0.CO;2.

Haeussler, P.J., O'sullivan, P., Berger, A.L., and Spotila, J.A., 2008, Neogene exhumation of the Tordrillo Mountains, Alaska, and correlations with Denali (Mount McKinley), *in* Freymueller, J.T., Haeussler, P.J., Wesson, R.L., and Ekström, G., eds., Active Tectonics and Seismic Potential of Alaska: American Geophysical Union Geophysical Monograph Series 179, p. 269–285, https://doi.org/10.1029/179GM15.

Hillhouse, J.W., and Coe, R.S., 1994, Paleomagnetic data from Alaska, *in* Plafker, G., and Berg, H.C., eds., The Geology of Alaska: Boulder, Colorado: Geological Society of America, Geology of North America, v. G-1, p. 797–812, https://doi.org/10.1130/DNAG-GNA-G1.797.

Hoffman, M.D., and Armstrong, P.A., 2006, Miocene exhumation of the southern Talkeetna Mountains, south-central Alaska, based on apatite (U-Th)/He thermochronology: Geological Society of America Abstracts with Programs, v. 38, no. 5, p. 9.

Jadamec, M.A., Billen, M.I., and Roeske, S.M., 2013, Three-dimensional numerical models of flat slab subduction and the Denali fault driving deformation in south-central Alaska: Earth and Planetary Science Letters, v. 376, p. 29–42, https://doi.org/10.1016/j.epsl.2013.06.009.

Jicha, B.R., Scholl, D.W., Singer, B.S., Yogodzinski, G.M., and Kay, S.M., 2006, Revised age of Aleutian Island Arc formation implies high rate of magma production: Geology, v. 34, p. 661–664, https://doi.org/10.1130/G22433.1.

Kalbas, J.L., Freed, A.M., and Ridgway, K.D., 2008, Contemporary fault mechanics in southern Alaska, *in* Freymueller, J.T., Haeussler, P.J., Wesson, R.L., and Ekström, G., eds., Active Tectonics and Seismic Potential of Alaska: American Geophysical Union Geophysical Monograph Series, v. 179, p. 321–336, https://doi.org/10.1029/179GM18.

Kassab, C.M., Kortyna, C.D., Ridgway, K.D., and Trop, J.M., 2009, Sedimentology, structural framework, and basin analysis of the eastern Arkose Ridge Formation, Talkeetna Mountains, Alaska: Geological Society of America Abstracts with Programs, v. 41, no. 7, p. 304.

Ketcham, R.A., 2005, Forward and inverse modeling of low-temperature thermochronometry data: Reviews in Mineralogy and Geochemistry, v. 58, p. 275–314, https://doi.org/10.2138/rmg.2005.58.11.

Kochelek, E.J., Amato, J.M., Pavlis, T.L., and Clift, P.D., 2011, Flysch deposition and preservation of coherent bedding in an accretionary complex: Detrital zircon ages from the Upper Cretaceous Valdez Group, Chugach terrane, Alaska: Lithosphere, v. 3, p. 265–274, https://doi.org/10.1130/L131.1.

Koehler, R.D., III, Reger, R.D., Carver, G.A., Spangler, E., and Gould, A., 2014, Castle Mountain fault southcentral Alaska: Observations on slip partitioning from lidar and paleoseismic trenching: Geological Society of America Abstracts with Programs, v. 46, no. 6, p. 661.

Kortyna, C., Donaghy, E., Trop, J.M., and Idleman, B., 2013, Integrated provenance record of a forearc basin modified by slab-window magmatism: Detrital- zircon geochronology and sandstone compositions of the Paleogene Arkose Ridge Formation, south-central Alaska: Basin Research, v. 26, p. 436–460, https://doi.org/10.1111/bre.12033.

Kusky, T.M., Bradley, D.C., and Haeussler, P., 1997, Progressive deformation of the Chugach accretionary complex, Alaska, during a Paleogene ridge-trench encounter: Journal of Structural Geology, v. 19, p. 139–157, https://doi.org/10.1016/S0191-8141(96)00084-3.

Kveton, K., 1989, Structure, thermochronology, provenance and tectonic history of the Orca Group in southwestern Prince William south Alaska [Ph.D. dissertation]: Seattle, Washington, University of Washington, 173 p.

Lease, R.O., Haeussler, P.J., and O'Sullivan, P., 2016, Changing exhumation patterns during Cenozoic growth and glaciation of the Alaska Range: Insights from detrital thermochronology and geochronology: Tectonics, v. 35, p. 934–955, https://doi.org/10.1002/2015TC004067.

Li, C., Zhang, M., Fu, P., Qian, Z., Hu, P., and Ripley, E.M., 2012a, The Kalatongke magmatic Ni–Cu deposits in the Central Asian Orogenic Belt, NW China: Product of slab window magmatism?: Mineralium Deposita, v. 47, p. 51–67, https://doi.org/10.1007/s00126-011-0354-7.

Li, Z.X., Li, X.H., Chung, S.L., Lo, C.H., Xu, X., and Li, W.X., 2012b, Magmatic switch-on and switch-off along the South China continental margin since the Permian: Transition from an Andean-type to a Western Pacific-type plate boundary: Tectonophysics, v. 532–535, p. 271–290, https://doi.org/10.1016/j.tecto.2012.02.011.

Little, T.A., 1990, Kinematics of wrench and divergent-wrench deformation along a central part of the Border Ranges Fault System, Northern Chugach Mountains, Alaska: Tectonics, v. 9, p. 585–611, https://doi.org/10.1029/TC009i004p00585.

Little, T.A., and Naeser, C.W., 1989, Tertiary tectonics of the Border Ranges fault system, Chugach Mountains, Alaska: Deformation and uplift in a forearc setting: Journal of Geophysical Research. Solid Earth, v. 94, p. 4333–4359, https://doi.org/10.1029/JB094iB04p04333.

Löbens, S., Oriolo, S., Benowitz, J., Wemmer, K., Layer, P., and Siegesmund, S., 2017, Late Paleozoic deformation and exhumation in the Sierras Pampeanas (Argentina): $^{40}Ar/^{39}Ar$-feldspar dating constraints: International Journal of Earth Sciences, v. 106, p. 1991–2003, https://doi.org/10.1007/s00531-016-1403-3.

Lovera, O.M., Grove, M., and Harrison, T.M., 2002, Systematic analysis of K-feldspar $^{40}Ar/^{39}Ar$ step heating results II: Relevance of laboratory argon diffusion properties to nature: Geochimica et Cosmochimica Acta, v. 66, p. 1237–1255, https://doi.org/10.1016/S0016-7037(01)00846-8.

Lowey, G.W., 1998, A new estimate of the amount of displacement on the Denali Fault system based on the occurrence of carbonate megaboulders in the Dezadeash Formation (Jura-Cretaceous), Yukon, and the Nutzotin Mountains sequence (Jura-Cretaceous), Alaska: Bulletin of Canadian Petroleum Geology, v. 46, p. 379–386.

Mankhemthong, N., Doser, D.I., and Pavlis, T.L., 2013, Interpretation of gravity and magnetic data and development of two-dimensional cross-sectional models for the border ranges fault system, south-central Alaska: Geosphere, v. 9, p. 242–259, https://doi.org/10.1130/GES00833.1.

Michaud, F., Royer, J.Y., Bourgois, J., Dyment, J., Calmus, T., Bandy, W., Sosson, M., Mortera-Gutiérrez, C., Sichler, B., Rebolledo-Viera, M., and Pontoise, B., 2006, Oceanic-ridge subduction vs. slab break off: Plate tectonic evolution along the Baja California Sur continental margin since 15 Ma: Geology, v. 34, p. 13–16, https://doi.org/10.1130/g22050.1.

O'Sullivan, P., Donelick, M., and Donelick, R., 2010, Apatite fission-track results from the region of the Pebble Deposit, southwest Alaska: Apatite to Zircon, Inc., Report no. 950.

O'Sullivan, P.B., and Currie, L.D., 1996, Thermotectonic history of Mt Logan, Yukon Territory, Canada: Implications of multiple episodes of middle to late Cenozoic denudation: Earth and Planetary Science Letters, v. 144, p. 251–261, https://doi.org/10.1016/0012-821X(96)00161-6.

Oswald, P.J., 2006, Eocene volcanic rocks of the southern Talkeetna Mountains, Alaska: Anomalous forearc volcanism in an extensional setting [M.S. thesis]: Moscow, Idaho, University of Idaho, 40 p., 6 tables, 18 figures.

Pallares, C., Maury, R.C., Bellon, H., Royer, J.Y., Calmus, T., Aguillón-Robles, A., Cotten, J., Benoit, M., Michaud, F., and Bourgois, J., 2007, Slab-tearing following ridge-trench collision: Evidence from Miocene volcanism in Baja California, México: Journal of Volcanology and Geothermal Research, v. 161, p. 95–117, https://doi.org/10.1016/j.tecto.2016.09.021.

Panuska, B.C., Stone, D.B., and Turner, D.L., 1990, Paleomagnetism of Eocene volcanic rocks, Talkeetna Mountains, Alaska: Journal of Geophysical Research. Solid Earth, v. 95, no. B5, p. 6737–6750, https://doi.org/10.1029/JB095iB05p06737.

Parry, W.T., Bunds, M.P., Bruhn, R.L., Hall, C.M., and Murphy, J.M., 2001, Mineralogy,$^{40}Ar/^{39}Ar$ dating and apatite fission track dating of rocks along the Castle Mountain fault, Alaska: Tectonophysics, v. 337, p. 149–172, https://doi.org/10.1016/S0040-1951(01)00117-2.

Pavlis, T.L., and Roeske, S.M., 2007, The Border Ranges fault system, southern Alaska, *in* Ridgway, K.D., Trop, J.M., Glen, J.M.G., and O'Neill, J.M., eds., Tectonic Growth of a Collisional Continental Margin: Crustal Evolution of Southern Alaska: Geological Society of America Special Paper 431, p. 95–127, https://doi.org/10.1130/2007.2431(05).

Pavlis, T.L., and Sisson, V.B., 2003, Development of a subhorizontal decoupling horizon in a transpressional system, Chugach metamorphic complex, Alaska: Evidence for rheological stratification of the crust, *in* Sisson, V.B., Roeske, S.M., and Pavlis, T.L., eds., Geology of a Transpressional Orogen Developed during Ridge-Trench Interaction along the North Pacific Margin: Geological Society of America Special Paper 371, p. 191–216, https://doi.org/10.1130/0-8137-2371-X.191.

Plafker, G., and Berg, H.C., 1994, Overview of the geology and tectonic evolution of Alaska, *in* Plafker, G., and Berg, H.C., eds., The Geology of Alaska: The Geology of North America Geological Society of America, v. G-1, p. 989–1021, http://doi.org/10.1130/DNAG-GNA-G1.989.

Reed, B.L., and Lanphere, M.A., 1972, Generalized geologic map of the Alaska-Aleutian Range batholith showing potassium-argon ages of the plutonic rocks: U.S. Geological Survey Miscellaneous Field Studies Map 372, 2 sheets, https://doi.org/10.3133/mf372.

Reiners, P.W., 2007, Thermochronologic Approaches to Paleotopography: Reviews in Mineralogy and Geochemistry, v. 66, p. 243–267, https://doi.org/10.2138/rmg.2007.66.10.

Reiners, P.W., and Brandon, M.T., 2006, Using thermochronology to understand orogenic erosion: Annual Review of Earth and Planetary Sciences, v. 34, p. 419–466, https://doi.org/10.1146/annurev.earth.34.031405.125202.

Reiners, P.W., and Farley, K.A., 2001, Influence of crystal size on apatite (U-Th)/He thermochronology: An example from the Bighorn Mountains, Wyoming: Earth and Planetary Science Letters, v. 188, p. 413–420, https://doi.org/10.1016/S0012-821X(01)00341-7.

Renne, P.R., Mundil, R., Balco, G., Min, K., and Ludwig, K.R., 2010, Joint determination of ^{40}K decay constants and $^{40}Ar^*/^{40}K$ for the Fish Canyon sanidine standard, and improved accuracy for $^{40}Ar/^{39}Ar$ geochronology: Geochimica et Cosmochimica Acta, v. 74, p. 5349–5367, https://doi.org/10.1016/j.gca.2010.06.017.

Riccio, S.J., Fitzgerald, P.G., Benowitz, J.A., and Roeske, S.M., 2014, The role of thrust faulting in the formation of the eastern Alaska Range: Thermochronological constraints from the Susitna Glacier Thrust Fault region of the intracontinental strike-slip Denali Fault system: Tectonics, v. 33, p. 2195–2217, https://doi.org/10.1002/2014TC003646.

Ridgway, K.D., Trop, J.M., Nokleberg, W.J., Davidson, C.M., and Eastham, K.R., 2002, Mesozoic and Cenozoic tectonics of the eastern and central Alaska Range: Progressive basin development and deformation in a suture zone: Geological Society of America Bulletin, v. 114, p. 1480–1504, https://doi.org/10.1130/0016-7606(2002)114%3C1480:MACTOT%3E2.0.CO;2.

Ridgway, K.D., Finzel, E.S., and Trop, J.M., 2012, Modification of Continental Forearc Basins by Flat-Slab Subduction Processes: A Case Study from Southern Alaska, *in* Busby, C., and Azor, A., eds., Tectonics of Sedimentary Basins: Recent Advances, p. 327–346, https://doi.org/10.1002/9781444347166.ch16.

Rioux, M., Hacker, B., Mattinson, J., Kelemen, P., Blusztajn, J., and Gehrels, G., 2007, Magmatic development of an intra-oceanic arc: High-precision U-Pb zircon and whole-rock isotopic analyses from the accreted Talkeetna arc, south-central Alaska: Geological Society of America Bulletin, v. 119, p. 1168–1184, https://doi.org/10.1130/B25964.1.

Rioux, M., Mattinson, J., Hacker, B., Kelemen, P., Blusztajn, J., Hanghøj, K., and Gehrels, G., 2010, Intermediate to felsic middle crust in the accreted Talkeetna arc, the Alaska Peninsula and Kodiak Island, Alaska: An analogue for low-velocity middle crust in modern arcs: Tectonics, v. 29, no. 3, https://doi.org/10.1029/2009TC002541.

Robertson, P.B., 2014, Structural configuration of a modified Mesozoic to Cenozoic forearc basin system, south-central Alaska [M.S. thesis]: West Lafayette, Indiana, Purdue University, 218 p.

Roden, M.K., and Miller, D.S., 1989, Apatite fission-track thermochronology of the Pennsylvania Appalachian Basin: Geomorphology, v. 2, p. 39–51, https://doi.org/10.1016/0169-555X(89)90005-6.

Roeske, S.M., Snee, L.W., and Pavlis, T.L., 2003, Dextral-slip reactivation of an arc-forearc boundary during Late Cretaceous–Early Eocene oblique convergence in the northern Cordillera, *in* Sisson, V.B., Roeske, S.M., and Pavlis, T.L., eds., Geology of a Transpressional Orogen Developed during Ridge-Trench Interaction along the North Pacific Margin: Geological Society of America Special Paper 371, p. 141–169, https://doi.org/10.1130/0-8137-2371-X.141.

Silberman, M.L., and Grantz, A., 1984, Paleogene volcanic rocks of the Matanuska Valley area and the displacement history of the Castle Mountain fault: U.S. Geological Survey Circular 868, p. 82–86.

Spotila, J.A., 2005, Applications of low-temperature thermochronometry to quantification of recent exhumation in mountain belts: Reviews in Mineralogy and Geochemistry, v. 58, p. 449–466, https://doi.org/10.2138/rmg.2005.58.17.

Spotila, J.A., and Berger, A.L., 2010, Exhumation at orogenic indentor corners under long-term glacial conditions: Example of the St. Elias orogen, Southern Alaska: Tectonophysics, v. 490, p. 241–256, https://doi.org/10.1016/j.tecto.2010.05.015.

Stamatakos, J.A., Trop, J.M., and Ridgway, K.D., 2001, Late cretaceous paleogeography of Wrangellia: Paleomagnetism of the MacColl Ridge Formation, southern Alaska, revisited: Geology, v. 29, p. 947–950, https://doi.org/10.1130/0091-7613(2001)029<0947:LCPOWP>2.0.CO;2.

Stanley, R.G., Haeussler, P.J., Benowitz, J.A., Lewis, K.A., Shellenbaum, D.P., Saltus, R.W., Shah, A.K., Phillips, J.D., and Potter,C.J., 2014, Tectonic implications of new geological and geophysical results from the Susitna basin, south-central Alaska: Search and Discovery Article, 10608.

Stern, R.J., and Gerya, T., 2017, Subduction initiation in nature and models: A review: Tectonophysics, v. 746, p. 173–198, https://doi.org/10.1016/j.tecto.2017.10.014.

Sunderlin, D., Trop, J.M., Idleman, B.D., Brannick, A., White, J.G., and Grande, L., 2014, Paleoenvironment and paleoecology of a Late Paleocene high-latitude terrestrial succession, Arkose Ridge Formation at Box Canyon, southern Talkeetna Mountains, Alaska: Palaeogeography, Palaeoclimatology, Palaeoecology, v. 401, p. 57–80, https://doi.org/10.1016/j.palaeo.2014.02.012.

Tagami, T., and O'Sullivan, P.B., 2005, Fundamentals of fission-track thermochronology: Reviews in Mineralogy and Geochemistry, v. 58, p. 19–47, https://doi.org/10.2138/rmg.2005.58.2.

Tempelman-Kluit, D.J., and Wanless, R.K., 1975, Potassium-argon age determinations of metamorphic and plutonic rocks in the Yukon Crystalline Terrane: Canadian Journal of Earth Sciences, v. 12, no. 11, p. 1895–1909, https://doi.org/10.1139/e75-167.

Thorkelson, D.J., 1996, Subduction of diverging plates and the principles of slab window formation: Tectonophysics, v. 255, p. 47–63, https://doi.org/10.1016/0040-1951(95)00106-9.

Torsvik, T.H., Doubrovine, P.V., Steinberger, B., Gaina, C., Spakman, W., and Domeier, M., 2017, Pacific plate motion change caused the Hawaiian-Emperor Bend: Nature Communications, v. 8, https://doi.org/10.1038/ncomms15660.

Trop, J.M., 2008, Latest Cretaceous forearc basin development along an accretionary convergent margin: South-central Alaska: Geological Society of America Bulletin, v. 120, p. 207–224, https://doi.org/10.1130/B26215.1.

Trop, J.M., and Ridgway, K.D., 2007, Mesozoic and Cenozoic tectonic growth of southern Alaska: A sedimentary basin perspective, *in* Ridgway, K.D., Trop, J.M., Glen, J.M.G., and O'Neill, J.M., eds., Tectonic Growth of a Collisional Continental Margin: Crustal Evolution of Southern Alaska: Geological Society of America Special Paper 431, p. 55–94, https://doi.org/10.1130/2007.2431(04).

Trop, J.M., Ridgway, K.D., and Spell, T.L., 2003, Sedimentary record of transpressional tectonics and ridge subduction in the Tertiary Matanuska Valley–Talkeetna Mountains forearc basin, southern Alaska, *in* Sisson, V.B., Roeske, S.M., and Pavlis, T.L., eds., Geology of a Transpressional Orogen Developed during Ridge-Trench Interaction along the North Pacific Margin: Geological Society of America Special Paper 371, p. 89–118, https://doi.org/10.1130/0-8137-2371-X.89.

Trop, J.M., Szuch, D.A., Rioux, M., and Blodgett, R.B., 2005, Sedimentology and provenance of the Upper Jurassic Naknek Formation, Talkeetna Mountains, Alaska: Bearings on the accretionary tectonic history of the Wrangellia composite terrane: Geological Society of America Bulletin, v. 117, p. 570–588, https://doi.org/10.1130/B25575.1.

Trop, J.M., Hart, W.K., Snyder, D., and Idleman, B., 2012, Miocene basin development and volcanism along a strike-slip to flat-slab subduction transition: Stratigraphy, geochemistry, and geochronology of the central Wrangell volcanic belt, Yakutat–North America collision zone: Geosphere, v. 8, no. 4, p. 805–834, https://doi.org/10.1130/GES00762.1.

Trop, J.M., Idleman, B., Ridgway, K.D., Sunderlin, D., Cole, R.B., Donaghy, E.E., and Robertson, P.B., 2015, Sedimentary record of Paleogene basin development deformation and exhumation during spreading ridge subduction on southern Alaska: Geological Society of America Abstracts with Programs, v. 47, no. 4, p. 9.

Valentino, J.D., Spotila, J.A., Owen, L.A., and Buscher, J.T., 2016, Rock uplift at the transition from flat-slab to normal subduction: The Kenai Mountains, southeast Alaska: Tectonophysics, v. 671, p. 63–75, https://doi.org/10.1016/j.tecto.2016.01.022.

Waldien, T.S., Roeske, S.M., Benowitz, J.A., Allen, W.K., Ridgway, K.D., and O'Sullivan, P.B., 2018, Late Miocene to Quaternary evolution of the McCallum Creek thrust system, Alaska: Insights for range-boundary thrusts in transpressional orogens: Geosphere, v. 14, no. 6, p. 2379–2406, https://doi.org/10.1130/GES01676.1.

Ward, D.J., Anderson, R.S., and Haeussler, P.J., 2012, Scaling the Teflon Peaks: Rock type and the generation of extreme relief in the glaciated western Alaska Range: Journal of Geophysical Research, v. 117, F01031, https://doi.org/10.1029/2011JF002068.

Williams, J.R., Carter, L.D., Hamilton, T.D., and Galloway, J.P., 1989, A working glacial chronology for the western Copper River basin, Alaska: Late Cenozoic history of the interior basins of Alaska and the Yukon: U.S. Geological Survey Circular 1026, p. 81–85.

Willis, J.B., Haeussler, P.J., Bruhn, R.L., and Willis, G.C., 2007, Holocene slip rate for the western segment of the Castle Mountain fault, Alaska: Bulletin of the Seismological Society of America, v. 97, p. 1019–1024, https://doi.org/10.1785/0120060109.

Wilson, F.H., Hults, C.P., Mull, C.G., and Karl, S.M., 2015, Geologic map of Alaska: U.S. Geological Survey Scientific Investigations Map 3340, pamphlet 197 p., 2 sheets, scale 1:1,584,000, http://doi.org/10.3133/sim3340.

Worthington, L.L., Van Avendonk, H.J.A., Gulick, S.P.S., Christeson, G.L., and Pavlis, T.L., 2012, Crustal structure of the Yakutat terrane and the evolution of subduction and collision in southern Alaska: Journal of Geophysical Research. Solid Earth, v. 117, no. B1, 20 p., http://doi.org/10.1029/2011JB008493.

Yin, A., Robinson, A., and Manning, C.E., 2001, Oroclinal bending and slab-break-off causing coeval east-west extension and east-west contraction in the Pamir-Nanga Parbat syntaxis in the past 10 my: American Geophysical Union Fall Meeting Abstracts, abstract T12F-03.